

IMAGING GENETICS AND BIOMARKER VARIATIONS OF CLINICALLY
DIAGNOSED ALZHEIMER'S DISEASE

Edwin Carl Stage Jr.

Submitted to the faculty of the University Graduate School
in partial fulfillment of the requirements
for the degree
Doctor of Philosophy
in the Program of Medical Neuroscience,
Indiana University

August 2020

Accepted by the Graduate Faculty of Indiana University, in partial fulfillment of the requirements for the degree of Doctor of Philosophy.

Doctoral Committee

Karmen K. Yoder, Ph.D., Chair

Liana G. Apostolova, M.D., MSc, FAAN

April 21, 2020

Shannon L. Risacher, Ph.D.

Sujuan Gao, Ph.D.

Andrew J. Saykin, Psy.D.

© 2020

Edwin Carl Stage Jr.

DEDICATION

This dissertation is dedicated to my family members, first and foremost to my rock and my best friend, Madeline. Every day you gave me the strength to continue giving my best and guided me towards my dreams. Through all of the late nights and missed dinners, thank you for your unwavering support and understanding. I love you.

To my parents, Ed and Vicki, thank you for your example. You taught me the importance of living with compassion, humility, and generosity. Most of all, you taught me the importance of enjoying life and spending time with those you love. I could never repay you what you've given me, but hopefully, now you'll at least let me contribute towards family dinners. I love you.

To my brother, Sam, I hope that you know what an absolute treasure it has been to watch you grow up into the magnificent man you are today. I believe that you still somehow think of me as a role model, but do you know that I look up to you as well? I love you.

To my grandparents, Ed, Ann, Juanita, and Randall, thank you for the loving environment and wisdom you always shared. Your stories continue to captivate me, regardless of how many times I've heard them. If I can have even a fraction of the impact on the world that you've all had, I surely will have lived my best life. I love you.

Finally, to my son Finnegan, there are a couple of things that you cannot yet know or understand. 1. Your mother and I do not know everything or even most things. We are simply doing the best we can. 2. You are the most beautiful

and perfect human I have ever held in my arms. I cannot wait to watch you grow up. I love you.

ACKNOWLEDGEMENTS

This work would not have been possible without the outstanding support and mentorship of Dr. Liana Apostolova, who not only trained me as a scientist to be more analytical and question everything, but challenged me to step outside of my comfort zone and accomplish things I never believed that I could. Her scientific fervor is contagious, as is the care and compassion she approaches her patients with. It is often easy to forget what we are fighting for, a world with a little less suffering, but Liana always keeps perspective and urges others to do the same. I could not have done this without you, thank you.

To my committee members, Drs. Karmen Yoder, Andrew Saykin, Shannon Risacher, and Sujuan Gao, you all have provided me such a nurturing scientific environment to grow. Your guidance and expertise have contributed greatly to this work, and your continual interest in my well-being has helped push me on during the darker times. Thank you all so much.

The analyses reported in this dissertation were funded by the NIA R56 AG057195, NIA U01 AG057195, NIA R01 AG040770, NIA K02 AG048240, NIA P30 AG010133 and NIA K01 AG049050.

Data collection and sharing for this project was funded by the Alzheimer's Disease Neuroimaging Initiative (ADNI) (National Institutes of Health Grant U01 AG024904) and DOD ADNI (Department of Defense award number W81XWH-12-2-0012). ADNI is funded by the National Institute on Aging, the National Institute of Biomedical Imaging and Bioengineering, and through generous contributions from the following: Alzheimer's Association; Alzheimer's Drug

Discovery Foundation; BioClinica, Inc.; Biogen Idec Inc.; Bristol-Myers Squibb Company; Eisai Inc.; Elan Pharmaceuticals, Inc.; Eli Lilly and Company; F. Hoffmann-La Roche Ltd and its affiliated company Genentech, Inc.; GE Healthcare; Innogenetics, N.V.; IXICO Ltd.; Janssen Alzheimer Immunotherapy Research & Development, LLC.; Johnson & Johnson Pharmaceutical Research & Development LLC.; Medpace, Inc.; Merck & Co., Inc.; Meso Scale Diagnostics, LLC.; NeuroRx Research; Novartis Pharmaceuticals Corporation; Pfizer Inc.; Piramal Imaging; Servier; Synarc Inc.; and Takeda Pharmaceutical Company.

The Canadian Institutes of Health Research is providing funds to support ADNI clinical sites in Canada. Private sector contributions are facilitated by the Foundation for the National Institutes of Health (www.fnih.org). The grantee organization is the Northern California Institute for Research and Education, and the study is coordinated by the Alzheimer's Disease Cooperative Study at the University of California, San Diego. ADNI data are disseminated by the Laboratory for Neuro Imaging at the University of Southern California.

Edwin Carl Stage Jr.

IMAGING GENETICS AND BIOMARKER VARIATIONS OF CLINICALLY
DIAGNOSED ALZHEIMER'S DISEASE

Neuroimaging biomarkers play a crucial role in our understanding of Alzheimer's disease. Beyond providing a fast and accurate *in vivo* picture of the neuronal structure and biochemistry, these biomarkers make up a research framework, defined in a 2018 as the A(amyloid)/T(tau)/N(neurodegeneration) framework after three of the hallmarks of Alzheimer's disease. I first used imaging measures of amyloid, tau and neurodegeneration to study clinically diagnosed Alzheimer's disease. After dividing subjects into early (onset younger than 65) and late-onset (onset of 65 and older) amyloid-positive (AD) and amyloid-negative (nonAD) groups, I saw radically differing topographical distribution of tau and neurodegeneration. AD subjects with an early disease onset had a much more severe amyloid, tau and neurodegeneration than late-onset AD. In the nonAD group, neurodegeneration was found only in early-onset FDG PET data and in a nonAlzheimer's-like MRI and FDG pattern for late-onset. The late-onset nonAD resembled that of limbic-predominant age-related TDP-43 encephalopathy.

I next utilized an imaging genetics approach to associate genome-wide significant Alzheimer's risk variants to structural (MRI), metabolic (FDG PET) and tau (tau PET) imaging biomarkers. Linear regression was used to select variants for each of the models and included a pooled sample, cognitively normal, mild cognitive impairment and dementia groups in order to fully capture the cognitive

spectrum from normal cognition to the most severely impaired. Model selected variants were replicated using voxelwise regression in an exploratory analysis of spatial associations for each modality. For each imaging type, I replicated some associations to the biomarkers previously seen, as well as identified several novel associations. Several variants identified with crucial Alzheimer's biomarkers may be potential future targets for drug interventions.

Karmen K. Yoder, Ph.D., Chair

TABLE OF CONTENTS

| | |
|--|-----|
| LIST OF TABLES | xii |
| LIST OF FIGURES | xiv |
| LIST OF ABBREVIATIONS | xvi |
| Chapter 1. Background and Justification..... | 1 |
| 1.1. Alzheimer’s Pathology | 1 |
| 1.2. Clinical Considerations for Alzheimer’s disease | 4 |
| 1.3. Genetics of Alzheimer’s disease | 10 |
| 1.4. Statement of Purpose | 12 |
| Chapter 2. Neurodegenerative Changes in Early & Late-Onset Cognitive Impairment with and without Brain Amyloidosis | 14 |
| 2.1. Introduction | 14 |
| 2.2. Methods | 16 |
| 2.3. Results | 20 |
| 2.4. Discussion..... | 41 |
| 2.5. Strengths and Limitations | 44 |
| 2.6. Conclusions | 44 |
| Chapter 3. The effect of the top 20 Alzheimer’s disease risk genes on gray matter density and FDG PET brain metabolism..... | 46 |
| 3.1. Introduction | 46 |
| 3.2. Methods | 50 |
| 3.3. Results | 60 |
| 3.4. Discussion..... | 74 |

| | |
|---|-----|
| 3.5. Strengths and Limitations | 80 |
| 3.6. Conclusions | 80 |
| Chapter 4. Association of the top 20 Alzheimer’s disease risk genes with [¹⁸ F]Flortaucipir PET | 82 |
| 4.1. Introduction | 82 |
| 4.2. Methods | 84 |
| 4.3. Results | 88 |
| 4.4. Discussion..... | 106 |
| 4.5. Strengths and limitations..... | 110 |
| 4.6. Conclusions | 111 |
| Chapter 5. Summary and Future Directions | 112 |
| 5.1. Neurodegenerative Changes in Early & Late-Onset Cognitive Impairment with and without Brain Amyloidosis..... | 112 |
| 5.2. The effect of the top 20 Alzheimer’s disease risk genes on gray matter density and FDG PET brain metabolism | 116 |
| 5.3. Association of the top 20 Alzheimer’s disease risk genes with [¹⁸ F]Flortaucipir PET | 118 |
| 5.4. Conclusion | 121 |
| References | 122 |
| Curriculum Vitae | |

LIST OF TABLES

| | |
|---|----|
| Table 1. EOAD and LOAD demographic comparisons to CN | 22 |
| Table 2. EOAD and LOAD demographic comparisons to the young and old CN groups, resp | 23 |
| Table 3. EO vs. LO demographic comparisons..... | 24 |
| Table 4. Regional amyloid PET (^{18}F Florbetapir) comparisons between amyloid positive subjects for frontal, cingulate, parietal and temporal cortices | 25 |
| Table 5. EOnonAD and LOnonAD demographic comparisons to CN | 33 |
| Table 6. EOnonAD and LOnonAD demographic comparisons to the young and old CN groups, resp..... | 34 |
| Table 7. Regional amyloid PET (^{18}F Florbetapir) comparisons between amyloid negative subjects for frontal, cingulate, parietal and temporal cortices | 35 |
| Table 8. All variants of the top 20 AD risk genes that were considered for inclusion in analyses | 54 |
| Table 9. List of variants that needed partial or full imputation | 55 |
| Table 10. Linkage analysis for genes with multiple variants included | 56 |
| Table 11. MRI descriptives | 62 |
| Table 12. FDG descriptives | 63 |
| Table 13. MRI FWE and/or FDR significant clusters | 64 |
| Table 14. FDG FWE and/or FDR significant clusters..... | 65 |
| Table 15. Demographic and biomarker data for each diagnostic group..... | 90 |

| | |
|--|-----|
| Table 16. Minor allele distribution for variants retained in the regression models | 91 |
| Table 17: Regression Selected Variants in a Pooled Sample | 94 |
| Table 18: Cluster and within-cluster peak level effects for each diagnostic group | 96 |
| Table 19: Regression Selected Variants in a CN Sample | 98 |
| Table 20: Regression Selected Variants in an MCI Sample | 101 |
| Table 21: Regression Selected Variants in a DEM Sample | 104 |

LIST OF FIGURES

| | |
|---|-----|
| Figure 1. MRI (top), FDG PET (middle), tau PET (bottom) comparisons between the AD groups and CN..... | 27 |
| Figure 2. MRI (top) and FDG PET (bottom) comparisons between the AD and CN groups restricted to only subjects with available tau PET scans..... | 28 |
| Figure 3. MRI (top), FDG PET (middle), tau PET (bottom) comparisons between young CN and EOnonAD and old CN and LOnonAD groups..... | 29 |
| Figure 4. MRI (top), FDG PET (middle), tau PET (bottom) comparisons between the nonAD groups and CN..... | 37 |
| Figure 5. MRI (top) and FDG PET (bottom) comparisons between the nonAD and CN groups restricted to only subjects with available tau PET scans | 38 |
| Figure 6. MRI (top), FDG PET (middle), tau PET (bottom) comparisons between young CN and EOAD and old CN and LOAD groups..... | 39 |
| Figure 7. LD analysis..... | 57 |
| Figure 8. <i>APOE4</i> effect | 67 |
| Figure 9. MRI SPM results | 70 |
| Figure 10. FDG SPM results | 73 |
| Figure 11. Association of the <i>APOE</i> e4 allele with tau deposition..... | 92 |
| Figure 12. Stepwise regression selected genes in a pooled sample (all diagnosis groups) | 95 |
| Figure 13. Stepwise regression selected genes in the CN group | 99 |
| Figure 14. Stepwise regression selected genes in the MCI group | 102 |

Figure 15. Stepwise regression selected genes in the DEM group..... 105

LIST OF ABBREVIATIONS

| | |
|--------------|---|
| 1.5T/3T | 1.5 or 3 Tesla |
| 3R/4R | 3 or 4 repeat (microtubule binding regions of tau) |
| χ^2 | Chi-squared value |
| A/T/N | Amyloid/Tau/Neurodegeneration |
| <i>ABCA7</i> | ATP Binding Cassette Subfamily A Member 7 |
| AChEI | Acetyl Cholinesterase Inhibitor |
| AD | Alzheimer's disease |
| ADNI | Alzheimer's Disease Neuroimaging Initiative |
| ADRDA | Alzheimer's disease and Related Disorders Association |
| AIC | Akaike information criterion |
| ANOVA | Analysis of variance |
| <i>APOE</i> | Apolipoprotein E |
| <i>APP</i> | Amyloid Beta Precursor Protein |
| AV-1451 | Flortaucipir |
| AV-45 | Florbetapir |
| A β | Amyloid beta |
| BACE | Beta-secretase |
| <i>BIN1</i> | Bridging Integrator 1 |
| bvFTD | behavior variant Frontotemporal Dementia |
| <i>CASS4</i> | Cas Scaffold Protein Family Member 4 |
| <i>CD2AP</i> | CD2 Associated Protein |
| <i>CD33</i> | CD33 Molecule |

| | |
|---------------|---|
| CDR | Clinical Dementia Rating |
| <i>CELF1</i> | CUGBP Elav-Like Family Member 1 |
| CERAD | Consortium to Establish ad Registry for Alzheimer's Disease |
| <i>CLU</i> | Clusterin |
| <i>CR1</i> | Complement C3b/C4b Receptor 1 |
| CSF | Cerebrospinal fluid |
| DEM | Dementia |
| <i>DSG2</i> | Desmoglein 2 |
| EOAD | Early-onset Alzheimer's disease |
| <i>EPHA1</i> | EPH Receptor A1 |
| eTIV | estimated Total Intracranial Volume |
| FDA | Food and drug administration |
| FDG | Fludeoxyglucose |
| FDR | False discovery rate |
| <i>FERMT2</i> | Fermitin Family Member 2 |
| FTLD | Frontotemporal lobar degeneration |
| FWE | Family-wise error |
| FWHM | Full width at half maximum |
| GM | Gray matter |
| GMD | Gray matter density |
| GTPase | A family of Guanosin triphosphate hydrolase enzymes |
| GWAS | Genome-wide association study |
| HS | Hippocampal sclerosis |

| | |
|---------------|---|
| HWE | Hardy-Weinberg Equilibrium |
| ICV | Intracranial volume |
| <i>INPP5D</i> | Inositol Polyphosphate-5-Phosphatase D |
| k | Cluster size (in voxels) |
| LATE | Limbic-predominant age-related TPD-43 encephalopathy |
| LD | Linkage disequilibrium |
| LEADS | Longitudinal Early-onset Alzheimer's disease study |
| LOAD | Late-onset Alzheimer's disease |
| <i>MAPT</i> | Microtubule Associated Protein Tau |
| MCI | Mild cognitive impairment |
| <i>MEF2C</i> | Myocyte Enhancer Factor 2C |
| mm | millimeter |
| MMSE | Mini-Mental State Examination |
| MNI | Montreal Neurological Institute |
| MRI | Magnetic Resonance Imaging |
| <i>MS4A6A</i> | Membrane Spanning 4-Domains A6A |
| MTL | Medial temporal lobe |
| NC/CN | Cognitively normal |
| NFT | Neurofibrillary tangles |
| NIA-AA | National Institute of Aging - Alzheimer's Association |
| NiftI | Neuroimaging Informatics Technology Initiative file format |
| NINCDS | National Institute of Neurological and Communicative Disorders and Stroke |

| | |
|---------------------|--|
| NMDA | N-Methyl-d-aspartic acid |
| <i>NME8</i> | NME/NM23 Family Member 8 |
| nonAD | Amyloid negative - non Alzheimer's disease |
| PART | Primary Age-Related Tauopathy |
| PCC | Posterior cingulate cortex |
| PET | Positron emission tomography |
| PHF | Paired helical filaments |
| <i>PICALM</i> | Phosphatidylinositol Binding Clathrin Assembly Protein |
| <i>PSEN1</i> | Presenilin 1 |
| <i>PSEN2</i> | Presenilin 2 |
| <i>PTK2B</i> | Protein Tyrosine Kinase 2 Beta |
| PVC | Partial volume correction |
| R ² | Coefficient of determination |
| RAB31 | Member RAS Oncogene Family 31 |
| RAB5B | Member RAS Oncogene Family 5B |
| ROI | Region of interest |
| SAS | Statistical Analysis Software |
| SE | Standard error |
| <i>SLC24A4/RIN3</i> | Solute Carrier Family 24 Member 4/Ras and Rab Interactor 3 |
| SNP/snp | Single-nucleotide polymorphism |
| <i>SORL1</i> | Sortilin Related Receptor 1 |
| SPECT | Single Photon Emission Computed Tomography |
| SPM 8/12 | Statistical parametric mapping version 8/12 |

| | |
|---------------|--|
| SPSS | Statistical Package for the Social Sciences |
| SUVR | Standardized uptake value ratio |
| TDP43 | TAR DNA Binding Protein 43 |
| VBM | Voxel-based morphometry |
| WM | White matter |
| <i>ZCWPW1</i> | Zinc Finger CW-Type and PWWP Domain Containing 1 |

Chapter 1. Background and Justification

Alzheimer's disease (AD) is the most common cause of dementia in the United States, currently affecting an estimated 5.8 million Americans, including as much as 10 percent of the U.S. population over the age of 65 ¹. The financial burden of dementia in 2019 on both caregivers and patients is estimated to be a staggering 290 billion dollars, underscoring the dire need for viable treatment options ². However, recent drug failures have highlighted how much is still unknown about AD ³⁻¹⁸. What we do know is that a solution or cure for AD will likely require the continued research of the clinical, pathological, genetic and environmental factors that contribute to the underlying disease.

1.1. Alzheimer's Pathology:

It's been 113 years since Alois Alzheimer published his landmark paper "Über eine eigenartige Erkrankung der Hirnrinde", a case description of a 55-year-old German woman with an early age of dementia onset ¹⁹. Upon autopsy, Alzheimer took note of peculiar dense bundles of neurofibrils and "miliar foci" throughout the cortex, what we now know as neurofibrillary tangles (NFTs) and amyloid-beta (A β) plaques ¹⁹. Though our techniques have become slightly more sophisticated, these pathological hallmarks of Alzheimer's disease (the name was aptly given by the German psychologist, Emil Kraepelin) remain central to the diagnosis.

Senile or neuritic plaque deposition follows a distinct distribution in AD described by Braak and Braak in 1991, following three stages, first appearing in

basal frontal, temporal and occipital cortex, then in isocortical association areas and finally depositing in primary isocortical areas^{20,21}. Though these plaques are associated with several abnormal components of the neuronal environment (including an abundance of microglia and astrocytes as well as paired helical filaments, PHFs), their primary core is the result of the accumulation of insoluble A β (largely A β 42, A β 40 to a lesser extent). A β 40 and A β 42 are released at the synapses of neurons after the proteolytic cleavage of amyloid precursor protein (APP) by β -secretase (BACE) and γ -secretase²². The accumulation of insoluble amyloid monomers into oligomers and plaques eventually leads to disruption of signaling at the synapses of cortical neurons, though it does not correlate temporally with cognitive decline²³. Abnormal amyloid accumulation can precede cognitive symptoms by as much as 20 years and seems to plateau in early disease stages, making it an attractive candidate for early detection of disease pathological changes²⁴⁻²⁶.

The second pathological hallmark of AD, intracellular NFTs, are largely composed of PHFs which consist of hyperphosphorylated tau, a microtubule-associated protein that loses its ability to stabilize the microtubule conformation when abnormally phosphorylated²⁷. In human brains, there are six isoforms of tau generated through alternative splicing of exons 2, 3 and 10 in the microtubule-associated protein tau or *MAPT* gene. These six isoforms are typically categorized as either three or four repeat (3R or 4R, respectively), depending on whether they contain three or four carboxy-terminal repeat domains²⁸. Tauopathies (neurodegenerative diseases involving the buildup of

tau protein) are often classified as **3R** (Pick's disease and some frontotemporal lobar degeneration *MAPT* mutations), **4R** (progressive supranuclear palsy, corticobasal degeneration, globular glial tauopathies, argyrophilic grain disease and some frontotemporal lobar degeneration *MAPT* mutations) or **3R+4R** (Alzheimer's disease (sometimes referred to as a secondary tauopathy), primary age-related tauopathy and frontotemporal lobar degeneration *MAPT* mutations) depending on the isoforms that make up the PHFs ²⁸. As with amyloid plaques, NFTs often follow a distinct pattern of deposition in AD, first restricted to the entorhinal cortex and hippocampus, then to limbic regions, and finally largely spanning isocortical regions ^{21,29}. However, contrary to amyloid, NFTs correlate well with the onset of clinical symptoms and severity of AD, which has prompted many to posit that targeting abnormal tau accumulation may be the most attractive target to stop or slow neurodegeneration ^{21,30,31}.

The combination of these pathologies may lead to downstream neuronal and synaptic loss, which can be seen as gross cortical atrophy, though the exact mechanisms to how this occurs are not well understood. The neuropathological criteria for AD are dependent on an "ABC" score that is a summary of A. A β /amyloid plaque Thal phase score, B. NFT Braak score and C. Neuritic plaque Consortium to Establish a Registry for Alzheimer's Disease (CERAD) score ³². The final score is determined to be either "Not", "Low", "Intermediate", or "High" degree of AD neuropathologic change.

1.2. Clinical Considerations for Alzheimer's disease:

In 1984, a special National Institute of Neurological and Communicative Disorders and Stroke and Alzheimer's Disease and Related Disorders (NINCDS-ADRDA) workgroup met to discuss what were the original clinical guidelines for dementia due to Alzheimer's disease ³³. Twenty-seven years later a similar meeting took place with several key additions to the original criteria ³⁴. First is the consideration of AD as a continuum, a slowly progressing disease with measurable stages that can be somewhat defined. The workgroup was divided into three separate groups to recognize the three stages of the disease process. Those stages are the asymptomatic or preclinical stage, the prodromal or mild cognitive impairment (MCI) stage and finally the AD dementia stage (which was the sole focus of the previous workgroup in 1984). The second major addition to the diagnostic criteria is the recognition of biomarkers as a useful tool for clinicians. The biomarkers considered are restricted to two categories indicative of AD pathophysiology 1) biomarkers of A β accumulation (abnormally high cortical retention of amyloid tracer as measured with positron emission tomography (PET) neuroimaging and/or low CSF A β 42) and 2) biomarkers of neuronal degeneration or injury (abnormally high CSF tau, decreased fluorodeoxyglucose (FDG) PET uptake in the posterior cingulate gyrus or evidence of mesial temporal lobe atrophy on structural imaging) (more information on these biomarkers on pages 6 and 7) ^{34,35}.

The core clinical criteria for dementia are severe functional impairment and decline of activities of daily living which cannot be explained by delirium or

another major psychiatric disorder^{35,36}. The impairment must be present in at least two cognitive domains from the list of memory, reasoning/handling of complex tasks, visuospatial, language or behavioral domains. Probable AD dementia patients have an insidious onset of dementia with a gradual worsening of cognition whose most prominent symptoms are either amnesic (by far the most common presentation) or nonamnesic (affecting language, visuospatial or executive function with relative sparing of memory function). This is a critical distinction from the previous criteria, which neglected the less common nonamnesic presenting AD dementias such as posterior cortical atrophy (PCA), logopenic primary progressive aphasia (PPA) and behavior variant AD. As with the other stages, a crucial step involves ruling out other neurologic, psychiatric or general medical disorders that may impact cognition. For the dementia stage, biomarkers are used to lend additional support to the clinical diagnosis of AD dementia.

Since the 1984 inception of the diagnostic criteria, MCI has emerged as a legitimate clinical entity, though the diagnostic group remains largely heterogeneous in terms of pathological burden and/or etiology. One of the key distinguishing factors between MCI and dementia is that MCI subjects, while cognitively impaired, generally maintain the independence of their day-to-day functional abilities. One of the main goals of the diagnostic criteria of 2011 was to help identify MCI who have cognitive symptoms most likely due to underlying AD pathology³⁷. This determination is largely done, as within the dementia stage, by ruling out other likely systemic or brain diseases potentially responsible for

cognitive decline, such as vascular, Lewy body dementia, traumatic brain injury, hormonal disorders, etc. Additional support may be given by the presence of a genetic mutation known to increase risk, such as those seen in mendelian forms of AD or *APOE* e4 allele carriers. The role of biomarkers in the MCI stage is to detect evidence of AD pathology to support the diagnosis.

The preclinical stage of AD is considered still a research entity (i.e. not a clinical diagnosis) and is defined by normal cognition with evidence of Alzheimer's pathology³⁸. As mentioned previously, Alzheimer's pathophysiological changes can begin as early as 20 years before cognitive symptoms arise, making the preclinical or asymptomatic stage the most attractive target to slow or even stop the progression of AD. The caveat, of course, is finding specific and sensitive biomarkers to correctly identify these preclinical subjects.

What is currently known about AD biomarkers is that they are dynamic throughout the disease progression and start first with measurable changes in amyloid²⁶. This is first detectable through a reduction in CSF A β 42 as more amyloid is sequestered into plaques (i.e. fewer free-floating A β 42), followed by retention of cortical amyloid PET tracers. Amyloid typically reaches its peak near or just after cognitive symptoms are detectable, which is likely why amyloid does not correlate tightly with cognitive decline. Amyloid PET tracers have been available since 2004 and currently there are three tracers which are FDA approved, [¹⁸F]Flortbetapir, [¹⁸F]Florbetaben and [¹⁸F]Flutemetamol, all which bind aggregated fibrillar forms of A β ³⁹. The advent of tau PET tracers adds an

additional detectable biomarker. Brain tau levels become abnormal sometime between amyloid accumulation and when CSF tau levels increase (as a result of cell death and subsequent release of intracellular tau into CSF). Current understanding how of tau PET uptake correlates to *postmortem* data is limited, though early results indicate that the most widely used tracer, [¹⁸F]Flortaucipir, provides an accurate *in vivo* measure of 3 and 4 repeat NFT pathology^{39,40}. As mentioned above, the abnormal accumulation of hyperphosphorylated tau into NFTs more closely correlates with cognitive symptoms than amyloidosis. Finally, biomarkers of neuronal degeneration, such as raised CSF tau levels, reduction in FDG PET uptake in the posterior cingulate and mesial temporal hippocampal atrophy on structural imaging, are the final biomarkers to become abnormal before the beginning of cognitive decline. FDG PET is used as an indirect measure of synapse loss, reflected by lower cellular intake of the tracer (also referred to as hypometabolism), whereas structural MR imaging provides excellent white/gray matter contrast that is crucial for tissue volumetric and thickness determinations. While both of these measures are nonspecific to a disease process, specific spatial changes may indicate potential etiologies³⁹.

A recent addition to the National Institute on Aging and Alzheimer's Association (NIA-AA) clinical diagnostic criteria utilizes the known *in vivo* fluid and imaging biomarkers to define an AD classification research framework^{34,36,37,41}. Biomarkers are divided into three categories according to their hypothetical dynamic progression, amyloid (A), tau (T) and neurodegeneration (N), with a classifying positive (+) or negative (-) added, and the "+" designation

indicating that the abnormal threshold for a category has been crossed ⁴¹. In this framework, amyloid-positive (A+) patients would fall within the Alzheimer's continuum regardless of the other biomarkers. The assumption made is that A+/T+/N+, A+/T+/N- or A+/T-/N- subjects are simply at various stages in the disease process. Those who are A- are either considered normal (if T and N are negative) or have a non-AD pathologic change if there is abnormal tau and/or neurodegeneration ⁴¹. The driving etiology behind non-AD pathologic change in AD phenocopies (clinically diagnosed AD without evidence of AD pathophysiology) is unknown, though they are likely a very heterogeneous group of pathologies (e.g., vascular, Lewy body, argyrophilic grain disease, frontotemporal dementia, hippocampal sclerosis, etc). This is explored further in Chapter 2, where I investigate the ATN changes in across the prodromal-dementia spectrum and discuss the presumed etiologies hypothesized from the observed tau and neurodegenerative patterns in amyloid-negative AD phenocopies or non-AD subjects.

An additional clinical consideration is the age of symptom onset, which can, among other things, drastically impact the severity and speed of disease course ⁴²⁻⁴⁶. An estimated 97% of all Alzheimer's cases occur in the elderly population (65 and older, late-onset or LO), making age the single biggest risk factor for AD ². However, among the 3% of AD with symptom onset before 65, termed early-onset (EO), a vast majority are sporadic in origin ^{41,42}. EOAD presents several challenges to families and clinicians, not the least of which is the devastating effects it can have on adults who are still essential financial

earners for their families. From a clinical perspective, EOAD patients often have greater cognitive impairment, decline faster and are significantly more likely to have a nonamnestic presentation than LOAD ⁴²⁻⁴⁷. The pathology echoes these differences between EO and LOAD, as EOAD typically present with far greater neuritic plaque and NFT burden ⁴⁸⁻⁵². More recently, imaging biomarkers of AD have been used to recapitulate the pathological findings and show that in general, EOAD patients have a far greater tau burden as well as greater hypometabolism and atrophy ⁵³⁻⁶¹. The driving factor for this is likely a multitude of reasons. At a surface level, rational arguments can be made that cognitive reserve, which in general is greater at younger ages, may require even greater pathologic burden to achieve the same level of cognitive deficit as in older patients. This means that a pathological comparison of relatively equally impaired EO to LOAD subjects would result in greater burden seen in the EO subjects. At a deeper level, why this pathology occurs at such a young age and to such a great extent is unknown, though it likely has strong genetic and environmental components. Currently, ongoing longitudinal observational studies, like the Longitudinal Early-Onset Alzheimer's Disease Study or LEADS, the first large multisite early-onset study of its kind, are using clinical and neuropsychological testing, neuroimaging, fluid biomarkers and genetics to attempt to answer some of these questions. In chapter 2, as mentioned above, I present a neuroimaging study of Alzheimer's vs non-AD pathologic changes, which includes further dividing subjects by age of onset. For this analysis, I subdivided AD groups into

EOAD and LOAD, while subdividing the non-AD groups into EOnonAD and LOnonAD.

1.3. Genetics of Alzheimer's disease:

AD has long been known to have a genetic component that was first identified in the small percentage of AD patients with dominantly inherited mutations, termed familial early-onset AD or Mendelian AD. Patients with familial AD have mutations in one of three genes directly impacting amyloid production. The first gene is *APP*, which encodes a 770 amino acid transmembrane protein containing sites for several nonsynonymous mutations that increase the release of A β ⁶²⁻⁶⁵. The remaining two genes, presenilin 1 (*PSEN1*) and presenilin 2 (*PSEN2*) encode proteins that are central to the function of the γ -secretase complex ^{66,67}. Mutations found in these genes are believed to result in increased production of A β 42, which is less soluble than other A β species (a full list of known mutations in *APP*, *PSEN1* and *PSEN2* can be found at <https://www.alzforum.org/mutations>) ⁶⁸⁻⁷².

In contrast to familial AD, sporadic AD is likely due to a combination of both genetic and environmental factors ². Over the last two decades, significant strides have been made towards better understanding the genetic risk factors contributing to this more genetically complex form, which has an estimated heritability of 70-80% ^{69,70}. Before the advent of large genome-wide association studies (GWAS), the apolipoprotein E (*APOE*) gene was the only highly accepted risk gene for sporadic AD. This is because *APOE* has a large, dose-dependent risk (one copy of the e4 allele triples AD risk while two copies increase risk by 15)

⁷³. The impact of *APOE* e4 is so great that it has been called a moderately penetrant gene with semi-dominant inheritance ⁷⁴. It is important to note, though, that carrying a copy of the e4 allele is not determinate nor is sufficiently causative of Alzheimer's disease. It is also noteworthy that *APOE* explains less than half of the overall genetic risk for sporadic AD, which was not understood until the last decade, when GWAS became available.

In an attempt to identify the remaining genetic risk, large-scale GWAS and meta-analysis of GWAS have identified genome-wide significant variants near over 20 genes ⁷⁵⁻⁸⁰. Each of the discovered alleles contributes to only a small amount of risk, leading some to hypothesize that these genes may have an additive or synergistic effect when multiple risk variants are inherited together. Additionally, understanding the biological roles of the risk genes, regardless of whether or not they are considered to have direct functional consequences, is imperative to a better overall biological understanding of AD. It is currently known that several risk genes are involved in pathways believed to be dysfunctional during the progression of AD, such as cholesterol metabolism (*ABCA7*, *APOE*, *CLU*, *SORL1*), immune response (*ABCA7*, *CR1*, *CD33*, *CLU*, *EPHA1*, *MS4A6A*) and endocytosis (*BIN1*, *CD2AP*, *EPHA1*, *PICALM*, *SORL1*) ⁸¹. Loci identified more recently are still being attributed to a dysfunctional Alzheimer's process, though early work suggests potential consequences for *CASS4*(tau metabolism), *CELF1*(cytoskeleton/axon development), *DSG2*(cytoskeleton/axon development), *FERMT2*(tau metabolism), *INPP5D*(*APP* metabolism), *MEF2C*(endocytosis), *NME8*(cytoskeleton/axon development),

PTK2B(endocytosis), *SLC24A4/RIN3*(cholesterol/endocytosis) and *ZCWPW1*(epigenetics).

One strategy used to associate gene to function is imaging genetics, which utilizes specific Alzheimer's phenotypes. This strategy has a distinct advantage over traditional gene to clinical diagnosis studies because imaging phenotypes are closer to biological changes due to genetics and remove much of the unwanted biomarker variation found with clinical Alzheimer's disease. In chapters 3 and 4, I use imaging genetics to test associations between identified GWAS risk genes with a temporoparietal tau PET region of interest, posterior cingulate FDG PET SUVR and medial temporal lobe thickness. Beyond testing for associations with genes across the full A/T/N biomarker spectrum, I investigate stage-specific genetic associations among cognitively normal (CN), mildly impaired (MCI) and subjects who have dementia (DEM). This additional stage-stratified analysis was direct extension of my previous work on the associations of the top AD genetic hits with brain amyloidosis (reviewed in greater detail in Chapter 3). Identifying variants associated with Alzheimer's pathophysiological changes in the preclinical and prodromal stages may provide critical insight to previously unknown disease mechanisms, which could ultimately lead to the discovery of new therapeutic targets.

1.4. Statement of Purpose:

In general, the goals of this work were to use imaging biomarkers of AD to better understand the driving factors of the heterogeneity of clinically diagnosed AD in

regard to age of disease onset, biomarker abnormalities and genetic risk. More specifically, this work aimed to:

1. Use imaging biomarkers of amyloid, tau and neurodegeneration to identify and both qualitatively and quantitatively characterize the differences between early vs. late and amyloid-positive vs. amyloid-negative clinically diagnosed Alzheimer's subjects.
2. Use imaging genetics to identify the genome-wide significant AD variants associated with neurodegeneration (FDG PET and MRI) and NFTs (tau PET).

Chapter 2. Neurodegenerative Changes in Early & Late-Onset Cognitive Impairment with and without Brain Amyloidosis

2.1. Introduction:

An estimated 5.8 million people in the United States are currently diagnosed with Alzheimer's disease (AD) ². Even when rendered by dementia experts, the clinical diagnosis of AD shows only modest accuracy ⁸². Twenty-nine to 56% of clinically diagnosed AD patients are AD phenocopies that fail to show AD pathology upon postmortem examination ⁸². With the development of amyloid tracers for positron emission tomography (PET) we can now readily distinguish the true AD cases from the amyloid-negative AD phenocopies (nonAD).

Ninety-seven percent of all AD cases have symptom onset at the age of 65 or older and are classified as "late-onset" (LO), while the remaining 3% have symptom onset before the age of 65 and are termed "early-onset" (EO) ^{2,83,84}. Pathologically, patients who are younger at disease onset show greater pathological burden ⁴⁸⁻⁵². Magnetic resonance imaging (MRI), [¹⁸F]Fluorodeoxyglucose (FDG) PET and [¹⁸F]Flortaucipir PET (tau PET) studies have shown that EO Alzheimer's subjects (EOAD) have more extensive atrophy, hypometabolism and tau burden compared to LO Alzheimer's subjects (LOAD) ⁵³⁻⁵⁷. The more advanced pathologic burden in EOAD has been associated with more aggressive clinical course and is more likely to have an atypical presentation ⁴²⁻⁴⁵. To date the imaging biomarker profiles of early-onset nonAD (EOnonAD) have not been studied.

The Alzheimer's Disease Neuroimaging Initiative (ADNI) is a multisite, longitudinal study that collects standardized imaging, genetic, clinical, and fluid biomarkers from clinically diagnosed amnesic mild cognitive impairment (MCI), clinically diagnosed Alzheimer's dementia (DEM) and cognitively normal (CN) control subjects as a part of a global research effort to better understand LOAD. While the majority of ADNI subjects are older than 65 years, ADNI contains a sizeable cohort of amnesic EO MCI or dementia subjects (age of symptom onset <65 years). The addition of amyloid imaging in the ADNI-GO/2 funding stages allowed researchers to ascertain the amyloid PET status of all ADNI participants and provided researchers the opportunity to study the biomarker-validated AD and non-AD phenocopies in greater detail.

In this study, my aim was to ascertain the extent and severity of tau and neurodegenerative pathology measured with tau PET, FDG PET and MRI in EO and LO ADNI cohorts stratified by amyloid status as follows: EOAD MCI and DEM (EOAD_{MCI}; EOAD_{DEM}), EOnonAD MCI and DEM (EOnonAD_{MCI}; EOnonAD_{DEM}), LOAD MCI and DEM (LOAD_{MCI}; LOAD_{DEM}) and LOnonAD MCI and DEM (LOnonAD_{MCI}; LOnonAD_{DEM}). I hypothesized that EOAD and EOnonAD subjects would have more severe neurodegeneration and greater tau burden relative to their LO counterparts, indicative of the greater disease burden likely required to have equivalent impairment to the significantly older LO group. I also hypothesized that nonAD cases would have a nonAD-like pattern of neurodegeneration.

2.2. Methods:

Subjects

Data used in the preparation of this article were obtained from the ADNI database (adni.loni.usc.edu). ADNI was launched in 2003 as a public-private partnership, led by Principal Investigator Michael W. Weiner, MD. The primary goal of ADNI has been to test whether serial MRI, PET, other biological markers, and clinical and neuropsychological assessments can be combined to accurately measure and predict the progression of MCI and Alzheimer's dementia. ADNI has undergone three complete funding cycles to date: ADNI1, ADNI-GO and ADNI2 and is now in the ADNI3 cycle. ADNI-GO, ADNI2 and ADNI3 included [¹⁸F]Florbetapir amyloid PET imaging.

The clinical and biomarker characteristics of the ADNI cohort have been previously published ⁸⁵. ADNI has enrolled clinically diagnosed CN, amnesic MCI and amnesic DEM subjects. Probable AD DEM diagnosis is based on the National Institute of Neurological and Communicative Disorders and Stroke and the AD and Related Disorders Association (NINCDS-ADRDA) criteria ³³. Probable AD DEM subjects were 56 to 90 years old at enrollment, scored between 20 and 26 on the Mini-Mental State Examination (MMSE) ⁸⁶ and 0.5–1 on the Clinical Dementia Rating (CDR) global score ⁸⁷. Subjects diagnosed as amnesic MCI ranged from 55 to 91 years old at enrollment, had no significant functional impairment, scored between 24 and 30 on the MMSE, had a global CDR of 0.5 (memory score \geq 0.5), and impairment on Wechsler Memory Scale – Logical Memory II test ⁸⁸. CN subjects had MMSE between 24 and 30, a global

CDR of 0 and did not meet criteria for MCI or DEM. Subjects were excluded due to inability to undergo MRI or if they had other neurological disorders, active depression, or history of psychiatric diagnosis, alcohol, or substance dependence within the past 2 years, less than 6 years of education or were not fluent in English or Spanish. The full list of inclusion/exclusion criteria may be accessed in the online ADNI protocol (<http://www.adni-info.org/Scientists/ADNIStudyProcedures.html>). Written informed consent was obtained from all participants and the institutional review board (IRB) at all ADNI sites have reviewed and approved ADNI data collection protocol.

For my analysis, I used 231 EO subjects with reported age of symptom onset ≤ 65 years from the ADNI database with available [^{18}F]Florbetapir amyloid PET or CSF A β data (219 of the 231 received [^{18}F]Florbetapir PET, the remaining 12 had CSF A β data). One hundred seventy-three EO subjects met criteria for MCI; 58 for DEM. 60 MCI and 50 DEM were amyloid-positive (EOAD_{MCI} and EOAD_{DEM}) and 113 and 8, respectively, were amyloid-negative (EOnonAD_{MCI} and EOnonAD_{DEM}) based on previously validated [^{18}F]Florbetapir global means standard uptake volume ratio (SUVR) cut-off of 1.17⁸⁹ or a CSF A β_{1-42} level < 192 pg/ml⁹⁰. The subset with tau PET, [^{18}F]Flortaucipir, included 10 EOAD_{MCI}, 7 EOAD_{DEM}, 38 EOnonAD_{MCI} and 3 EOnonAD_{DEM}.

LO subjects included had either [^{18}F]Florbetapir amyloid PET (488/539 subjects) or CSF A β data (51/539 subjects), and all had FDG PET and MR imaging. Special care was taken to ensure that no LO diagnostic group was significantly more or less cognitively impaired than their EO counterpart

(measured by MMSE) by removing outlier subjects, resulting in 539 subjects. Three hundred sixty-seven met criteria for MCI and 172 for DEM. Two hundred sixteen LO MCI and 148 LO DEM were amyloid-positive ($LOAD_{MCI}$ and $LOAD_{DEM}$), while 151 LO MCI and 24 LO DEM were amyloid-negative ($LONonAD_{MCI}$; $LONonAD_{DEM}$). The subset with tau PET included 53 $LOAD_{MCI}$, 27 $LOAD_{DEM}$, 51 $LONonAD_{MCI}$ and 2 $LONonAD_{DEM}$. Due to the low numbers of EO and LO nonAD_{DEM} subjects with [¹⁸F]Flortaucipir scans (3 and 2, respectively) they were grouped together with the EO and LO nonAD_{MCI}, resulting in 41 EOnonAD and 53 LOnonAD subjects in the tau comparisons.

Since EO and LO groups cannot be directly compared because neurodegenerative changes associated with aging could inadvertently confound the results, I conducted two sets of analyses. I first compared each EO and LO group to the same CN comparison group comprised of the 291 amyloid-negative ($SUVR < 1.17$) CN subjects within the age range of 55 to 90 years old. This comparison allowed for a straightforward interpretation of the effect sizes as a measure of disease impact. Next, I repeated the analyses comparing the LO and EO groups to only the older ($N=146$) and younger half ($N=145$) of CN, respectively.

MRI and PET acquisition and analyses

ADNI MRI and PET acquisition and preprocessing protocols can be found at www.adni-info.org. The MRI data acquisition and preprocessing have been previously described elsewhere³³. I downloaded preprocessed MRI data from LONI IDA (<https://ida.loni.usc.edu>). Scans were spatially warped to Montreal

Neurological Institute (MNI) space and segmented into gray matter (GM), white matter, and CSF components using voxel-based morphometry (VBM) in Statistical Parametric Mapping version 12 (SPM12), as described previously⁹¹. GM maps were normalized and smoothed using 10 mm full-width half maximum (FWHM) Gaussian kernel, which yielded gray matter density (GMD) data. Intracranial volume (ICV) was also calculated using FreeSurfer version 5.1.

PET scanners across sites were held to rigorous qualifications, calibration, and normalization standards as described in detail elsewhere⁸⁷. I downloaded preprocessed amyloid, FDG PET and tau PET data from LONI IDA (<https://ida.loni.usc.edu>). The scans were already averaged, aligned to standard space, re-sampled to a standard image and voxel size (2mm × 2mm × 2mm), and smoothed to a uniform resolution as previously described⁹². I aligned the images to the corresponding MRI scan from the same visit and normalized them to MNI space using parameters obtained from the MRI segmentation using SPM12. PET scans were intensity normalized to mean pons uptake for FDG, whole cerebellum for amyloid and cerebellar crus for tau PET, resulting in whole brain SUVR images as previously described^{93,94}. To assign subjects into groups by amyloid status, I used an amyloid PET cutoff of SUVR ≥ 1.17 or CSF A β ₁₋₄₂ level < 192 pg/ml^{89,90}.

Statistical Analyses

Clinical and Demographic Analyses:

The statistical distribution of clinical and demographic characteristics (age, education, global CDR, MMSE, and amyloid PET mean global SUVR) were

analyzed in SPSS version 24.2 using one-way ANOVA. ANOVA p-values are listed in the tables and Bonferroni-corrected multiple comparisons p-values are listed in the results text. *APOE4* genotype and sex frequency comparisons were done using a chi-square test with two-sided p-values. The alpha value for all comparisons was $p < 0.05$.

Parametric Mapping:

I used voxel-wise linear regression models in SPM12 to study the extent and severity of neurodegeneration and tau burden in EO and LO AD and nonAD groups relative to CN while controlling for age, sex and education. Additionally, in the MRI analyses, I covaried for MRI field strength (1.5T vs. 3T) and ICV. Family-wise error (FWE) cluster-level correction was applied to correct for multiple comparisons with a significance threshold of $p < 0.01$. Because side-by-side interpretation of significance maps generated with unequal sample sizes can be misleading, I also derived β -coefficient maps to demonstrate the effect sizes in each comparison, which are visualized using the MRICrogl version 2.1 software.

2.3. Results:

AD analyses

Demographic comparisons:

The demographic, neuropsychological, and amyloid burden comparisons of the amyloid positive diagnostic groups relative to CN are shown in **Table 1**. The CN were significantly older than the EO and significantly younger than the

LO subjects ($p < 0.001$, both). The CN subjects had significantly fewer *APOE4* carriers compared to all other groups ($p < 0.001$, all). The age and *APOE4* effects remained when the data were split into younger and older subgroups (**Table 2**).

As expected, the EOAD_{MCI} and EOAD_{DEM} subjects were significantly younger compared to the LOAD_{MCI} and LOAD_{DEM} groups ($p < 0.001$, **Table 3**, top). Compared to EOAD_{MCI}, LOAD_{MCI} had significantly fewer years of education ($p = 0.021$). The EOAD_{DEM} and LOAD_{DEM} groups showed similar education. Both EOAD groups had a significantly higher percentage of *APOE e4* homozygotes compared to LOAD subjects (MCI $p = 0.004$, DEM $p = 0.022$). There were no significant differences in global [¹⁸F]Florbetapir SUVR, global CDR or MMSE between the EO and LOAD groups.

Regional amyloid comparisons between the AD subjects showed a significant difference ($p = 0.044$) in parietal cortices and significant ($p = 0.048$) difference in temporal amyloid SUVR between EOAD_{MCI} and EOAD_{DEM} (**Table 4**).

Table 1. EOAD and LOAD demographic comparisons to CN. The comparisons were done using ANOVA and chi-square tests with two-sided p-values. The Bonferroni-corrected pairwise differences are discussed in the Results section. Significant p-values (<0.05) are bolded.

*Significantly different than CN group at p<0.05

**Significantly different than CN group at p<0.01

***Significantly different than CN group at p<0.001

| Variable | CN (N=291) | EOAD _{MCI} (N=60) | EOAD _{DEM} (N=50) | p-value | LOAD _{MCI} (N=216) | LOAD _{DEM} (N=148) | p-value |
|--|----------------|-------------------------------|-------------------------------|------------------|--------------------------------|--------------------------------|------------------|
| Age, years, Mean (SD) | 74.3 (6.4) | 65.4 (6.0)*** | 64.7 (6.3)*** | <0.001 | 76.4 (5.8)*** | 78.3 (5.9)*** | <0.001 |
| Sex, Male % | 52.2 | 46.7 | 44.0 | 0.461 | 60.2 | 58.8 | 0.174 |
| Education, years, Mean (SD) | 16.7 (2.6) | 16.7 (2.8) | 15.6 (2.4)** | 0.022 | 15.8 (2.8)*** | 15.4 (3.0)*** | <0.001 |
| % APOE e4, 0/1/2 alleles | 77/22/1 | 18/52/30*** | 26/38/36*** | <0.001 | 34/52/14*** | 26/56/18*** | <0.001 |
| Global CDR, Mean (SD) | 0.02 (0.09) | 0.50 (0.00)*** | 0.87 (0.33)*** | <0.001 | 0.50 (0.16)*** | 0.84 (0.36)*** | <0.001 |
| MMSE, Mean (SD) | 29.0 (1.3) | 27.8 (1.8)*** | 22.5 (3.3)*** | <0.001 | 27.4 (1.9)*** | 23.0 (2.8)*** | <0.001 |
| Global Cortical [¹⁸ F]Florbet apir SUVR, Mean (SD) | 1.03 (0.06) | 1.41 (0.15)*** | 1.48 (0.13)*** | <0.001 | 1.43 (0.17)*** | 1.47 (0.16)*** | <0.001 |
| Tau Scans, N | 126 | 10 | 7 | N/A | 53 | 27 | N/A |

Table 2. EOAD and LOAD demographic comparisons to the young and old CN groups, resp. The comparisons were done using ANOVA and chi-square tests with two-sided p-values. The Bonferroni-corrected pairwise differences are discussed in the Results section. Significant p-values (<0.05) are bolded.

*Significantly different than CN group at p<0.05

**Significantly different than CN group at p<0.01

***Significantly different than CN group at p<0.001

| Variable | Young CN (N=145) | EOAD _{MCI} (N=60) | EOAD _{DEM} (N=50) | p-value | Old CN (N=146) | LOAD _{MCI} (N=216) | LOAD _{DEM} (N=148) | p-value |
|---|------------------|----------------------------|----------------------------|------------------|----------------|-----------------------------|-----------------------------|------------------|
| Age, years, Mean (SD) | 69.1 (3.3) | 65.4 (6.0)*** | 64.7 (6.3)*** | <0.001 | 79.4 (4.3) | 76.4 (5.8)*** | 78.3 (5.9) | <0.001 |
| Sex, Male % | 50.3 | 46.7 | 44.0 | 0.713 | 54.1 | 60.2 | 58.8 | 0.505 |
| Education, years, Mean (SD) | 16.7 (2.5) | 16.7 (2.8) | 15.6 (2.4)** | 0.027 | 16.7 (2.7) | 15.8 (2.8)** | 15.4 (3.0)*** | <0.001 |
| % APOE ε4, 0/1/2 alleles | 74/25/1 | 18/52/30*** | 26/38/36*** | <0.001 | 80/18/2 | 34/52/14*** | 26/56/18*** | <0.001 |
| Global CDR, Mean (SD) | 0.02 (0.10) | 0.50 (0.00)*** | 0.87 (0.33)*** | <0.001 | 0.01 (0.07) | 0.50 (0.16)*** | 0.84 (0.36)*** | <0.001 |
| MMSE, Mean (SD) | 29.1 (1.1) | 27.8 (1.8)*** | 22.5 (3.3)*** | <0.001 | 28.8 (1.4) | 27.4 (1.9)*** | 23.0 (2.8)*** | <0.001 |
| Global Cortical [¹⁸ F]Florbetapir SUVR, Mean (SD) | 1.04 (0.06) | 1.41 (0.15)*** | 1.48 (0.13)*** | <0.001 | 1.01 (0.06) | 1.43 (0.17)*** | 1.47 (0.16)*** | <0.001 |
| Tau Scans, N | 55 | 10 | 7 | | 71 | 53 | 27 | |

Table 3. EO vs. LO demographic comparisons. The comparisons were done using ANOVA and chi-square tests with two-sided p-values. Significant p-values (<0.05) are bolded. In addition, pairwise comparisons of MCI to DEM for each group are displayed using the following symbols to denote a significant difference.

*Significantly different between MCI and DEM at $p < 0.05$

**Significantly different between MCI and DEM at $p < 0.01$

***Significantly different between MCI and DEM at $p < 0.001$

| Diagnostic group (N) | EOAD _{MCI} (N=60) | LOAD _{MCI} (N=216) | p-value | EOnonAD _{MCI} (N=113) | LOnonAD _{MCI} (N=151) | p-value |
|---|-------------------------------|--------------------------------|------------------|-----------------------------------|-----------------------------------|------------------|
| Age, years, Mean (SD) | 65.4 (6.0) | 76.4 (5.8)** | <0.001 | 65.5 (5.8) | 77.6 (6.2) | <0.001 |
| Sex, Male % | 46.7 | 60.2 | 0.065 | 50.4 | 59.6* | 0.138 |
| Education, years, Mean (SD) | 16.7 (2.8)* | 15.8 (2.8) | 0.021 | 16.2 (2.5) | 16.3 (2.5) | 0.848 |
| % APOE e4, 0/1/2 alleles | 18/52/30 | 34/52/14 | 0.004 | 68/30/2 | 86/13/2 | 0.005 |
| Global CDR, Mean (SD) | 0.50 (0.00)*** | 0.50 (0.16)*** | 0.823 | 0.46 (0.17)*** | 0.48 (0.11)*** | 0.167 |
| MMSE, Mean (SD) | 27.8 (1.8)*** | 27.4 (1.9)*** | 0.229 | 28.6 (1.5)*** | 28.4 (1.6)*** | 0.175 |
| Global Cortical [¹⁸ F]Florbetapir SUVR, Mean (SD) | 1.41 (0.15)* | 1.43 (0.17)* | 0.315 | 1.03 (0.08) | 1.01 (0.09) | 0.115 |
| Tau scans, N | 10 | 53 | N/A | 38 | 51 | N/A |
| Diagnostic group (N) | EOAD _{DEM} (N=50) | LOAD _{DEM} (N=148) | p-value | EOnonAD _{DEM} (N=8) | LOnonAD _{DEM} (N=24) | p-value |
| Age, years, Mean (SD) | 64.7 (6.3) | 78.3 (5.9)** | <0.001 | 66.3 (5.8) | 79.4 (5.8) | <0.001 |
| Sex, Male % | 44.0 | 58.8 | 0.069 | 50.0 | 83.3* | 0.059 |
| Education, years, Mean (SD) | 15.6 (2.4)* | 15.4 (3.0) | 0.668 | 15.6 (3.5) | 15.6 (3.0) | 1.000 |
| % APOE e4, 0/1/2 alleles | 26/38/36 | 26/56/18 | 0.022 | 71/14/14 | 83/13/4 | 0.642 |
| Global CDR, Mean (SD) | 0.87 (0.33)*** | 0.84 (0.36)*** | 0.579 | 0.69 (0.26)*** | 0.83 (0.24)*** | 0.155 |
| MMSE, Mean (SD) | 22.5 (3.3)*** | 23.0 (2.8)*** | 0.283 | 23.0 (2.4)*** | 23.6 (1.9)*** | 0.453 |
| Global Cortical [¹⁸ F]Florbetapir SUVR, Mean (SD) | 1.48 (0.13)* | 1.47 (0.16)* | 0.616 | 1.04 (0.08) | 1.01 (0.10) | 0.485 |
| Tau scans, N | 7 | 27 | N/A | 3 | 2 | N/A |

Table 4. Regional amyloid PET ($[^{18}\text{F}]$ Florbetapir) comparisons between amyloid positive subjects for frontal, cingulate, parietal and temporal cortices. *Temporal SUVR was significantly different ($p=0.048$) between EOAD_{MCI} and EOAD_{DEM} subjects

| Amyloid Regions | EOAD_{MCI} | EOAD_{DEM} | LOAD_{MCI} | LOAD_{DEM} | ANOVA p-values |
|-----------------|----------------------------|----------------------------|----------------------------|----------------------------|----------------|
| Frontal SUVR | 1.38 (0.18) | 1.47 (0.17) | 1.41 (0.17) | 1.43 (0.17) | 0.083 |
| Cingulate SUVR | 1.47 (0.19) | 1.55 (0.15) | 1.50 (0.18) | 1.53 (0.18) | 0.112 |
| Parietal SUVR | 1.38 (0.19) | 1.47 (0.15) | 1.40 (0.17) | 1.44 (0.17) | 0.044 |
| Temporal SUVR | 1.27 (0.18)* | 1.37 (0.17)* | 1.30 (0.16) | 1.33 (0.16) | 0.023 |

Imaging comparisons:

The FWE cluster-level corrected maps of the MRI, FDG PET and tau PET comparisons of EOAD and LOAD spectrum individuals to CN are shown in **Figure 1**. The same analyses limited to only subjects with tau PET scans are shown in **Figure 2** while **Figure 3** displays comparisons of EOAD and LOAD to younger and older CN subgroups, resp. The pattern of neurodegeneration and tau deposition seen in **Figure 1** and **Figures 2** and **3** are very similar discounting the probability of exaggerated age or selection bias.

Figure 1. MRI (top), FDG PET (middle), tau PET (bottom) comparisons between the AD groups and CN. The significance maps show $p < 0.05$ thresholded FWE cluster-level corrected results of EOAD_{MCI} (N=60), EOAD_{DEM} (N=50), LOAD_{MCI} (N=216) and LOAD_{DEM} (N=148) vs. CN (N=291). The results displayed here are for all subjects with available scans in each modality.

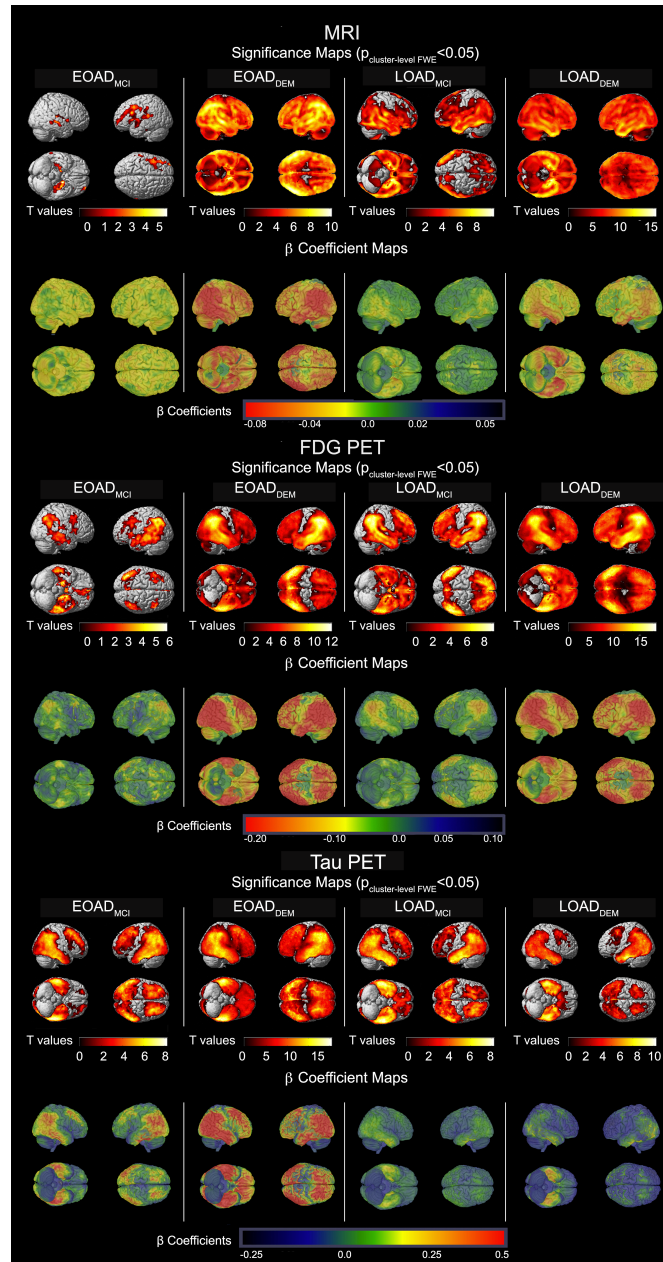


Figure 2. MRI (top) and FDG PET (bottom) comparisons between the AD and CN groups restricted to only subjects with available tau PET scans. The significance maps show $p < 0.05$ thresholded FWE cluster-level corrected results. of EOAD_{MCI} (N=10), EOAD_{DEM} (N=7), LOAD_{MCI} (N=53) and LOAD_{DEM} (N=27) vs. CN (N=126)

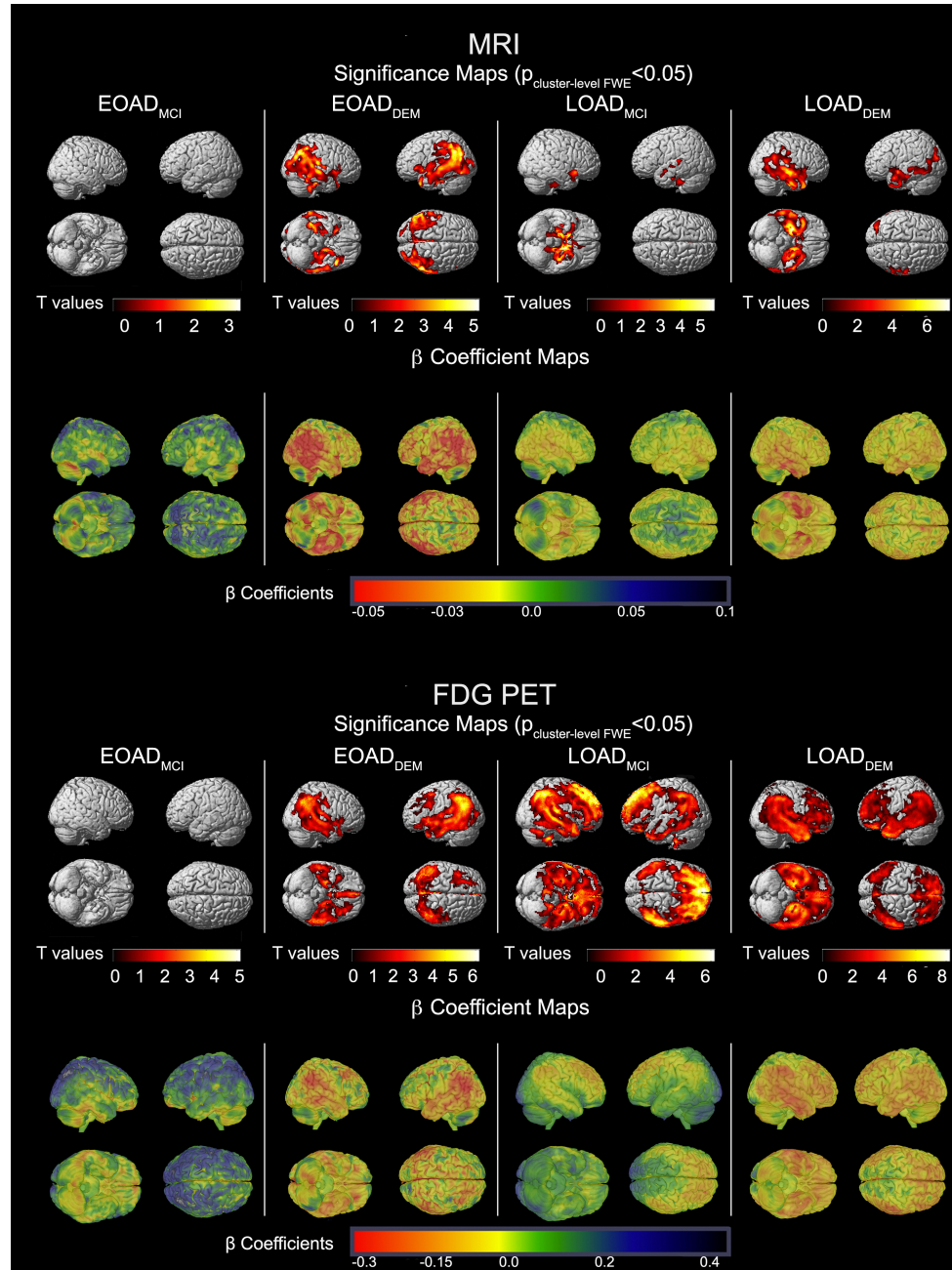
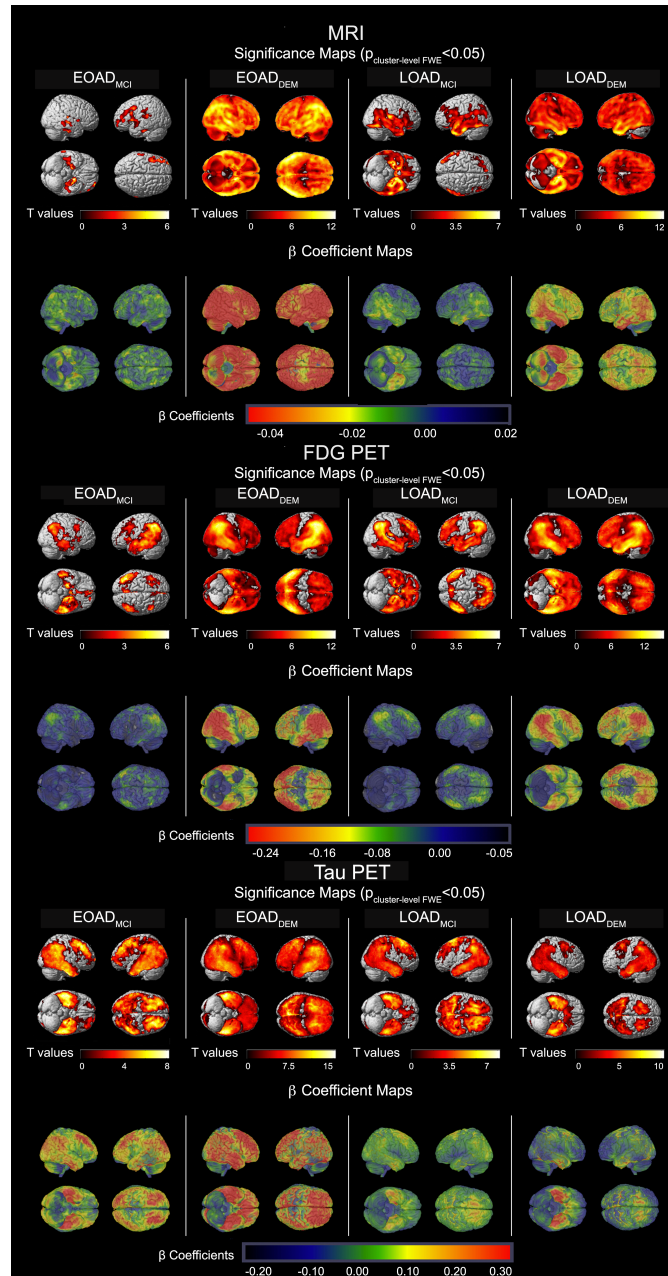


Figure 3. MRI (top), FDG PET (middle), tau PET (bottom) comparisons between young CN and EOnonAD and old CN and LOnonAD groups. The significance maps show $p < 0.05$ thresholded FWE cluster-level corrected results of EOAD_{MCI} (N=60) and EOAD_{DEM} (N=50) vs young CN (N=145), LOAD_{MCI} (N=216) and LOAD_{DEM} (N=148) vs. old CN (N=146).



MRI (Figure 1, top panel)

The EOAD_{MCI} group showed two significant clusters of atrophy in the left and right medial and lateral temporal and left frontal cortices relative to the CN group (left cluster: cluster size $k=45797$, cluster $p_{FWE}<0.001$; right cluster: $k=20760$, cluster $p_{FWE}=0.003$). Compared to the CN group, the LOAD_{MCI} cohort showed significant atrophy of the bilateral medial and lateral temporal, temporoparietal, insular, occipital and frontal regions (single cluster $k=688646$, cluster $p_{FWE}<0.001$). The EOAD_{MCI} group visually showed a larger effect size (i.e., more severe atrophy) than LOAD_{MCI} in overlapping regions (see β -coefficient maps in **Figure 1**, top panel).

Both EOAD_{DEM} and LOAD_{DEM} showed extensive atrophy throughout the brain compared to CN (single clusters, $k_{EO}=1541575$, $k_{LO}=1503763$, cluster $p_{FWE}<0.001$ for both). The significance and β -coefficient maps show a stronger effect size (i.e., more severe atrophy) in the EOAD_{DEM} than the LOAD_{DEM} group (see β -coefficient maps in **Figure 1**, top panel).

FDG PET (Figure 1, middle panel)

Compared to CN, EOAD_{MCI} showed a significant hypometabolic cluster in bilateral medial and lateral temporal and lateral, temporoparietal cortices ($k=32246$, cluster $p_{FWE}<0.001$). Additionally, there was a small cluster of hypometabolism in bilateral dorsolateral prefrontal cortex ($k=3396$, cluster $p_{FWE}<0.001$). LOAD_{MCI} subjects showed hypometabolism of the bilateral inferior temporal, medial and lateral temporal and parietal cortices as well as bilateral

frontal cortex (single cluster, $k=94307$, cluster $p_{FWE}<0.001$, **Figure 1**, middle panel).

Both the EOAD_{DEM} and LOAD_{DEM} groups showed extensive hypometabolism relative to CN in bilateral parietal, temporal, and frontal lobes, as well as insular and cingulate cortices (single clusters, $k_{EO}=148701$, $k_{LO}=185998$, cluster $p_{FWE}<0.001$ for both). As with the MRI analysis, the EOAD_{DEM} group showed a stronger effect size (i.e., more severe hypometabolism) than the LOAD_{DEM} group (see β -coefficient maps in **Figure 1**, middle panel).

Tau PET (Figure 1, bottom panel)

These analyses were limited to the subset of individuals with available tau PET imaging. Compared to the CN group, the EOAD_{MCI} group had a significant cluster of tau binding covering temporal, parietal, parietooccipital and right frontal cortices ($k=74981$, cluster $p_{FWE}<0.001$). An additional significant cluster of tau binding was present in the left prefrontal cortex ($k=9800$, cluster $p_{FWE}<0.001$). The LOAD_{MCI} cohort showed tau deposition in a similar pattern (single cluster, $k=96885$, cluster $p_{FWE}<0.001$). The beta coefficient maps demonstrated greater tau burden in EOAD_{MCI} compared to LOAD_{MCI} (see β -coefficient maps in **Figure 1**, bottom panel).

EOAD_{DEM} showed tau binding in all cortical regions save for the primary sensorimotor and visual cortices (single cluster, $k=157966$, cluster $p_{FWE}<0.001$). LOAD_{DEM} showed two significant clusters of tau binding – one in the posterior

association cortices ($k=67260$, cluster $p_{FWE}<0.001$) and a smaller one in the bilateral prefrontal cortices ($k=4931$, cluster $p_{FWE}<0.001$). The β -coefficient maps show much more severe and extensive tau deposition in $EOAD_{DEM}$ compared to $LOAD_{DEM}$ (see β -coefficient maps in **Figure 1**, bottom panel).

NonAD analyses:

Demographic comparisons:

Direct comparisons of CN to $EOnonAD_{MCI}$, $LOnonAD_{MCI}$, $EOnonAD_{DEM}$ and $LOnonAD_{DEM}$ showed the expected significant difference in age, global CDR and MMSE ($p<0.001$, **Table 5**). Compared to CN, $LOnonAD_{DEM}$ had a greater proportion of men ($p=0.003$) and lower education ($p=0.044$). Even when split in younger and older subgroups, the age differences between CN and the respective disease groups remained significant (**Table 6**).

By definition, $EOnonAD_{MCI}$ and $EOnonAD_{DEM}$ were significantly younger than the corresponding $LOnonAD$ groups ($p<0.001$). The $EOnonAD_{MCI}$ group had a higher proportion of *APOE e4* carriers compared to the $LOnonAD_{MCI}$ group ($p=0.005$). There were no significant differences in sex, education, global CDR, MMSE or global [^{18}F]Florbetapir SUVR between the groups.

A closer look into regional amyloid differences among nonAD subjects revealed significant differences between $LOnonAD_{MCI}$ and $LOnonAD_{DEM}$ parietal amyloid SUVR ($p=0.045$, **Table 7**). No other region was significantly different across nonAD groups.

Table 5. EOnonAD and LOnonAD demographic comparisons to CN. The comparisons were done using ANOVA and chi-square tests with two-sided p-values. The Bonferroni-corrected pairwise differences are discussed in the Results section. Significant p-values (<0.05) are bolded.

*Significantly different than CN group at p<0.05

**Significantly different than CN group at p<0.01

***Significantly different than CN group at p<0.001

| Variable | CN (N=291) | EOnonAD _{MCI} (N=113) | EOnonAD _{DEM} (N=8) | p-value | LOnonAD _{MCI} (N=151) | LOnonAD _{DE} M(N=24) | p-value |
|--|---------------|-----------------------------------|---------------------------------|------------------|-----------------------------------|----------------------------------|------------------|
| Age, years, Mean (SD) | 74.3 (6.4) | 65.5 (5.8)*** | 66.3 (5.8)*** | <0.001 | 77.6 (6.2)*** | 79.4 (5.8)*** | <0.001 |
| Sex, Male % | 52.2 | 50.4 | 50.0 | 0.944 | 59.6 | 83.3** | 0.008 |
| Education, years, Mean (SD) | 16.7 (2.6) | 16.2 (2.5) | 15.6 (3.5) | 0.095 | 16.3 (2.5) | 15.6 (3.0)* | 0.037 |
| % APOE e4, 0/1/2 alleles | 77/22/1 | 68/30/2 | 71/14/14 | 0.028 | 86/13/2* | 83/13/4 | 0.173 |
| Global CDR, Mean (SD) | 0.02 (0.09) | 0.46 (0.17)*** | 0.69 (0.26)*** | <0.001 | 0.48 (0.11)*** | 0.83 (0.24)*** | <0.001 |
| MMSE, Mean (SD) | 29.0 (1.3) | 28.6 (1.5)* | 23.0 (2.4)*** | <0.001 | 28.4 (1.6)*** | 23.6 (1.9)*** | <0.001 |
| Global Cortical [¹⁸ F]Florbeta pir SUVR, Mean (SD) | 1.03 (0.06) | 1.03 (0.08) | 1.04 (0.08) | 0.214 | 1.01 (0.09) | 1.01 (0.10) | 0.160 |
| Tau scans, N | 126 | 38 | 3 | N/A | 51 | 2 | N/A |

Table 6. EOnonAD and LOnonAD demographic comparisons to the young and old CN groups, resp. The comparisons were done using ANOVA and chi-square tests with two-sided p-values. The Bonferroni-corrected pairwise differences are discussed in the Results section. Significant p-values (<0.05) are bolded.

*Significantly different than CN group at p<0.05

**Significantly different than CN group at p<0.01

***Significantly different than CN group at p<0.001

| Variable | Young CN (N=145) | EOnonADMCI (N=113) | EOnonADM (N=8) | p- value | Old CN (N=146) | LOnonADMCI (N=151) | LOnonADM (N=24) | p- value |
|--|---------------------|-----------------------|-------------------|------------------|-------------------|-----------------------|--------------------|------------------|
| Age, years, Mean (SD) | 69.1 (3.3) | 65.5 (5.8)*** | 66.3 (5.8)* | <0.001 | 79.4 (4.3) | 77.6 (6.2)** | 79.4 (5.8) | 0.010 |
| Sex, Male % | 50.3 | 50.4 | 50.0 | 0.990 | 54.1 | 59.6 | 83.3** | 0.026 |
| Education, years, Mean (SD) | 16.7 (2.5) | 16.2 (2.5) | 15.6 (3.5) | 0.138 | 16.7 (2.7) | 16.3 (2.5) | 15.6 (3.0) | 0.078 |
| % APOE e4, 0/1/2 alleles | 74/25/1 | 68/30/2 | 71/14/14* | 0.066 | 80/18/2 | 86/13/2 | 83/13/4 | 0.630 |
| Global CDR, Mean (SD) | 0.02 (0.10) | 0.46 (0.17)*** | 0.69 (0.26)*** | <0.001 | 0.01 (0.07) | 0.48 (0.11)*** | 0.83 (0.24)*** | <0.001 |
| MMSE, Mean (SD) | 29.1 (1.1) | 28.6 (1.5)** | 23.0 (2.4)*** | <0.001 | 28.8 (1.4) | 28.4 (1.6)** | 23.6 (1.9)*** | <0.001 |
| Global Cortical [¹⁸ F]Florbet apir SUVR, Mean (SD) | 1.04 (0.06) | 1.03 (0.08) | 1.04 (0.08) | 0.749 | 1.01 (0.06) | 1.01 (0.09) | 1.01 (0.10) | 0.986 |
| Tau Scans, N | 55 | 38 | 3 | | 71 | 51 | 2 | |

Table 7. Regional amyloid PET ($[^{18}\text{F}]$ Florbetapir) comparisons between amyloid negative subjects for frontal, cingulate, parietal and temporal cortices.

| Amyloid Regions | CN | EOnonAD _{MCI} | EOnonAD _{DEM} | LOnonAD-MCI | LOnonAD _{DEM} | ANOVA p-values |
|-----------------|-------------|------------------------|------------------------|-------------|------------------------|----------------|
| Frontal SUVR | 1.01 (0.07) | 1.01 (0.06) | 1.05 (0.08) | 1.00 (0.08) | 0.99 (0.12) | 0.304 |
| Cingulate SUVR | 1.11 (0.08) | 1.11 (0.09) | 1.16 (0.07) | 1.09 (0.09) | 1.09 (0.11) | 0.187 |
| Parietal SUVR | 1.02 (0.07) | 1.02 (0.07) | 1.06 (0.06) | 1.01 (0.08) | 1.02 (0.10) | 0.394 |
| Temporal SUVR | 0.96 (0.06) | 0.95 (0.06) | 0.99 (0.05) | 0.95 (0.07) | 1.01 (0.08) | 0.112 |

Imaging comparisons:

The FWE cluster-level corrected MRI, FDG PET and tau PET comparison maps of the nonAD groups to CN are shown in **Figure 4**. The same analyses limited to only subjects with tau PET scans are shown in **Figure 5**, while **Figure 6** displays comparisons of EOnonAD and LOnonAD to younger and older CN subgroups, resp. The pattern of neurodegeneration and tau deposition seen in **Figure 16** is largely identical to the one in **Figure 4**, with the exception of emerging tau deposition in bilateral frontal and right parietal lobes in EOnonAD when compared to the young CN.

Figure 4. MRI (top), FDG PET (middle), tau PET (bottom) comparisons between the nonAD groups and CN. The significance maps show $p < 0.05$ thresholded FWE cluster-level corrected results of EOnonAD_{MCI} (N=113), EOnonAD_{DEM} (N=8), LOnonAD_{MCI} (N=151) and LOnonAD_{DEM} (N=24) vs. CN (N=291). The results displayed here are for all subjects with available scans in each modality.

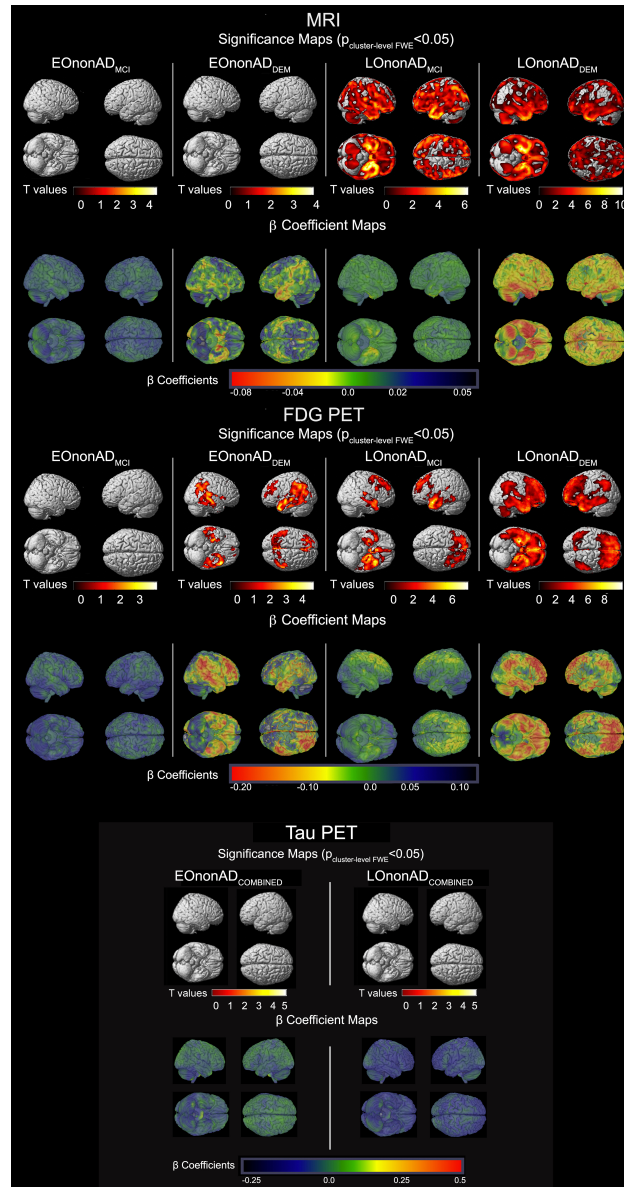


Figure 5. MRI (top) and FDG PET (bottom) comparisons between the nonAD and CN groups restricted to only subjects with available tau PET scans. The significance maps show $p < 0.05$ thresholded FWE cluster-level corrected results of EOnonAD_{MCI} (N=38), EOnonAD_{DEM} (N=3), LOnonAD_{MCI} (N=51) and LOnonAD_{DEM} (N=2) vs. CN (N=126).

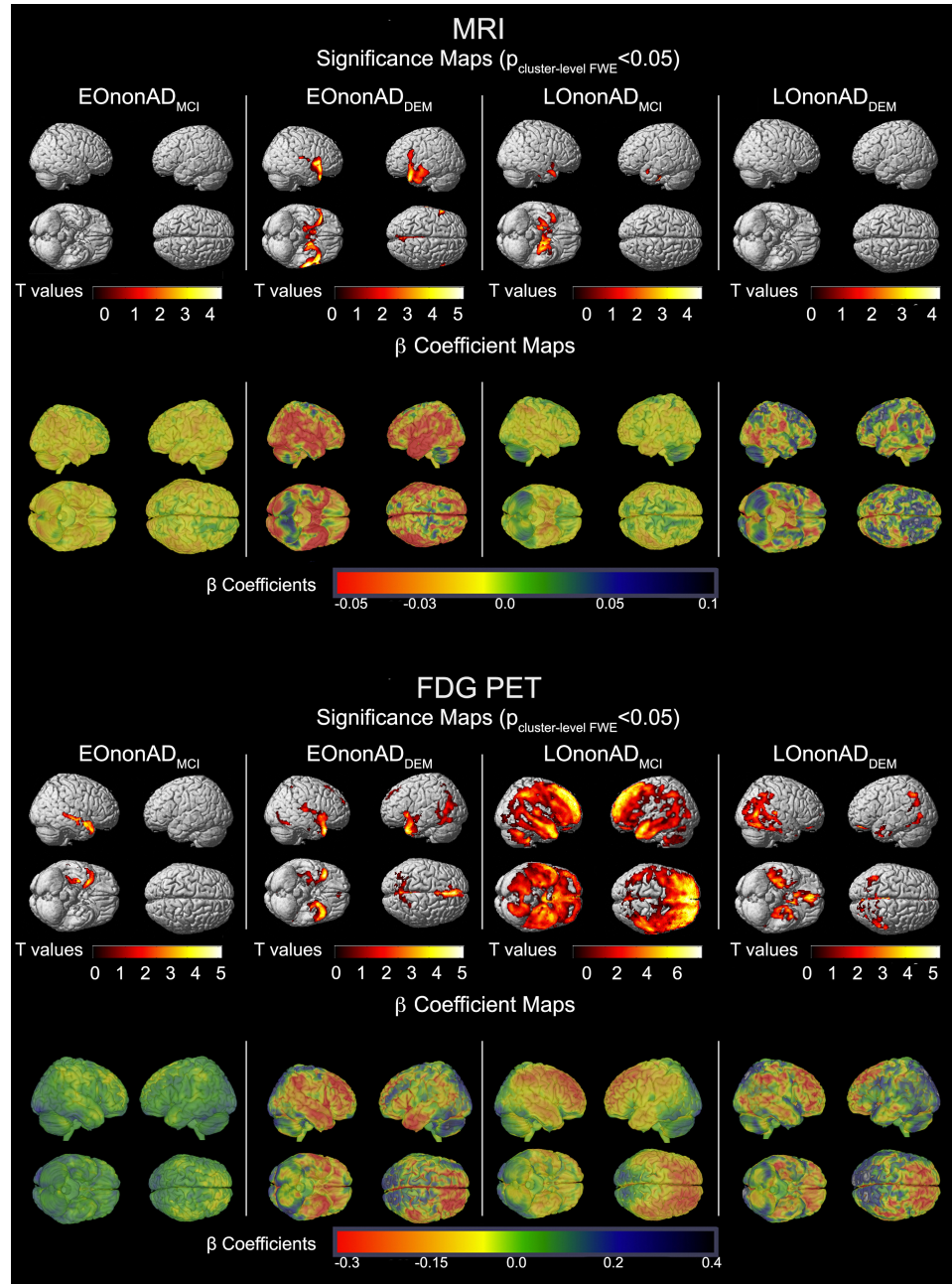
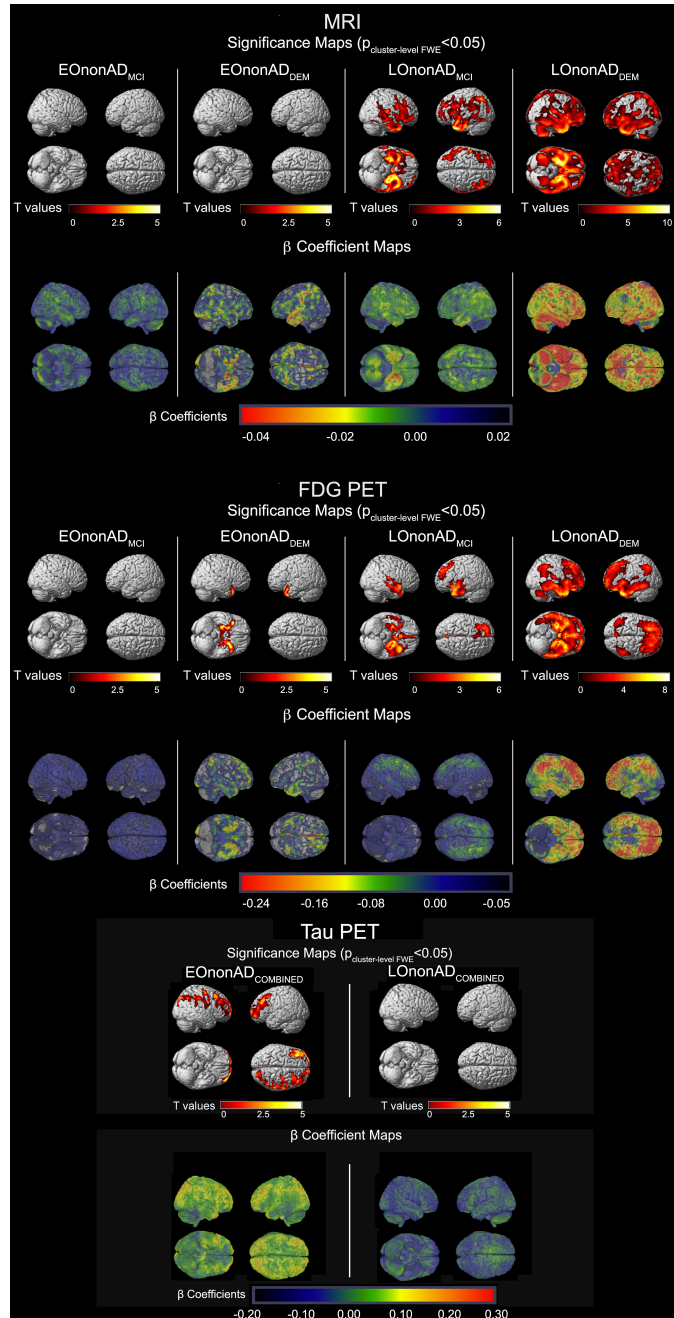


Figure 6. MRI (top), FDG PET (middle), tau PET (bottom) comparisons between young CN and EOAD and old CN and LOAD groups. The significance maps show $p < 0.05$ thresholded FWE cluster-level corrected results of EOnonAD_{MCI} (N=113) and EOnonAD_{DEM} (N=8) vs young CN (N=145), LOnonAD_{MCI} (N=151) and LOnonAD_{DEM} (N=24) vs. old CN (N=146).



MRI (Figure 4, top panel)

EOnonAD showed no significant atrophy compared to the CN group. LOnonAD_{MCI} showed extensive atrophy in the bilateral medial and lateral temporal, temporoparietal, parietooccipital and frontal cortices (single cluster, $k=569219$, cluster $p_{FWE}<0.001$). LOnonAD_{DEM} had similarly widespread atrophy showing two significant clusters – one in bilateral temporoparietal and frontal cortices ($k=602716$, cluster $p_{FWE}<0.001$) and another in the cerebellum ($k=13494$, cluster $p_{FWE}=0.020$). The largest effect size was observed in LOnonAD_{DEM} with greatest predilection for the medial and inferior temporal lobes (see β -coefficient maps in **Figure 4**, top panel).

FDG PET (Figure 4, middle panel)

Compared to CN, EOnonAD_{MCI} showed no significant hypometabolism, while the EOnonAD_{DEM} group showed three significant clusters in left and right temporoparietal (left: $k=15114$, cluster $p_{FWE}<0.001$; right: $k=6104$, cluster $p_{FWE}<0.001$) and bilateral frontal cortices (single cluster, $k=3002$, cluster $p_{FWE}<0.001$). LOnonAD_{MCI} showed a significant cluster of hypometabolism in bilateral temporal and prefrontal cortices ($k=24278$, cluster $p_{FWE}<0.001$). A similar fronto-temporal pattern of hypometabolism was also observed in LOnonAD_{DEM}; however, it also extended to the parietal lobes (single cluster, $k=78550$, cluster $p_{FWE}<0.001$).

Tau PET (Figure 4, bottom panel)

Due to the small sample sizes, the EOnonAD and LOnonAD groups were not split by disease stage. There were no significant tau binding in either EOnonAD or LOnonAD. As mentioned above, EOnonAD showed tau deposition in bilateral frontal (single cluster, $k=7215$, cluster $p_{FWE}<0.001$) and right parietal lobes (single cluster, $k=4664$, cluster $p_{FWE}<0.001$) when compared to young CN only (**Figure 4**).

2.4. Discussion:

The current study aimed to map neurofibrillary, structural and metabolic differences between EO and LO MCI and DEM subjects stratified by amyloid positivity. As expected I found that EOAD_{MCI} and EOAD_{DEM} subjects show more severe neurodegeneration and greater tau deposition compared to LOAD_{MCI} and LOAD_{DEM}, respectively, a finding that is consistent with previous imaging reports^{45,48-54,57}, and with the fact that EO individuals have a much more aggressive disease course^{42,45}.

The availability of amyloid PET imaging or CSF A β measurements allowed me to identify nonAD cases that were enrolled as Alzheimer's phenocopies. While I failed to find significant neurodegeneration in EOnonAD_{MCI}, I observed significant hypometabolism in EOnonAD_{DEM} in the absence of significant atrophy, a finding that could be indicative of synaptic dysfunction before cellular loss. The lack of findings, particularly in the EOnonAD_{MCI} subjects, where the neurodegenerative changes are likely subtle, may be due to the inability to properly account for age-related degeneration (despite covarying for age during

the analysis) when comparing directly to the CN subjects who are significantly older. In the EOnonAD_{DEM} subjects, the lack of visible atrophy on statistical maps may be due to a relatively small sample size, as the beta-coefficient maps indicate a pattern of neurodegeneration similar to that seen in the FDG PET analysis. Furthermore, the EOnonAD_{DEM} subjects may be a heterogeneous group of multiple etiologies, making detection of significant clusters of atrophy difficult.

LOnonAD cases showed pronounced atrophy and hypometabolism with greatest predilection for the temporal and frontal lobes. This pattern of neurodegeneration has been reported in primary age-related tauopathy (PART) and hippocampal sclerosis with TAR-DNA binding protein 43 (TDP-43) inclusions (HS-TDP-43)^{95,96}. Both conditions are highly prevalent among the elderly with and without cognitive deficit^{95,96}, however, of these two, HS-TDP-43 (also known as limbic-predominant age-related TDP-43 encephalopathy (LATE)⁹⁷) is the more likely etiology due to the lack of tau binding in the medial temporal lobes which is expected in PART. It is worth noting that though [¹⁸F]Flortaucipir binds well to mature tangles in 3R+4R tauopathies, such as in AD and PART^{98,99}, further *post mortem* studies are needed to say with confidence which tauopathy tau variants can reliably be bound with Flortaucipir.

The hypometabolic pattern I observed in LOnonAD fits well with previous pathologic and imaging reports of LATE. TDP-43 inclusions and neurite deposits first appear in the hippocampal dentate granule cells, subiculum and the amygdala^{96,100,101}. In more advanced stages, TDP-43 pathology is also found in

frontal and temporal neocortex^{96,100,101}. TDP-43 pathology is extremely prevalent among cognitively impaired elderly and is the stand-alone pathology in 4.2% of these cases^{96,100,102,103}. 86% of TDP-43 positive cases have HS-TDP-43^{96,104-106}. HS-TDP-43 oftentimes show episodic and semantic memory dysfunction, explaining how they could easily be diagnosed clinically with AD¹⁰⁷. Individuals with HS-TDP-43 have greater hippocampal atrophy and greater cognitive impairment than those with HS without TDP-43^{100,101,104}. Additional support for my hypothesis that the LOnonAD subjects likely harbor HS-TDP-43 are the recent reports that HS-TDP-43 cases show hypometabolic changes in the medial and lateral temporal, posterior and middle cingulate, precuneus, and prefrontal cortex, similar to the FDG PET pattern I observed in LOnonAD_{MCI} and LOnonAD_{DEM}¹⁰⁸. Similar hypometabolic and atrophy patterns involving medial and lateral temporal and prefrontal cortices were recently reported in two additional clinic-pathologic studies^{109,110}.

An additional possibility is that some LOnonAD subjects may suffer from behavioral variant frontotemporal dementia (bvFTD). However, this is less likely given the mean age of the LOnonAD cohorts (77.6 and 79.4 years, respectively) and their amnesic predominant presentation at enrollment as required by ADNI (see <http://www.adni-info.org/Scientists/ADNIStudyProcedures.html>). It is worth noting, however, that in rare cases (10% of pathologically confirmed bvFTD cases), patients presented with primarily amnesic symptoms and some studies have even reported as much as 25% of pathologically confirmed FTLN cases to have a disease onset after the age of 65^{111,112}.

2.5. Strengths and Limitations:

Several strengths and limitations of my study should be noted. One of the strengths is the relatively large sample size of EO subjects available through ADNI. Additionally, ADNI employs meticulously standardized clinical and imaging data collection, which is routinely subjected to quality control. One of the limitations of my analyses is the cross-sectional design and the measurement of atrophy, which has a temporal component. This means that I am actually measuring differences in gray matter density, which implies atrophy, but is not synonymous. Longitudinal analyses are needed to assess atrophy and metabolic changes over time. Additionally, while the rigorous exclusion criteria employed in ADNI are typical of clinical trials, this renders the ADNI's population as not representative of the general population. Furthermore, there is very little *post mortem* data currently available for ADNI, which means diagnosis of AD largely lacks pathological verification. Finally, while I am including the EOnonAD_{DEM} in my report for completeness, one must keep in mind that the number of subjects in this group is very small, thus, the findings should be interpreted with caution. Larger research studies such as the recently funded Longitudinal Early-onset Alzheimer's Disease Study (LEADS) which will use amyloid imaging and detect EOnonAD cases will be able to define the neurodegenerative pattern in this group.

2.6. Conclusions:

In conclusion, my study found a similar neurodegenerative pattern between amnesic amyloid-positive EO and LO MCI and DEM subjects. These processes were more severe in the EO group indicating a more aggressive disease course. I also found that LOnonAD_{DEM} subjects show anterior temporal neurodegeneration which might reflect the presence HS-TDP-43 or LATE. In the absence of reliable *in vivo* TDP-43 biomarker, the only feasible method of confirmation is through post-mortem examination of the brains. Other large research consortia such as the recently funded LEADS project will allow the opportunity to systematically study EOAD and EOnonAD and further characterize these highly understudied disease states.

Chapter 3. The effect of the top 20 Alzheimer's disease risk genes on gray matter density and FDG PET brain metabolism

3.1. Introduction:

Alzheimer's disease (AD) is a chronic neurodegenerative disease characterized by short-term memory loss in the early disease stages and progressive cognitive and functional deficits as the disease advances. The clinical symptoms result from the deposition of two toxic proteins - β -amyloid ($A\beta$) and tau, which give rise to neuritic plaques and neurofibrillary tangles respectively ¹¹⁵. The clinical appearance of AD is the direct result of neuronal dysfunction and death, which is manifested by brain atrophy and hypometabolism.

Brain imaging is increasingly utilized to measure AD-associated changes in vivo. Amyloid positron emission tomography (PET), a novel Food and Drug Administration approved imaging technology, uses selective $A\beta$ tracers to visualize brain amyloidosis and can reliably detect the presence of neuritic plaques in the symptomatic and presymptomatic stages. Brain atrophy is best evaluated with longitudinal studies of high-field magnetic resonance imaging (MRI). The atrophic changes are first noticeable in the medial temporal lobe, eventually spreading through the remainder of the brain as the disease progresses ¹¹⁶. Brain hypometabolism, a decrease in brain metabolic activity, can be visualized using [¹⁸F]Fluorodeoxyglucose (FDG) PET or single-photon emission tomography (SPECT) with ^{99m}Tc exametazime. The hallmark pattern in

AD is early hypometabolism of the posterior cingulate, lateral temporal and parietal lobes with spread to the frontal lobes as the disease progresses ¹¹⁷.

Seventy-80% of sporadic Alzheimer's disease can be attributed to genetic risk ^{118,119}. Recent large-scale genome-wide association studies (GWAS) have discovered more than 20 AD gene variants that confer genetic risk ⁷⁵⁻⁸⁰. Among these variants is the apolipoprotein E (*APOE*) gene, which is the most established genetic risk factor for AD. Individuals with a single *APOE4* allele have a three-fold increase in AD risk while homozygotes have a 15-fold increase ¹²⁰. *APOE* is a major protein component of chylomicrons and is highly expressed in both liver and brain, where it plays a role in lipid metabolism and is thought to be involved in the breakdown of A β , both inside and outside of cells. The *APOE4* protein is less effective in clearing A β than the e3 allele, providing a possible explanation for the increased risk of amyloid buildup ¹²¹. With the help of imaging studies, *APOE4* was found to be strongly associated with brain amyloidosis ^{122,123}, atrophy ¹²⁴ and hypometabolism ^{125,126}. These data indicate that valuable observations related to gene function can be made with imaging phenotypes.

Many of the remaining top 20 AD variants have also been implicated in brain metabolism and neurodegeneration. Several *SORL1* variants, *EPHA1* rs11771145 and *CR1* rs6656401 were found to be associated with hippocampal atrophy and cerebro- or cardio-vascular disease ^{127,128}. Additionally, various research groups have shown that *ABCA7* rs3764650, *MS4A6A* rs983392, *MS4A6A* rs610932 and rs11230161, *BIN1* rs6733839 and rs744373, *CR1* rs1408077, *CR1* rs6656401, *CR1* rs3818361, *PICALM* rs3851179, *CLU*

rs11136000 and rs2279590, *CD2AP* rs10948363, and *CD33* rs3865444 are all associated with MRI-measured brain atrophy¹²⁹⁻¹³⁵. *BIN1* rs7561528 was found to be significantly associated with both hippocampal volume and FDG PET brain metabolism¹³⁶. The studies mentioned have unquestionably contributed to the field of imaging genetics and AD research as a whole, but many of these papers have either analyzed the effect of a single gene variant at a time^{127-130,132,134,135} or investigated the association between a polygenic risk score with the imaging trait, which does not allow for the interpretation of the individual contribution of genetic variants¹³¹. The commonly used univariate imaging genetics approach ignores the fact that in any given human subject, many of these risk variants are simultaneously present, and the genetic contribution of each variant should be investigated in the presence of the rest and not in isolation. Additionally, these studies have investigated the effects in the pooled samples consisting of asymptomatic individuals, of whom only a portion harbor AD pathology, as well as symptomatic individuals who are in different stages of the disease. Such an approach would miss any stage-specific associations that might occur for genes that influence the timing and course of development of disease traits (e.g., early vs. late neurodegeneration or amyloidosis, early vs. late impairment in a specific cognitive domain), and/or could explain, at least in part, AD heterogeneity.

Using a multivariable approach across the disease spectrum allows for accurate modeling of this complex polygenic disease that is constantly evolving. Here, I report a comprehensive analysis of the associations of well-validated AD risk variants from recent large-scale GWAS studies with two markers of

neurodegeneration – brain gray matter density (GMD) and brain glucose metabolism. My goal was to establish the relative contribution of the top 20 AD risk genes to changes in GMD and metabolic dysfunction. I hypothesized that I would find gene variants that show a profound effect on these two neurodegenerative phenotypes and that some variants will show associations in a stage-specific manner.

This work was performed in conjunction with the published findings of Apostolova et al in 2018, which used imaging genetics to explore the association of the top 20 Alzheimer's risk variants to cortical amyloid PET retention¹¹³. The study design, as in the chapters below, uses a multivariable regression model to select variants in a polygenic fashion as to establish relative contribution of selected genes to amyloidosis. This study also emphasized the importance of modeling throughout each of the disease stages, preclinical to dementia, to potentially capture stage-dependent associations. The results of the regression models were then reproduced in a voxelwise fashion as exploratory analysis of regional associations.

Data included were from 322 cognitively normal, 496 MCI and 159 dementia subjects from the Alzheimer's Disease Neuroimaging Initiative (ADNI) who were genotyped and received [¹⁸F]Flortbetapir PET scans.

The main findings of this work were that outside of the *APOE* e4 allele, *ABCA7* rs3752246 had the largest association to amyloidosis. *ABCA7*'s association with the early stages of the disease (preclinical and MCI) aligns with

neurodegeneration dementia findings presented below in chapter 3 and fits along the hypothetical dynamic biomarker model proposed by Jack et al in 2010 ¹¹⁴.

Additionally, I found evidence of a stage dependent gene effects in AD. The association for *FERMT2* *rs17125944* was strongest in the MCI stage. This observation indicates that a subset of AD genes might exhibit dynamic associations across the cognitive continuum.

3.2. Methods:

Subjects

I sourced the study data from the Alzheimer's Disease Neuroimaging Initiative (ADNI) database (<http://adni.loni.usc.edu>). ADNI is an international longitudinal study with approximately 50 sites across the United States and Canada that was launched in 2003. ADNI's goal is to track the progression of AD using clinical and cognitive tests, MRI, FDG PET, amyloid PET, cerebrospinal fluid and blood biomarkers (<http://adni.loni.usc.edu/study-design>).

ADNI has undergone three study cycles: ADNI1, ADNI GO and ADNI2. The study population was composed of participants from all three phases ¹³⁷. The MRI and FDG PET analyses included all subjects with GWAS and baseline MRI or FDG PET data that were successfully preprocessed. A total of 1564 ADNI subjects had baseline MRI and GWAS data. Of those, 65 failed in the MRI preprocessing steps and were excluded from the structural analyses. The final MRI cohort consisted of 441 cognitively normal (NC) subjects, 764 mild cognitive impairment (MCI) subjects and 294 dementia subjects (total N=1499). As not all

ADNI1 subjects received FDG PET, the FDG PET cohort was smaller and consisted of 381 NC, 634 MCI and 243 dementia subjects (total N=1258). There were 59 subjects with available FDG PET data whose MRI scans failed in the preprocessing steps as described above. These subjects were included in the FDG PET analyses.

The clinical characteristics of the ADNI cohort were described previously⁸⁵. Diagnosis of AD was based on the National Institute of Neurological and Communicative Disorders and Stroke and the AD and Related Disorders Association (NINCDS-ADRDA) criteria³³. AD subjects were required to have Mini-Mental State Examination (MMSE)⁸⁶ scores between 20 and 26 and a Clinical Dementia Rating scale (CDR) score of 0.5–1 at baseline⁸⁷. Qualifying MCI subjects had memory complaints but no significant functional impairment, scored between 24 and 30 on the MMSE, had a global CDR score of 0.5, a CDR memory score of 0.5 or greater, and objective memory impairment on Wechsler Memory Scale – Logical Memory II test¹³⁸. NC subjects had MMSE scores between 24 and 30, a global CDR of 0 and did not meet criteria for MCI and AD. Subjects were excluded if they refused or were unable to undergo MRI, had other neurological disorders, active depression, or history of psychiatric diagnosis, alcohol, or substance dependence within the past 2 years, less than 6 years of education, or were not fluent in English or Spanish. The full list of inclusion/exclusion criteria may be accessed on pages 23–29 of the online ADNI protocol (<http://www.adni-info.org/Scientists/ADNIStudyProcedures.html>). Written informed consent was obtained from all participants.

Gene Variant Selection and Imputation

ADNI-1 participants were genotyped using the Illumina Human610-Quad BeadChip array, while ADNI-2/GO participants were genotyped using the Illumina HumanOmniExpress BeadChip (Illumina, Inc., San Diego, CA). The decision to include gene variants was based on the AD GWAS studies that discovered these variants to date. Genes previously associated with the defining AD pathologic hallmark - amyloid pathology, were also included in the study (**Table 8**)¹³⁹⁻¹⁴¹. The total number of variants selected was 36.

ABCA7 rs3752246, *BIN1* rs6733839, *CASS4* rs7274581, *CD2AP* rs9349407, *CELF1* rs10838725, *INPP5D* rs35349669, *PTK2B* rs2883497, *SORL1* rs11218343 and *SORL1* rs1131497 were not genotyped on either ADNI GWAS array or needed full imputation. The following variants were only genotyped on one of the platforms and needed partial imputation: *NME8* rs2718058 in ADNI1 and *CLU* rs933194, *DSG2* rs8093731, *MEF2C* rs190982 and *ZCWPW1* rs1476679 in ADNI-GO/2 (**Table 9**). The imputation procedures have been previously described¹⁴². Imputation was performed using MACH and minimac methodology and the 1000 Genomes project (www.1000genomes.org) as the reference panel. The accuracy threshold was set at $r^2=0.30$.

I assessed Hardy-Weinberg equilibrium (HWE) using the --hardy option in PLINK. In the test, I used a quantitative phenotype (global cortical metabolism) and a case-control phenotype. The result indicates that all 27 single nucleotide polymorphisms (SNPs) do not show any evidence of deviation from HWE (p-

value > 0.01). The accepted significance threshold for declaring SNPs to be in HWE is p-value < 0.001.

Nine of the 20 genes were represented by more than one SNP. Given that such variants could be in linkage disequilibrium (LD) and introduce co-linearity bias, I performed LD analyses followed by Cohen's kappa (κ) statistics (**Table 10** and **Figure 7**). When variants providing identical information (those with high LD and high κ) were detected I chose the SNP with the smallest amount of missing data. This reduced the variants from 36 to 27.

I assessed the allele frequencies for each gene variant. SNPs were coded by minor allele dosage except for the following: *ABCA7* rs3764650 GG/GT vs. TT, *CASS4* rs7274581 CC/TC vs. TT, *CLU* rs9331949 AG/GG vs. AA, *DSG2* rs8093731 TT/TC vs. CC, *FERMT2* rs17125944 CC/TC vs. TT and *SORL1* rs112183431 CC/TC vs. TT where the minor allele homozygote frequency was less than 2%.

Table 8. All variants of the top 20 AD risk genes that were considered for inclusion in analyses

Variants selected were identified in AD GWAS. Included is minor allele, minor allele frequency, odds ratio and the paper(s) where the association was found.

| SNPs | PAPER MINOR | MAF | OR | CITATIONS |
|-------------------------|-------------|------|------------------|--|
| ABCA7 rs3752246 | G | 0.17 | 1.15 [1.09-1.21] | Hughes et al., 2014 |
| ABCA7 rs3764650 | G | 0.2 | 1.23 [1.18-1.30] | Hollingworth et al., 2011; Shulman et al., 2013 |
| ABCA7 rs4147929 | A | 0.18 | 1.15 [1.11-1.19] | Lambert et al., 2013 |
| BIN1 rs6733839 | T | 0.39 | 1.22 [1.18-1.25] | Lambert et al., 2009 |
| BIN1 rs744373 | G | 0.36 | 1.17 [1.12-1.21] | Seshadri et al., 2010; Hohman et al., 2013; Gharesouran et al., 2014 |
| BIN1 rs7561528 | A | 0.2 | 1.17 [1.13-1.22] | Biffi et al., 2010; Naj et al., 2011; Hohman et al., 2013 |
| CASS4 rs7274581 | C | 0.09 | 0.88 [0.84-0.92] | Lambert et al., 2013 |
| CD2AP rs9349407 | C | 0.19 | 1.12 [1.07-1.17] | Hollingworth et al., 2011; Naj et al., 2011; Shulman et al., 2013 |
| CD2AP rs10948363 | G | 0.19 | 1.1 [1.07-1.13] | Lambert et al., 2013 |
| CD33 rs3865444 | A | 0.21 | 0.94 [0.91-0.96] | Hollingworth et al., 2011; Naj et al., 2011; Lambert et al., 2013 |
| CELF1 rs10838725 | C | 0.26 | 1.08 [1.05-1.11] | Lambert et al., 2013 |
| CLU rs11136000 | T | 0.38 | 0.84 [0.79-0.89] | Harold et al., 2009; Lambert et al., 2009; Seshadri et al., 2010 |
| CLU rs9331949 | C | 0.1 | 1.29 [1.09-1.52] | Yu et al., 2013 |
| CLU rs1532278 | T | 0.26 | 0.89 [0.85-0.93] | Naj et al., 2011 |
| CLU rs9331896 | C | 0.38 | 0.86 [0.84-0.89] | Lambert et al., 2013 |
| CR1 rs12034383 | A | 0.41 | 1.32 [1.10-1.59] | Brouwers et al., 2012 |
| CR1 rs3818361 | A | 0.25 | 1.18 [1.13-1.24] | Thambisetty et al., 2013 |
| CR1 rs6656401 | A | 0.07 | 1.18 [1.14-1.22] | Lambert et al., 2009; Lambert et al., 2013 |
| CR1 rs6701713 | A | 0.25 | 1.16 [1.11-1.22] | Naj et al., 2011; Shulman et al., 2013 |
| DSG2 rs8093731 | T | 0.12 | 0.73 [0.62-0.86] | Lambert et al., 2013 |
| EPHA1 rs11767557 | C | 0.2 | 0.87 [0.83-0.91] | Hollingworth et al., 2011; Naj et al., 2011; Hughes et al., 2014 |
| EPHA1 rs11771145 | A | 0.43 | 0.9 [0.88-0.93] | Lambert et al., 2013 |
| FERMT2 rs17125944 | C | 0.11 | 1.14 [1.09-1.19] | Lambert et al., 2013 |
| INPP5D rs35349669 | T | 0.21 | 1.08 [1.05-1.11] | Lambert et al., 2013 |
| MEF2C rs190982 | G | 0.22 | 0.93 [0.90-0.95] | Lambert et al., 2013 |
| MS4A6A rs610932 | A | 0.45 | 0.9 [0.87-0.92] | Hollingworth et al., 2011 |
| MS4A6A rs983392 | G | 0.23 | 0.9 [0.87-0.92] | Lambert et al., 2013 |
| NME8 rs2718058 | G | 0.34 | 0.93 [0.90-0.95] | Lambert et al., 2013 |
| PICALM rs3851179 | T | 0.31 | 0.9 [0.83-0.99] | Harold et al., 2009; Biffi et al., 2010; Seshadri et al., 2010 |
| PICALM rs10792832 | A | 0.31 | 0.87 [0.85-0.89] | Lambert et al., 2013 |
| PICALM rs561655 | G | 0.34 | 0.87 [0.84-0.91] | Naj et al., 2011 |
| PTK2B rs28834970 | C | 0.32 | 1.1 [1.08-1.13] | Lambert et al., 2013 |
| SLC24A4/RIN3 rs10498633 | T | 0.15 | 0.91 [0.88-0.94] | Lambert et al., 2013 |
| SORL1 rs11218343 | C | 0.11 | 0.77 [0.72-0.82] | Lambert et al., 2013 |
| SORL1 rs1131497 | G | 0.37 | 1.92 [1.28-2.90] | Seshadri et al., 2007; Zhang et al., 2015 |
| ZCWPW1 rs1476679 | C | 0.21 | 0.91 [0.89-0.94] | Lambert et al., 2013 |

Table 9. List of variants that needed partial or full imputation

Some variants required imputation using data from the 1000 Genomes project. Need for imputation was dependent on the phase which subjects were genotyped.

| SNP | Imputed in |
|-------------------|-------------------|
| ABCA7 rs3752246 | ADNI-1, ADNI-2/GO |
| BIN1 rs6733839 | ADNI-1, ADNI-2/GO |
| CASS4 rs7274581 | ADNI-1, ADNI-2/GO |
| CD2AP rs9349407 | ADNI-1, ADNI-2/GO |
| CELF1 rs10838725 | ADNI-1, ADNI-2/GO |
| CLU rs9331949 | ADNI-1 |
| DSG2 rs8093731 | ADNI-1 |
| INPP5D rs35349669 | ADNI-1, ADNI-2/GO |
| MEF2C rs190982 | ADNI-1 |
| NME8 rs2718058 | ADNI-2/GO |
| PTK2B rs28834970 | ADNI-1, ADNI-2/GO |
| SORL1 rs11218343 | ADNI-1, ADNI-2/GO |
| SORL1 rs1131497 | ADNI-1, ADNI-2/GO |
| ZCWPW1 rs1476679 | ADNI-1 |

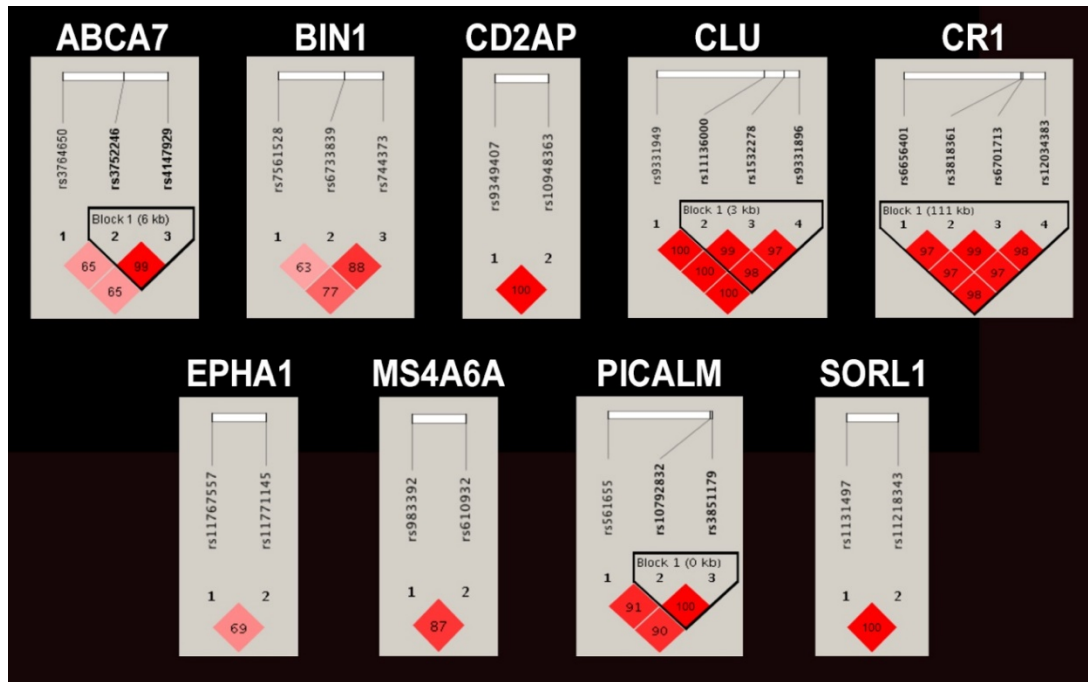
Table 10. Linkage analysis for genes with multiple variants included

Linkage disequilibrium and kappa statistics results for the variants retained in the analyses.

| GENE | SNP 1 | SNP 2 | LD (D') | KAPPA |
|--------------|--------------|--------------|----------------|--------------|
| <i>ABCA7</i> | rs3752246 | rs3764650 | 65 | 0.38 |
| <i>BIN1</i> | rs6733839 | rs744373 | 88 | 0.58 |
| | rs744373 | rs7561528 | 77 | 0.7 |
| | rs7561528 | rs6733839 | 63 | 0.45 |
| <i>CLU</i> | rs11136000 | rs9331949 | 100 | -0.01 |
| <i>CR1</i> | rs12034383 | rs3818361 | 97 | 0.03 |
| <i>EPHA1</i> | rs11767557 | rs11771145 | 69 | 0.32 |
| <i>SORL1</i> | rs11218343 | rs1131497 | 100 | -0.02 |

Figure 7. LD analysis

Results from the linkage analysis. For variants with significant overlap, the variant with the least missing data was retained for maximum N. Figure 7 shows variants who reside within a linkage block outline in black.



MRI and FDG PET data acquisition and analyses

The MRI acquisition and preprocessing protocols can be found on www.adni-info.org. ADNI MRI data acquisition and preprocessing have been previously described elsewhere ¹⁴³⁻¹⁴⁵. Briefly, I downloaded pre-processed MRI data from LONI IDA (<https://ida.loni.usc.edu>)¹⁴⁶. 785 subjects had 3T scans available and for the remaining 715 subjects, I used 1.5T data. MRI field strength was included as a covariate in all MRI analyses. I analyzed all scans using voxel-based morphometry (VBM) in Statistical Parametric Mapping (SPM8), as described previously ^{91,147}. Scans were downloaded from the ADNI site in NifTI format, co-registered to MNI space, bias corrected, and segmented into gray matter (GM), white matter (WM), and cerebrospinal fluid (CSF) compartments using SPM templates. GM density maps were converted to 1mm × 1mm × 1mm voxel resolution and smoothed using 10 mm full-width half maximum (FWHM) Gaussian kernel. Total intracranial volume (ICV) and baseline mean medial temporal lobe thickness measures were extracted for each subject using Freesurfer version 5.1, as described previously ^{148,149}. The medial temporal region of interest included the entorhinal, fusiform, parahippocampal and temporopolar cortical areas.

The FDG PET acquisition and preprocessing protocols can be found on www.adni-info.org. PET scanners and related equipment across sites were held to the same qualifications, calibration, and normalization standards, as described in detail ⁹². I downloaded preprocessed FDG PET data from LONI IDA (<https://ida.loni.usc.edu>). These scans were already averaged, aligned to a

standard space, re-sampled to a standard image and voxel size (2mm × 2mm × 2mm), smoothed to a uniform resolution as previously described⁹². The downloaded images were aligned to each corresponding MRI image on a subject-by-subject basis in MNI space using SPM8, as previously described¹⁴⁹. Each scan's intensity was scaled to the pons to create standard uptake value ratio (SUVR) images. Finally, baseline mean FDG SUVR in bilateral posterior cingulate was extracted for each subject^{150,151}.

Statistical Analyses

R Statistical Analyses:

The distributions of clinical and demographic characteristics [age, sex, education, MMSE, *APOE4* genotype, diagnosis] for each variant were analyzed using t-tests or Chi-square tests with two-sided p-values as appropriate.

My main analyses were done in R v3.3.0 (<https://www.r-project.org/>). First, I performed stepwise linear regression with all 27 AD risk variants as predictors and age, gender, education and *APOE4* genotype as covariates in the pooled sample and then in each diagnostic group. I used medial temporal lobe thickness or posterior cingulate SUVR, AD biomarkers of neurodegeneration, as outcome measures. Additional covariates were the diagnosis in the pooled analyses and magnetic field strength and ICV in all MRI analyses. The decision to exclude variables in the stepwise regression models was based on the Akaike Information Criterion (AIC) using the critical p-value of 0.157¹⁵². Given that all the risk genes were previously validated (i.e., all were candidate genes) and I used a multivariable model, I set the significance threshold at $p < 0.05$. After

discovering stage-specific genetic influences I repeated the pooled sample analyses introducing interaction terms between the genetic variants retained in the models and diagnosis.

Analyses in Imaging Space:

All imaging analyses were done in an exploratory fashion. I reproduced the final stepwise regression models using voxel-wise regression in SPM8 for visualization purposes in order to explore, on a whole-brain level, the extent and spatial pattern of these imaging genetic associations established using a region of interest approach. These models included all variants retained in the R stepwise linear regression models and were covaried for age, gender and *APOE4* genotype. Consistent with the original regression model, the pooled analyses also included diagnosis as a covariate and the MRI analyses were additionally controlled for MRI field strength and ICV. Due to the exploratory nature of the secondary results, I used a less stringent visualization voxel-wise threshold, which was uncorrected $p < 0.01$ with a minimum cluster size (k) of 50 voxels. Next, I report all family-wise error (FWE) and false discovery rate (FDR) significant within-cluster peak effects for all genetic variants identified in the models.

3.3. Results:

Group comparisons of demographic characteristics and distributions of the genotypes that were retained in the regression models are shown in **Tables 11** and **12** for the MRI and PET samples, respectively. As expected, AD subjects

were the oldest, least educated, had the greatest frequency of *APOE4* and performed the worst on MMSE (**Tables 11 and 12**). There were no significant differences in age, gender, education, MMSE and *APOE4* distribution between carriers and non-carriers or by allele dosage for any of the genotypes except the following: *DSG2* minor allele carriers were more likely to be male ($p=0.028$ in the FDG sample) and less likely to be *APOE4* carriers ($p=0.04$ in the MRI sample); *EPHA1* rs11767557 minor allele carriers were less likely to be *APOE4* carriers and had significantly higher MMSE scores in the FDG sample ($p=0.037$ and $p=0.047$, respectively); *SORL1* rs11218343 minor allele carriers were less educated and more likely to be male in both samples (MRI: $p=0.01$ and $p=0.008$, and FDG $p=0.008$ and $p=0.026$, respectively), and *ZCWPW1* risk allele carriers were significantly less educated and had higher MMSE scores in both samples (MRI $p=0.0012$ and $p=0.034$, and FDG $p=0.025$ and $p=0.034$, respectively). For completeness, the allele dosage for all 27 variants including the ones not retained in the models can be seen in **Tables 13 and 14**.

Table 11. MRI descriptives

Descriptive characteristics and distribution of the genotypes of the study groups who received MRI.

| VARIABLES | NC (N=441) | MCI (N=764) | DEM (N=294) | p-value |
|---|-----------------------|------------------------|------------------------|------------------|
| Age , mean years (SD) | 74.1 (5.7) | 72.6 (7.6) | 74.6 (7.9) | <0.001 |
| Sex , N male (%) | 222 (50%) | 453 (59%) | 165 (56%) | 0.010 |
| Education , mean years (SD) | 16.4 (2.6) | 16.0 (2.8) | 15.2 (3.0) | <0.001 |
| MMSE , Mean (SD) | 29.1 (1.1) | 27.6 (1.8) | 23.3 (2.1) | <0.001 |
| APOE4 , %0/1/2 | 71/27/2 | 49/40/11 | 34/47/19 | <0.001 |
| ABCA7 rs3752246 , % 0/1/2 | 69/29/2 | 68/28/4 | 67/30/3 | 0.580 |
| CELF1 rs10838725 , % 0/1/2 | 46/45/9 | 44/46/10 | 45/48/7 | 0.450 |
| EPHA1 rs11771145 , % 0/1/2 | 44/44/12 | 43/45/12 | 45/42/13 | 0.950 |
| FERMT2 rs17125944 , % 0/1 | 85/15 | 84/16 | 78/22 | 0.020 |
| INPP5D rs35349669 , % 0/1/2 | 30/48/22 | 30/46/24 | 26/51/23 | 0.520 |
| SLC24A4/RIN3 rs10498633 , % 0/1/2 | 60/35/5 | 61/34/5 | 60/35/5 | 0.990 |
| ZCWPW1 rs1476679 , % 0/1/2 | 50/41/9 | 51/41/8 | 60/33/7 | 0.080 |

Table 12. FDG descriptives

Descriptive characteristics and distribution of the genotypes of the study groups who received FDG PET

| VARIABLES | NC (N=381) | MCI (N=634) | DEM (N=243) | p-value |
|---|-----------------------|------------------------|--------------------|------------------|
| Age, mean years (SD) | 74.3 (6.2) | 72.6 (7.6) | 75.0 (7.7) | <0.001 |
| Sex, N male (%) | 190 (50%) | 380 (60%) | 148 (61%) | 0.003 |
| Education, mean years (SD) | 16.4 (2.7) | 16.1 (2.7) | 15.4 (2.9) | <0.001 |
| MMSE, Mean (SD) | 29.0 (1.2) | 27.8 (1.8) | 23.1 (2.8) | <0.001 |
| APOE4, %0/1/2 | 73/25/2 | 51/38/11 | 33/50/17 | <0.001 |
| CD2AP rs9349407, % 0/1/2 | 49/44/7 | 53/40/7 | 49/40/11 | 0.220 |
| CELF1 rs10838725, % 0/1/2 | 48/42/10 | 44/46/10 | 43/50/4 | 0.270 |
| CLU rs11136000, % 0/1/2 | 36/50/14 | 37/50/13 | 43/42/15 | 0.280 |
| CLU rs9331949, % 0/1 | 95/5 | 97/3 | 95/5 | 0.310 |
| CR1 rs12034383, % 0/1/2 | 14/49/37 | 15/48/37 | 21/46/33 | 0.190 |
| DSG2 rs8093731, % 0/1 | 98/2 | 98/2 | 97/3 | 0.840 |
| EPHA1 rs11771145, % 0/1/2 | 44/44/12 | 45/42/13 | 43/44/13 | 0.940 |
| EPHA1 rs11767557, % 0/1/2 | 66/30/4 | 70/27/3 | 63/34/3 | 0.290 |
| MS4A6A rs610932, % 0/1/2 | 31/48/21 | 37/47/16 | 38/45/17 | 0.250 |
| NME8 rs2718058, % 0/1/2 | 39/47/14 | 40/45/15 | 38/49/13 | 0.880 |
| PTK2B rs28834970, % 0/1/2 | 42/42/16 | 42/42/16 | 39/49/12 | 0.390 |
| SLC24A4/RIN3 rs10498633, % 0/1/2 | 61/34/5 | 62/34/4 | 58/37/5 | 0.870 |
| SORL1 rs11218343, % 0/1 | 91/9 | 92/8 | 93/7 | 0.550 |

Table 13. MRI FWE and/or FDR significant clusters

Family-wise error (FWE) and False Discovery Rate (FDR) corrected cluster analyses and within-cluster peak effects for the genetic variants identified in the exploratory MRI analyses

| DX Group | Gene variant | cluster-level | | | | peak level | | Talairach coordinates | Brain Region (Brodmann Area, BA) |
|----------|-----------------------------------|-------------------|-------------------|-----------|-----------------|------------|-----------------|-----------------------|----------------------------------|
| | | <i>p</i> FWE-corr | <i>q</i> FDR-corr | <i>kE</i> | <i>p</i> uncorr | <i>T</i> | <i>p</i> uncorr | | |
| DEM | <i>ABCA7</i> rs3752246 | <0.0001 | <0.0001 | 924757 | <0.0001 | 9.72 | <0.0001 | -11 -23 63 | L medial frontal gyrus (BA6) |
| | <i>EPHA1</i> rs11771145 | 0.04 | 0.051 | 13081 | 0.001 | 3.86 | <0.0001 | -52 -28 61 | L postcentral gyrus (BA2) |
| | | 0.007 | 0.017 | 1889 | <0.0001 | 4.01 | <0.0001 | 52 -30 59 | R postcentral gyrus (BA2) |
| | <i>SLC24A4/RIN3</i> rs10498633 | 0.007 | 0.012 | 18621 | <0.0001 | 3.78 | <0.0001 | -14 1 46 | L cingulate gyrus (BA24) |

NC – Cognitively normal; DEM - Dementia; *p*FWE-corr - Family Wise Error-corrected p-value; *q*FDR-corr - False Discovery Rate-corrected q-value; *kE* - cluster size; *p*uncorr: - uncorrected p-value; *T* -T statistic

Table 14. FDG FWE and/or FDR significant clusters

Family-wise error (FWE) and False Discovery Rate (FDR) corrected cluster-level analyses and within-cluster peak effects for genetic variants identified in the exploratory FDG PET analyses

| Dx Group | Gene variant | Cluster | | | | Peak Effect | | Talairach coordinates | Brain Region (Brodmann Area, BA) |
|---------------|----------------------------|-----------|-----------|--------|---------------------|-------------|---------------------|--------------------------------|------------------------------------|
| | | pFWE-corr | qFDR-corr | kE | p _{uncorr} | T | p _{uncorr} | | |
| POOLED SAMPLE | CLU rs1113600 | <0.0001 | <0.0001 | 5979 | <0.0001 | 4.02 | <0.0001 | -48 -4 -32 | L inferior temporal gyrus (BA20) |
| | | 0.027 | 0.025 | 1493 | <0.0001 | 4.01 | <0.0001 | 64 -18 8 | R transverse temporal gyrus (BA42) |
| | EPHA1 rs11771145 | 0.049 | 0.102 | 1314 | 0.0001 | 3.8 | <0.0001 | -14 -50 60 | L superior parietal lobule (BA7) |
| | MS4A6A rs610932 | 0.001 | 0.001 | 2723 | <0.0001 | 4.28 | <0.0001 | 40 -14 42 | R precentral gyrus (BA4) |
| | PTK2B rs28834970 | 0.002 | 0.003 | 2426 | <0.0001 | 3.96 | <0.0001 | -2 -74 -2 | L lingual gyrus (BA18) |
| NC | CELFI rs10838725 | 0.004 | 0.004 | 1960 | <0.0001 | 4.19 | <0.0001 | 20 -66 44 | R precuneus (BA7) |
| | | <0.0001 | <0.0001 | 2718 | <0.0001 | 3.88 | <0.0001 | 0 52 -12 | L medial frontal gyrus (BA10) |
| | | 0.017 | 0.012 | 1514 | <0.0001 | 3.5 | <0.0001 | 32 -38 -4 | R sub-gyral, hippocampus |
| | CR1 rs12034383 | <0.0001 | <0.0001 | 37014 | <0.0001 | 4.98 | <0.0001 | 18 -36 30 | R cingulate gyrus (BA31) |
| | DSG2 rs8093731 | 0.017 | 0.008 | 1515 | <0.0001 | 4.15 | <0.0001 | 6 -4 50 | R medial frontal gyrus (BA6) |
| | PTK2B rs28834970 | <0.0001 | <0.0001 | 6279 | <0.0001 | 4.24 | <0.0001 | 44 -22 6 | L superior temporal gyrus (BA13) |
| | | <0.0001 | <0.0001 | 6722 | <0.0001 | 3.98 | <0.0001 | -42 -36 12 | L superior temporal gyrus (BA41) |
| | SLC24A4/RIN3 rs10498633 | <0.0001 | <0.0001 | 20054 | <0.0001 | 4.38 | <0.0001 | 22 -4 -30 | R parahippocampal gyrus (BA36) |
| 0.007 | | 0.004 | 1767 | <0.001 | 3.71 | <0.0001 | -22 -8 -30 | L parahippocampal gyrus (BA36) | |
| DEM | NME8 rs2718058 | <0.001 | <0.001 | 3551 | <0.001 | 4.52 | <0.0001 | -14 -88 30 | L cuneus (BA19) |

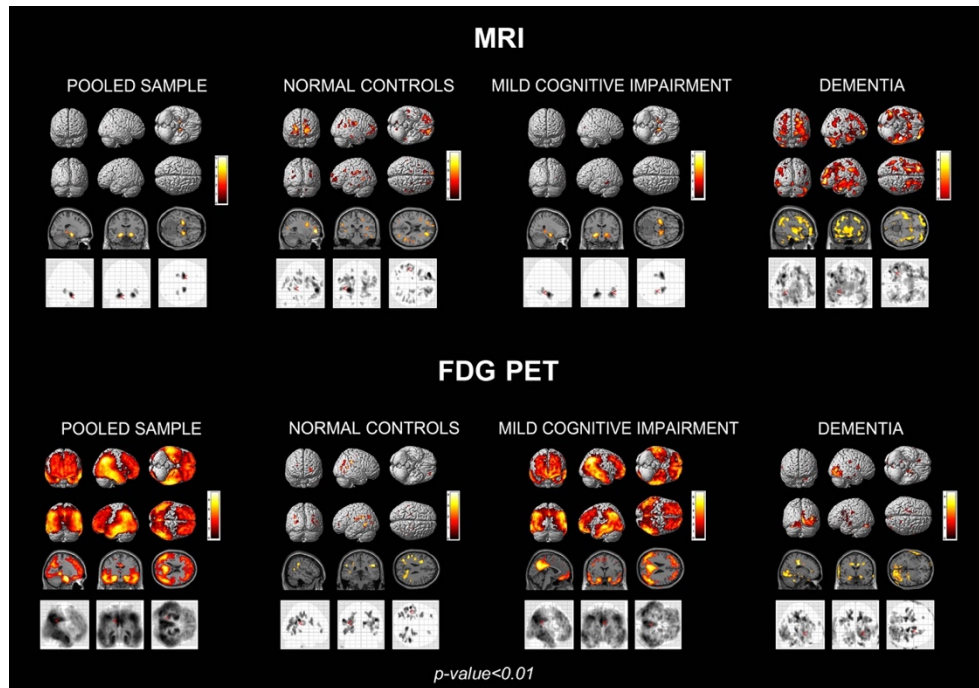
NC – Cognitively normal; DEM - Dementia; pFWE-corr - Family Wise Error-corrected p-value; qFDR-corr - False Discovery Rate-corrected q-value; kE - cluster size; p_{uncorr} - uncorrected p-value; T - T statistic

APOE4 showed the expected negative association with GMD in the NC and MCI group (**Figure 8** top). In the symptomatic MCI group, I saw a strong hippocampo-centric pattern, indicating that MCI carriers had greater hippocampal loss of GMD compared to MCI noncarriers. In the dementia group, I found the opposite association. *APOE4*-negative dementia subjects had greater cortical loss of GMD than *APOE4*-positive subjects, indicative of greater cortical neurodegeneration. *APOE4* was associated with widespread hypometabolism in the MCI group (**Figure 8** bottom). *APOE4* showed a much less pronounced effect in the dementia stage indicating that both carriers and noncarriers experienced significant, widespread hypometabolic changes.

Figure 8. APOE4 effect

APOE4 Effect on brain atrophy (top) and hypometabolism (bottom).

Results are displayed using $p < 0.01$ (uncorrected) and cluster size (k) of 50 voxels.



MRI Analyses

Pooled sample:

In the pooled sample the stepwise linear regression model achieved an $R^2=0.4$, $p<0.0001$. *SLC24A4/RIN3* rs10498633 was the only variant that was significantly associated with mean medial temporal lobe thickness in the pooled sample ($\chi^2=11.8$, $p=0.003$). *ABCA7* rs3752246 and *FERMT2* rs17125944 were retained in the regression output based on the selection criteria but were not statistically significant. See **Figure 9** for the exploratory visualization of these associations and **Table 13** for FWE- and FDR-corrected cluster-level results and within-cluster peak effects for genetic variants identified in the models.

Analyses within diagnostic groups:

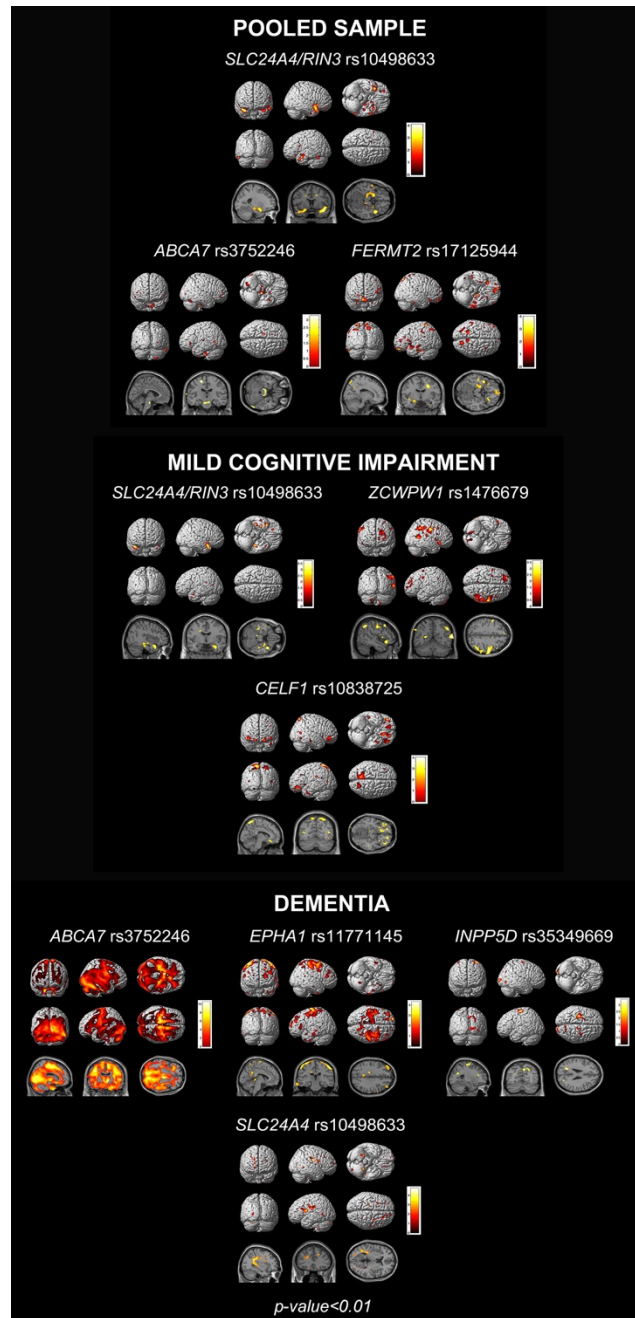
I found neither significant nor trend level associations in the NC group. In the MCI group the model achieved an $R^2=0.26$. *SLC24A4/RIN3* rs10498633 ($\chi^2=11.3$, $p=0.004$) and *ZCWPW1* rs1476679 ($\chi^2=7.3$, $p=0.026$) reached significance. *CELF1* rs10838725 ($\chi^2=5.2$, $p=0.073$) was trending. In the dementia group the model achieved an $R^2=0.19$, $p<0.0001$. *ABCA7* rs3752246 ($\chi^2=8.5$, $p=0.014$), *EPHA1* rs11771145 ($\chi^2=11.6$, $p=0.003$) and *INPP5D* rs35349669 ($\chi^2=6.4$, $p=0.042$) were significantly associated with mean medial temporal lobe thickness. *SLC24A4/RIN3* rs10498633 ($\chi^2=5.4$, $p=0.068$) was trending. See **Figure 9** for the exploratory pattern of these associations.

Next, I repeated the pooled sample analyses introducing interaction terms between the genetic variants retained in the models and diagnosis. The following variants showed significant interaction effect with diagnosis - *EPHA1* rs11771145

($F=3.2$, $p=0.01$) and *SLC24A4/RIN3* ($F=2.7$, $p=0.03$). Please note that the R statistical analyses and the analyses in imaging space might differ as in the R statistics model I use a circumscribed ROI – in the case of MRI the medial temporal region while the whole brain exploratory results show the effect of the variant across the brain.

Figure 9. MRI SPM results

Regression selected genes associated with MRI measured GMD. Results are displayed at significance threshold of uncorrected $p < 0.01$ and minimum cluster size (k) of 50 voxels.



FDG PET Analyses

Pooled sample:

In the pooled sample, the stepwise linear regression model achieved an $R^2=0.13$, $p<0.0001$. *EPHA1* rs11767557 showed significant associations with brain metabolism ($\chi^2=6.3$, $p=0.042$). *PTK2B* rs28834970 ($\chi^2=5.6$, $p=0.059$), *MS4A6A* rs610932 ($\chi^2=5.5$, $p=0.065$) and *SLC24A4/RIN3* rs10498533 ($\chi^2=4.6$, $p=0.098$) showed trend level associations. *CLU* rs11136000 and *EPHA1* rs11771145 were included in the model based on the selection criteria but were not statistically significant.

See **Figure 10** for the exploratory visualization of these associations and **Table 14** for FWE- and FDR-corrected cluster-level results and within-cluster peak effects for genetic variants identified in the models.

Analyses within diagnostic groups:

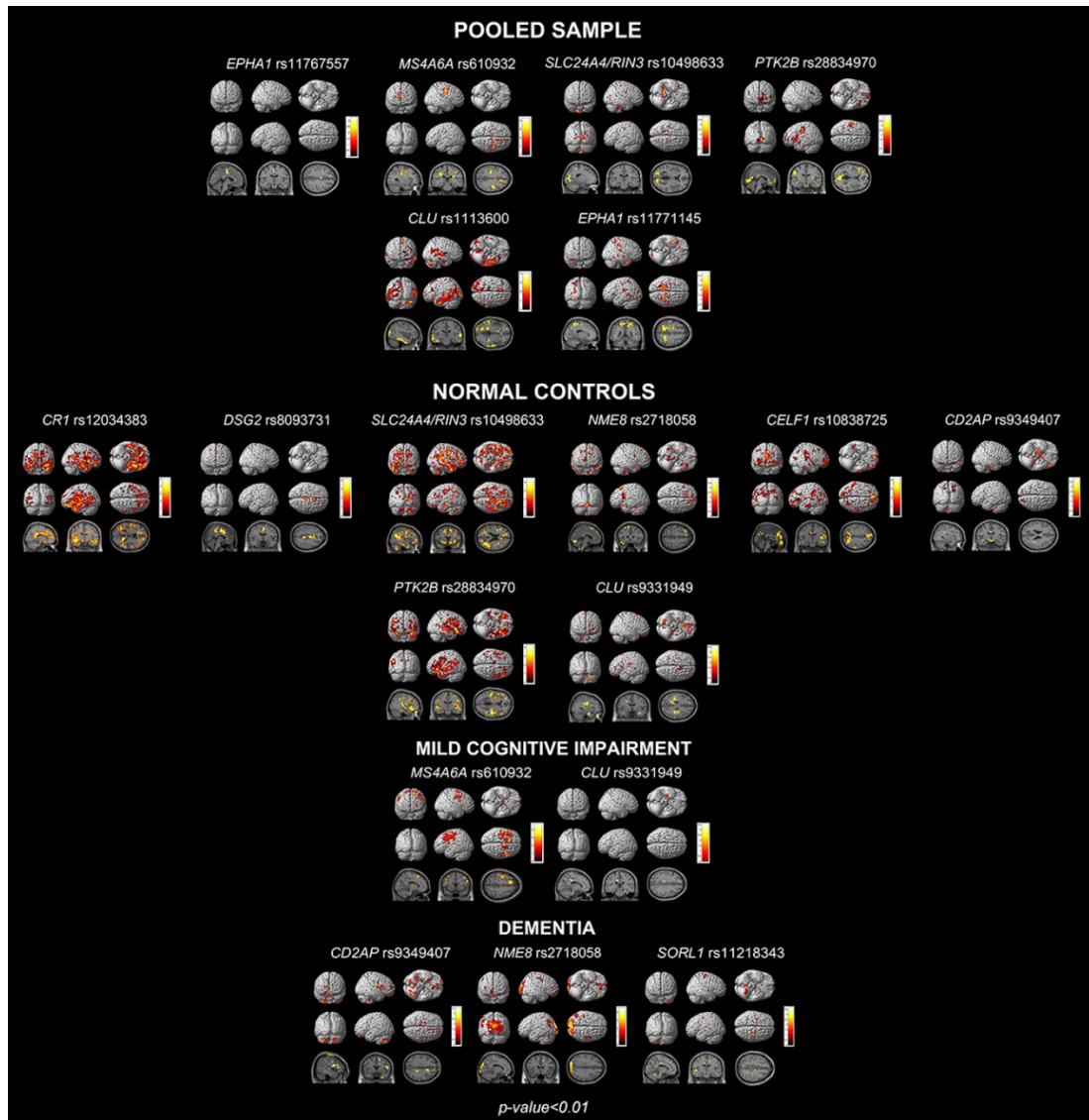
In the NC group the stepwise linear regression model achieved an $R^2=0.14$, $p<0.0001$. *SLC24A4/RIN3* rs10498533 ($\chi^2=6.3$, $p=0.043$), *NME8* rs2718058 ($\chi^2=6.0$, $p=0.049$) and *CD2AP* rs9349407 ($\chi^2=6.1$, $p=0.048$) showed significant associations, while *DSG2* rs8093731 ($\chi^2=3.4$, $p=0.064$), *CR1* rs12034383 ($\chi^2=4.9$, $p=0.087$), and *CELF1* rs10838725 ($\chi^2=5.386$, $p=0.068$) were trending. *CLU* rs9331949 and *PTK2B* rs28834970 were included in the model based on the selection criteria but were not statistically significant. In the MCI group, the stepwise linear regression model achieved an $R^2=0.09$, $p<0.0001$. *CLU* rs9331949 was trending ($\chi^2=3.4$, $p=0.065$) while *MS4A6A* rs610932 was included based on the selection criteria but was not statistically significant. In the

dementia stage the model achieved an $R^2=0.07$, $p=0.034$. *SORL1* rs11218343 showed trend level significance ($\chi^2=3.5$, $p=0.063$) while *NME8* rs2718058 and *CD2AP* rs9349407 were included based on the selection criteria but were not statistically significant. See **Figure 10** for the exploratory visualization of these associations.

Next, I repeated the pooled sample analyses introducing interaction terms between the genetic variants retained in the models and diagnosis. The following variants showed significant interaction effect with diagnosis - *CD2AP* rs9349407 ($F=2.4$, $p=0.04$), *CLU* rs9331949 ($F=3.5$, $p=0.03$) and *NME8* rs2718058 ($F=3.1$, $p=0.01$). *CR1* rs12034383 ($F=2.3$, $p=0.06$) and *SORL1* rs11218343 ($F=2.9$, $p=0.06$) showed trend level interactions. Please note that the R statistical analyses and the analyses in imaging space might differ as in the R statistics model I use a circumscribed ROI – in the case of FDG PET the posterior cingulate region while the whole brain exploratory results show the effect of the variant across the brain.

Figure 10. FDG SPM results

Regression selected genes associated with FDG PET measured brain metabolism. Results are displayed at significance threshold of uncorrected $p < 0.01$ and minimum cluster size (k) of 50 voxels.



3.4. Discussion:

To my knowledge, this is the first comprehensive analysis of the effect of the top 20 AD risk variants on MTL GMD and PCC brain metabolism. In the MRI analyses, I found no genetic influences on GMD in NC. In the MCI stage, *SLC24A4/RIN3* rs10498633 and *ZCWPW1* rs1476679 showed significant effects while in the dementia stage *ABCA7* rs3752246, *EPHA1* rs11771145 and *INPP5D* rs35349669 were significantly associated with GMD. In the FDG PET analyses, the only significant associations were seen in the NC control group for *SLC24A4/RIN3* rs10498533, *NME8* rs2718058 and *CD2AP* rs9349407. The reported associations of *ABCA7*, *ZCWPW1*, and *INPP5D* with GMD, and *CD2AP* with PCC brain metabolism are novel.

Many of the variants displayed stage-specific associations, which is likely due to the nature of AD pathological biomarker changes from the presymptomatic stage to dementia. These stage-specific associations are in agreement with the biomarker progression as proposed by Jack et al.¹¹⁴. Jack's biomarker progression model postulates that neurodegenerative changes begin in the late asymptomatic stages as NC individuals start to transition to MCI¹¹⁴ and that FDG PET abnormalities precede brain atrophy¹¹⁴. Both neurodegenerative biomarkers become progressively more abnormal over the course of the disease. My findings agree with this model. The results indicate neither significant nor trend level associations with GMD in the NC group, but significant associations were detected in the MCI and dementia stages. I also see a modality effect progression that fits with the Jack model. *SLC24A4/RIN3*

shows significant association with brain metabolism in the presymptomatic stages and associations with GMD in the MCI group.

Recent analyses on the top 20 AD genes and brain amyloidosis revealed that, after *APOE4*, *ABCA7* had the strongest effect on brain amyloidosis, with the effect being most pronounced in the MCI stage ¹⁵³. In the present study, I observe a strong association of *ABCA7* with GMD in the dementia group. These associations also seem to follow the biomarker progression, as A β deposition begins in the presymptomatic to early MCI phase and global decreases in GMD begins in late MCI to dementia phase. Associations of *ABCA7* with brain atrophy ¹²⁹ and amyloidosis ¹³⁹⁻¹⁴¹ have been previously reported.

In a similar manner, my previous work showed that *EPHA1*'s strongest effect on brain amyloidosis is in the prodromal phase ¹⁵³. In the present study, the MRI results show a significant association with GMD in the dementia stages only. To date, two additional studies have described *EPHA1* associations with brain atrophy ^{154,155} and one also detected an association with brain metabolism as I did here ¹⁵⁴.

Next, I found it pertinent to briefly review the literature on the function and central nervous system associations for each of the genes in the models.

ABCA7

ATP-Binding Cassette Sub-Family A Member 7 (*ABCA7*) encodes a 2,146 amino acid member of the ABC transporter family comprised of proteins involved in lipid transport ¹⁵⁶. *ABCA7* is highly expressed in the central nervous system

and in microglia ¹⁵⁷. Loss of function of endogenous *ABCA7* increases β -secretase cleavage of APP to A β in brain lysates and in murine models ¹⁵⁸. 15 *ABCA7* loci were recently evaluated for associations with cerebrospinal fluid A β and tau levels, brain atrophy, and brain hypometabolism. Several *ABCA7* variants had significant associations with amyloid deposition, though an association with brain atrophy was not reported there ¹⁵⁹. However, another group has previously found such an association in a different independent imaging genetic cohort ¹²⁹. Additionally, one rare missense mutation variant of *ABCA7*, rs7297358, was found to be protective for AD ¹⁶⁰.

CD2AP

The CD2 associated protein gene (*CD2AP*) encodes a 639 amino acid scaffolding protein that is named by its association with the T-cell and natural killer cell adhesion molecule cluster of differentiation 2 (CD2). *CD2AP* is a cytokinetic regulator that might be influencing neuronal survival by reducing the potency of glial cell derived neurotrophic factor ¹⁶¹. In cell culture, *CD2AP* suppression results in lower levels of APP, less A β release, and a lower A β_{42} /A β_{40} ratio while having little to no effect on A β deposition ¹⁶². *CD2AP* knockdown significantly increases A β protein levels while APP remained at a similar level to the wild-type ¹⁶³. Recent research in *CD2AP* knockout mice shows that *CD2AP*'s association with LOAD risk may be at least in part due to an effect on the cerebrovascular unit ¹⁶⁴. To my knowledge, there are no reported imaging associations of *CD2AP* to date.

EPHA1

EPH Receptor A1 (*EPHA1*) belongs to the EPH family of receptor tyrosine kinases. *EPHA1* codes for a 976 amino acid protein with a single kinase domain¹⁶⁵. *EPHA1* is highly expressed in cerebral cortex and hippocampus (<http://www.proteinatlas.org/ENSG00000146904-EPHA1/tissue>) and plays a crucial role in cortical and axonal development^{166,167}. *EPHA1* directs contact-dependent bidirectional signaling by binding the membrane-bound ephrin-A family of ligands^{168,169}. As already discussed, *EPHA1* has been previously associated with brain atrophy and brain metabolism^{154,155}.

INPP5D

Inositol Polyphosphate-5-Phosphatase D (*INPP5D*) encodes a 1,888 amino acid protein that plays a role in a number of inflammatory pathways and in regulation, of cytokine signaling^{170,171}. *INPP5E*, a closely related gene to *INPP5D*, is a crucial regulator of autophagy¹⁷². Autophagy has been shown in many instances to be dysregulated in AD¹⁷³⁻¹⁷⁵. *INPP5D* may also play a role in suppression of cytokine release from microglia or astrocytes¹⁷⁶. *INPP5D* has been significantly associated with several central nervous system pathologies, including macroscopic and microscopic infarcts, Lewy bodies, and hippocampal sclerosis¹⁷⁷.

NME8

NME Family Member 8 (*NME8*) encodes a 588 amino acid protein kinase. Until recently *NME8* was associated with non-neurologic diseases such as primary ciliary dyskinesia ¹⁷⁸ and osteoarthritis ^{179,180}. In a recent ADNI study, however, *NME8* rs2718058 was shown to have a neuroprotective effect against hippocampal atrophy and brain hypometabolism ¹⁸¹.

SLC24A4/RIN3

Solute Carrier Family 24 (Sodium/Potassium/Calcium Exchanger) Member 4 (*SLC24A4*)/Ras and Rab Interactor 3 (*RIN3*) are indicated in AD together because the candidate polymorphism lies between both genes on chromosome 14q32.12. *SLC24A4* encodes a 622 amino acid potassium-dependent sodium-calcium exchanger ¹⁸². *SLC24A4* appears to take part in lipid metabolism ¹⁸³. *SLC24A4* CpG methylation sites were also associated with A β burden and tau pathology ¹⁸⁴. In a recent study, *SLC24A4* knockout mice showed brain glucose hypometabolism ¹⁸⁵. Interestingly, I found a similar effect in NC.

RIN3 encodes a 985 amino acid guanine exchange factor for RAB5B and RAB31 and plays an important role in the transport of early endosomes ^{186,187}. In a transgenic model, a mutation in APP was shown to contribute to early endosomal abnormalities and enlargement, which leads to loss of cholinergic neurons ¹⁸⁸. RAB GTPase expression is increased in MCI subjects and in aging brains ¹⁸⁹. *RIN3* also interacts with *BIN1*, which has recently been linked to tau

pathology¹⁹⁰. To my knowledge there are no reported imaging associations of *RIN3* to date.

ZCWPW1

Zinc Finger CW-Type and PWWP Domain Containing 1 (*ZCWPW1*) codes for a 648 amino acid protein that has recently been identified as a risk variant for late-onset AD¹⁹¹. Zinc fingers including *ZCWPW1* are crucial components of epigenetic regulation¹⁹²⁻¹⁹⁴. To my knowledge, there are no reported imaging associations of *ZCWPW1* to date.

The *APOE4* effect on cortical gray matter density warrants some discussion. Structurally, I found the expected negative association of *APOE4* with gray matter density in NC and MCI with a strong predilection for the medial temporal lobe. In the dementia group, however, *APOE4*-negative individuals showed more profound atrophy than *APOE4* carriers with a broad neocortical distribution. Given that a far greater proportion of *APOE4* negative dementia subjects were amyloid negative (94% vs. 28% of the amyloid positive dementia subjects, $p < 0.0001$) one could safely conclude that the profound cognitive decline of many of these subjects is due to other neurodegenerative diseases. Thus, the finding greater atrophy in *APOE4* noncarrier dementia subjects in extra-hippocampal locations is not surprising.

3.5. Strengths and Limitations:

Several strengths and limitations of my work are worth noting. The major strength of my study is the multivariable approach. This allows for more accurate modeling of the associations with AD biomarkers as they exist *in vivo*. Using ADNI is another strength as the ADNI protocol includes a rigorous clinical, biomarker, and genetic characterization for all enrolled subjects. By standardizing their data collection and processing strategies ADNI minimizes between-site variations as much as possible. ADNI is a multisite study modeled by clinical trials. As such, ADNI uses more stringent inclusion and exclusion criteria typical of clinical trial methodology. Hence all observations made here need to be further replicated in the general population. Another limitation is that the study design is a cross-sectional analysis. From the data alone it is not possible to reliably draw conclusions about changes in metabolism or atrophy over time. I do, however, intend to address this in future studies by taking a longitudinal approach to my work. Despite this limitation, this study has identified several key genes they may exert their effect in specific stages, which need to be examined in future research.

3.6. Conclusions:

In conclusion, I found several AD risks and protective loci that may play a key role in GMD and brain metabolism. I also noted stage-specific associations for certain variants, which may follow a specific progression of AD biomarkers

throughout the disease. Importantly, many of these stage associations take place in the context of the proposed biomarker timeline.

Chapter 4. Association of the top 20 Alzheimer's disease risk genes with [¹⁸F]Flortaucipir PET

4.1. Introduction:

An estimated 5.8 million people in the United States currently living with Alzheimer's disease (AD) ². In contrast to the dominantly inherited mutations attributed to familial early-onset AD, which are seen in amyloid precursor protein (*APP*), presenilin 1 (*PSEN1*) and presenilin 2 (*PSEN2*) genes, sporadic AD arises from a variety of risk factors both genetic and environmental ⁶⁸⁻⁷⁰.

Understanding the complex network of genetic risk factors contributing to sporadic AD has been challenging. For a long time, the only risk gene associated with sporadic AD was the apolipoprotein E (*APOE*) gene. *APOE* has a dose-dependent risk, where one copy of the e4 allele triples AD risk while two copies increase risk by as much as 15-fold. Although this variant confers a large amount of risk, current estimations cite *APOE* e4 (*APOE4*) as accounting for less than half of the total genetic hazard ^{73,195}.

To explain the remaining genetic component, large-scale genome-wide association studies (GWAS) and meta-analysis of GWAS have identified risk variants near 20 genes involved in pathways such as cholesterol metabolism, immune response and endocytosis ^{78-80,196-198}. Though each of these variants contributes to a relatively small amount of the overall risk, inheriting multiple risk alleles may result in summation and a greater overall risk profile. Though function is known for many of the genes, a small number have no certain

function, and even fewer are understood as they relate to dysfunction seen during the progression of Alzheimer's.

Through the use of imaging genetics, I previously associated the top AD GWAS-identified variants with amyloidosis, brain metabolism and atrophy ^{113,199}. In addition to using a polygenic model to find variant associations with AD-specific disease biomarkers or endophenotypes, I found *stage-dependent* associations with *FERMT2* (amyloid positron emission tomography, PET), *EPHA1* and *SLC24A4/RIN3* (MRI) and *CD2AP*, *CLU* and *NME8* (FDG PET) in each of the three diagnostic groups, cognitively normal (CN), mild cognitive impairment (MCI) and AD dementia (DEM) subjects, indicating that the genetic impact on AD evolves as the disease progresses. This strategy was particularly important to better understanding genotype-endophenotype interactions in AD, which follows a known pathophysiologic progression consisting of early amyloid deposition followed many years later by the accumulation of tau and finally neuronal degeneration ²⁶.

The addition of tau PET neuroimaging to ADNI protocol affords the opportunity to conduct a comprehensive polygenic analysis of the associations of GWAS-validated AD risk variants with cortical tau burden, which was measured via [¹⁸F]Flortaucipir PET. The goal of this study was to establish the relative genetic contribution to tau burden using stepwise multivariable regression as I have done previously for brain amyloidosis and neurodegeneration ^{113,199}.

4.2. Methods:

Participants

Data used in the preparation of this article were obtained from the Alzheimer's Disease Neuroimaging Initiative (ADNI) database (adni.loni.usc.edu). ADNI was launched in 2003 as a public-private partnership, led by Principal Investigator Michael W. Weiner, MD. The primary goal of ADNI has been to test whether serial MRI, PET, other biological markers, and clinical and neuropsychological assessment can be combined to measure the progression of MCI and early AD. For up-to-date information, see www.adni-info.org.

The clinical description of the ADNI cohort has been previously published^{85,200,201}. Diagnosis of AD was based on the National Institute of Neurological and Communicative Disorders and Stroke and the Alzheimer's Disease and Related Disorders Association criteria^{33,34,202}. Individuals with AD dementia were required to have Mini-Mental State Examination (MMSE)⁸⁶ scores between 20 and 26 and a Clinical Dementia Rating (CDR) score of 0.5 to 1 at baseline⁸⁷. Qualifying individuals with MCI had memory concerns but no significant functional impairment, scored between 24 and 30 on the MMSE, had a global CDR score of 0.5, had a CDR memory score of 0.5 or greater, and had objective memory impairment on the Wechsler Memory Scale–Logical Memory II test²⁰³. The controls had MMSE scores between 24 and 30, had a global CDR score of 0 and did not meet criteria for MCI and AD. Individuals were excluded if they refused or were unable to undergo MRI, had other neurologic disorders, active depression, a history of psychiatric diagnosis, a history of alcohol or other

substance dependence within the past 2 years, had less than 6 years of education, or were not fluent in English or Spanish. The full list of inclusion and exclusion criteria are listed in the online ADNI protocol (http://adni.loni.usc.edu/wp-content/uploads/2010/09/ADNI_GeneralProceduresManual.pdf). Written informed consent was obtained from all participants. Only de-identified data were used in these analyses.

I included all ADNI subjects with available genetic data and [¹⁸F]Flortaucipir scans. This resulted in a sample containing 135 CN, 98 MCI and 43 DEM subjects.

Gene Variant Selection and Imputation

Participants were genotyped using either the Illumina Human610-Quad BeadChip (ADNI 1) or Illumina HumanOmniExpress BeadChip (ADNI GO/2) arrays and intensity data was processed using GenomeStudio v2009.1 according to Illumina Inc. protocols.

Similar to my previous studies, I narrowed my focus to variants in the top 20 well-established AD risk genes identified and validated in the largest AD GWAS to date. I also included all other variants contained within these genes that have previously been associated with brain amyloidosis. The full list, which contained a total of 36 variants, can be seen in **Table 8**.

Missing genotypes (**Table 9**) were imputed using MACH and minimac, relying on the 1000 Genomes project data as a reference panel. Posterior

probabilities of the imputed genotypes for each individual were determined in minimac, where I used a threshold of $r^2=0.30$ to accept the imputed genotype.

For the nine genes containing more than one SNP, I performed linkage disequilibrium analysis (LD), followed by Cohen κ statistics to guard against collinearity bias (**Table 10** and **Figure 7**). In situations where variants had significant overlap (high LD and high κ), I retained the variant with the least amount of missing data. 27 variants were included in the final regression models including multiple variants from the *ABCA7*, *BIN1*, *CLU*, *CR1*, *EPHA1* and *SORL1* genes that were not in LD.

Genotypes were coded by the copy number of the minor alleles (0/1/2 copies), however, when minor allele homozygote frequency was less than 2% the genotype was collapsed into the presence or absence of minor allele (coded as 1 and 0, resp.). This was the case for five of the variants; *ABCA7* rs3764650, *CASS4* rs7274581, *CLU* rs9331949, *DSG2* rs8093731, *FERMT2* rs17125944, and *SORL1* rs11218343.

[¹⁸F]Flortaucipir PET Data Acquisition Protocol and Analyses

Standardized [¹⁸F]Flortaucipir acquisition and preprocessing protocols can be found at www.adni-info.org. In the main analysis, I downloaded the ADNI UC Berkeley [¹⁸F]Flortaucipir partial volume corrected (PVC) standardized uptake value ratio (SUVR) Freesurfer 6.0 defined regions from ADNI's website (<http://adni.loni.usc.edu>), where the processing methods for UC Berkeley can also be found. I computed a size-weighted Alzheimer's-specific meta-ROI using the *a priori* regions defined by Jack et al. in 2016, which contains entorhinal,

amygdala, parahippocampal, fusiform, inferior temporal, and middle temporal regions^{204,205}. The meta-ROI was then intensity-normalized to the inferior cerebellar grey-matter reference region (defined by UC Berkeley using the SUI template)²⁰⁶. Meta-ROI SUVRs were then matched to subject genotype data.

Statistical Analysis

Clinical, demographic, and biomarker values of interest (age, sex, educational level, *APOE* e4 genotype, MMSE, [¹⁸F]Florbetapir mean cortical SUVR and [¹⁸F]Flortaucipir meta-ROI SUVR) for each diagnostic group (CN, MCI and DEM) were compared using ANOVA or χ^2 tests with 2-sided p-values as appropriate. Variant association with [¹⁸F]Flortaucipir meta-ROI SUVR was determined using multivariable stepwise linear regression models in SAS 9.4, with all 27 AD risk variants, first in the pooled sample and then in each diagnostic category using [¹⁸F]Flortaucipir meta-ROI SUVR as the outcome measure. All regression models included age, sex, and *APOE* e4 genotype as covariates, while the pooled sample also controlled for diagnosis. Model selection was based on the Akaike information criterion (AIC) critical p-value threshold of 0.157¹⁵². I also provide false discovery rate (FDR)-corrected p-values for each variant retained to protect against type I errors.

Analysis in Imaging Space

Next, I visualized the selected variant spatial effects in SPM12. Preprocessed [¹⁸F]Flortaucipir scans were downloaded from ADNI, where PET frames were coregistered, averaged, image and voxel size were standardized and smoothed to a uniform resolution. Using SPM12, each subject's pre-

processed [¹⁸F]Flortaucipir scan was then coregistered to that subject's closest-visit MRI, normalized into MNI space and intensity normalized to the cerebellar crus to generate SUVR images. To visualize the spatial distribution of the genetic associations, I reproduced the regression models using voxelwise regression in SPM12, limited to those which survived AIC thresholding. As with the regression modeling in SAS, I covaried for age, sex, and *APOE* e4 genotype, including diagnosis as a covariate in the pooled sample. Due to the exploratory nature of these secondary results, I employed a less stringent voxelwise threshold of uncorrected $p < 0.01$ with a minimum cluster size (k) of 50 voxels. Following this I displayed familywise error (FWE)- and false discover rate (FDR)-corrected cluster-level and within-cluster peak effects for each variant.

4.3. Results:

Group comparisons of demographic, biomarker and carrier distribution of variants retained in the regression models are seen in **Tables 15** and **16**. The sample included 135 CN, 98 MCI and 43 DEM subjects who had available GWAS and [¹⁸F]Flortaucipir data. There were no significant differences in age between groups ($p=0.078$). There were, however, significantly more male participants in the MCI than in the other groups ($p=0.041$). DEM subjects had significantly less education and more *APOE4* carriers than the other two groups ($p=0.015$ and $p=0.003$). I also observed the expected differences in MMSE, [¹⁸F]Flortaucipir SUVR and [¹⁸F]Florbetapir SUVR across diagnostic groups ($p<0.001$ for all). There were no significant diagnostic group differences in minor

allele distribution for any of the gene variants selected in the regression models except for *SLC24A4/RIN3* rs10498633, which had significantly more homozygous carriers in the MCI group ($p=0.030$). *APOE4* showed significant association with tau in the pooled, CN and MCI sample while only minimally so in the DEM group (**Figure 11**).

Investigating for demographic differences between risk gene dosages, I observed no significant differences in age, sex, education or *APOE4* carrier percentage by minor allele distribution among the variants retained in the regression. All the models were corrected for age, gender and *APOE4*.

Table 15. Demographic and biomarker data for each diagnostic group

This table shows a demographic, neuropsychological and imaging measure comparison across each of the diagnostic groups, using ANOVA and chi-square p-values where necessary.

| Variables | CN (N=135) | MCI (N=98) | DEM (N=43) | p-value |
|---|-----------------------|-----------------------|-----------------------|------------------|
| Age, mean years (SD) | 77.7 (6.7) | 79.1 (7.1) | 80.3 (8.1) | 0.078 |
| Sex, % male | 50.4 | 66.3 | 51.2 | 0.041 |
| Education, mean years (SD) | 16.9 (2.4) | 16.2 (3.1) | 15.6 (2.6) | 0.015 |
| APOE4 carrier, % Yes | 30.4 | 38.8 | 51.2 | 0.003 |
| MMSE, mean (SD) | 29.0 (1.3) | 27.5 (2.3) | 21.2 (5.3) | <0.001 |
| Meta-ROI Flortaucipir SUVR (SD) | 1.50 (0.22) | 1.61 (0.29) | 2.32 (1.02) | <0.001 |
| Whole Cerebral Cortical Florbetapir SUVR (SD) | 1.13 (0.18) | 1.18 (0.26) | 1.37 (0.21) | <0.001 |

Table 16. Minor allele distribution for variants retained in the regression models

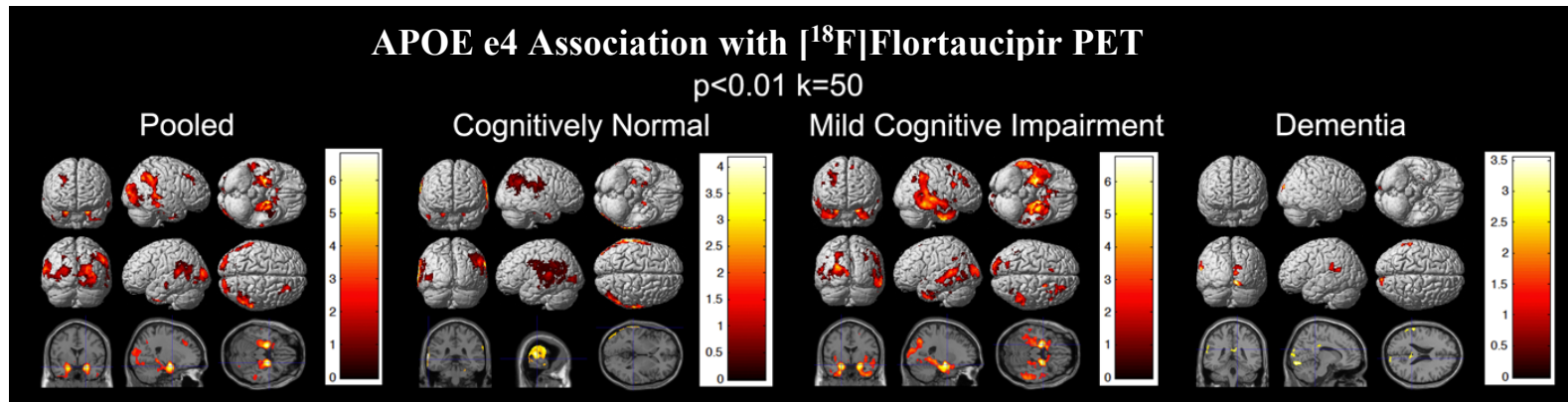
This table shows the percentage of subjects who had each copy number for the genes retained in any of the four regression models. I display by diagnostic group.

| Variables | CN (N=135) | MCI (N=98) | DEM (N=43) | p- value |
|--|-----------------------|-----------------------|-----------------------|---------------------|
| <i>ABCA7</i> rs3752246 %0/1/2 | 68/30/2 | 76/22/2 | 70/28/2 | 0.747 |
| <i>BIN1</i> rs744373 %0/1/2 | 50/39/10 [†] | 42/46/12 | 58/37/5 | 0.361 |
| <i>CLU</i> rs11136000 %0/1/2 | 27/59/13 [†] | 38/45/17 | 40/44/16 | 0.201 |
| <i>CLU</i> rs9331949 %0/1* | 93/7 | 96/4 | 98/2 | 0.336 |
| <i>EPHA1</i> rs11771145 %0/1/2 | 48/39/13 | 45/43/12 | 33/54/14 [†] | 0.463 |
| <i>PICALM</i> rs3851179 %0/1/2 | 40/45/15 | 55/38/7 | 40/51/9 | 0.100 |
| <i>SLC24A4/RIN3</i> rs10498633 %0/1/2 | 64/33/2 [†] | 67/22/10 [†] | 63/35/2 | 0.030 |
| <i>ZCWPW1</i> rs1476679 %0/1/2 | 47/44/10 [†] | 48/41/11 | 70/28/2 | 0.078 |

* Collapsed because minor allele homozygote frequency was <2%

[†] Does not add up to 100% due to rounding

Figure 11. Association of the *APOE* e4 allele with tau deposition



Pooled Sample

In the pooled sample, the stepwise regression model achieved an R^2 value of 0.3294 (**Table 17**). *ABCA7* 3752246 (coefficient=0.093, SE=0.055, p-value=0.0907) and *CLU* rs9331949 (coefficient=0.200, SE=0.120, p-value=0.0987) were associated with tau at a trend level. An exploratory analysis into the patterns of association can be seen in **Figure 12** while the cluster-level and within-cluster peak effects can be seen in **Table 18**.

Table 17. Regression Selected Variants in a Pooled Sample

The selected genes under the AIC threshold of 0.157. In addition to reporting model parameters, I show [¹⁸F]Flortaucipir meta-ROI SUVR by copy number of risk alleles

| Pooled Sample, Model R ² = 0.3294 | | | | | |
|--|--------------------|----------------|--------------------------------|--|--|
| Covariates Selected | Parameter Estimate | Standard Error | p-value/FD R-corrected p-value | [¹⁸ F]Flortaucipir SUVR by risk allele | [¹⁸ F]Flortaucipir p-value |
| <i>ABCA7</i> rs3752246 | 0.093 | 0.055 | 0.0907/0.0987 | 1.64/1.71/ 2.13 | 0.096 |
| <i>CLU</i> rs9331949 | 0.200 | 0.120 | 0.0987/0.0987 | 1.66/1.77 | 0.472 |

Figure 12. Stepwise regression selected genes in a pooled sample (all diagnosis groups)

SPM visualization of association patterns for regression selected genes.

Due to the exploratory nature of this analysis, the p-value was set at an uncorrected $p < 0.01$ and minimum cluster size of 50

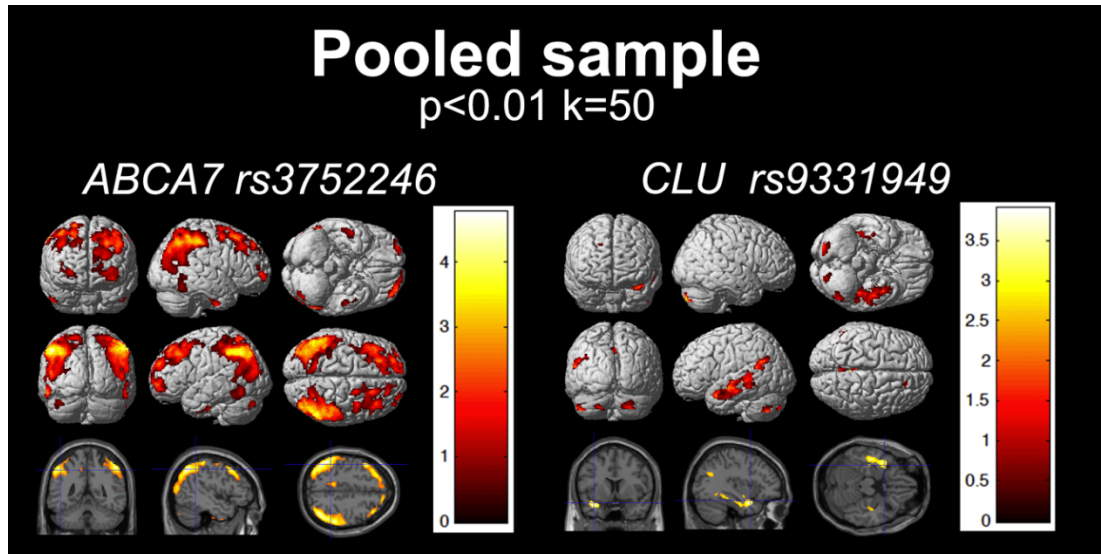


Table 18. Cluster and within-cluster peak level effects for each diagnostic group

This table shows FWE- and FDR-corrected cluster and peak-level values for variants which had at least one cluster FWE- or FDR-corrected $p < 0.05$ (determined in SPM).

| Gene Variant | Cluster Level | | | | Peak Level | | | Brain Region |
|---|-----------------------|-----------------------|----------------------|---------------------|------------|---------------------|----------------------------------|---------------------------------------|
| | FWE-Corrected p-value | FDR-Corrected q-value | Cluster Size, Voxels | Uncorrected p-value | T-value | Uncorrected p-value | Peak Talairach Coordinates x/y/z | |
| Pooled Group | | | | | | | | |
| ABCA7 rs3752246 | 0.001 | 0.004 | 3759 | <0.001 | 4.75 | <0.001 | -50/-54/46 | Left angular gyrus (BA39) |
| | 0.001 | 0.004 | 3540 | <0.001 | 4.57 | <0.001 | 54/-42/50 | Right supramarginal gyrus (BA40) |
| | 0.010 | 0.029 | 2504 | <0.001 | 4.27 | <0.001 | -44/16/48 | Left premotor cortex (BA6) |
| CLU rs9331949 | 0.031 | 0.063 | 1973 | 0.001 | 3.67 | <0.001 | -36/6/-24 | Left temporopolar cortex (BA38) |
| Cognitively Normal Group | | | | | | | | |
| <i>no clusters surviving correction</i> | | | | | | | | |
| Mild Cognitive Impairment Group | | | | | | | | |
| CLU rs9331949 | 0.038 | 0.295 | 1334 | 0.001 | 4.49 | <0.001 | -40/-90/16 | Left associative visual cortex (BA19) |
| PICALM rs3851179 | 0.001 | 0.001 | 2669 | <0.001 | 4.36 | <0.001 | -46/-4/-26 | Left temporopolar cortex (BA38) |
| | <0.001 | 0.001 | 8748 | <0.001 | 4.01 | <0.001 | 32/16/-34 | Right temporopolar cortex (BA38) |
| | 0.043 | 0.033 | 1303 | 0.001 | 3.59 | <0.001 | 46/4/22 | Right pars opercularis (BA44) |
| SLC24A4/RIN3 rs10498633 | 0.039 | 0.052 | 1329 | 0.001 | 3.98 | <0.001 | -62/-32/-2 | Left middle temporal gyrus (BA21) |
| | 0.002 | 0.006 | 2222 | <0.001 | 3.77 | <0.001 | 30/-28/-22 | Right fusiform gyrus (BA37) |
| Dementia Group | | | | | | | | |
| ZCWPW1 rs1476679 | <0.001 | 0.282 | 12855 | <0.001 | 4.44 | <0.001 | -16/8/-20 | Left orbitofrontal cortex (BA11) |

CN Sample

In the sample of CN subjects, the regression model achieved an R^2 of 0.1314 (**Table 19**). *CLU rs9331949* (coefficient=0.200, SE=0.071, p-value=0.0934) was associated with tau burden at a trend-level. Visualization of the patterns of association and the cluster and peak effects can be seen in **Figure 13** and **Table 18**, respectively.

Table 19. Regression Selected Variants in a CN Sample

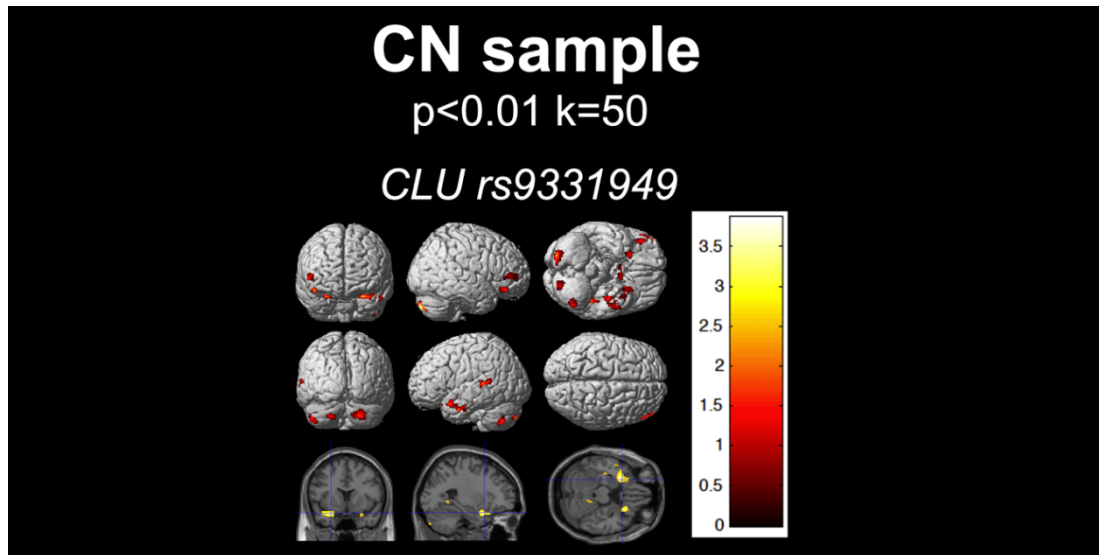
The selected genes under the AIC threshold of 0.157. In addition to reporting model parameters, I show [¹⁸F]Flortaucipir meta-ROI SUVR by copy number of risk alleles

| CN Sample, Model R ² = 0.1314 | | | | | |
|--|--------------------|----------------|--------------------------------|--|--|
| Covariates Selected | Parameter Estimate | Standard Error | p-value/F DR-corrected p-value | [¹⁸ F]Flortaucipir SUVR by risk allele | [¹⁸ F]Flortaucipir p-value |
| <i>CLU</i> rs9331949 | 0.200 | 0.071 | 0.0934/0.0934 | 1.50/1.63 | 0.076 |

Figure 13. Stepwise regression selected genes in the CN group

SPM visualization of association patterns for regression selected genes.

Due to the exploratory nature of this analysis, the p-value was set at an uncorrected $p < 0.01$ and minimum cluster size of 50



MCI Sample

In the MCI sample, the regression model achieved an R^2 of 0.2651 (**Table 20**). *BIN1* rs744373 (coefficient=0.086, SE=0.041, p-value=0.0366) was significantly associated with the Alzheimer's specific tau deposition, while *CLU* rs11136000 (coefficient=-0.071, SE=0.038, p-value=0.0647), *EPHA1* rs11771145 (coefficient=0.069, SE=0.041, p-value=0.0946), *PICALM* rs3851179 (coefficient=-0.079, SE=0.046, p-value=0.0853) and *SLC24A4/RIN3* rs10498633 (coefficient=-0.069, SE=0.040, p-value=0.0872) were associated at a trend level. *CLU* rs9331949 (coefficient=0.202, SE=0.134, p-value=0.1386) was included in the model by meeting the AIC model selection threshold. Visualization of the patterns of association and the cluster and peak effects can be seen in **Figure 14** and **Table 18**, respectively.

Table 20. Regression Selected Variants in an MCI Sample

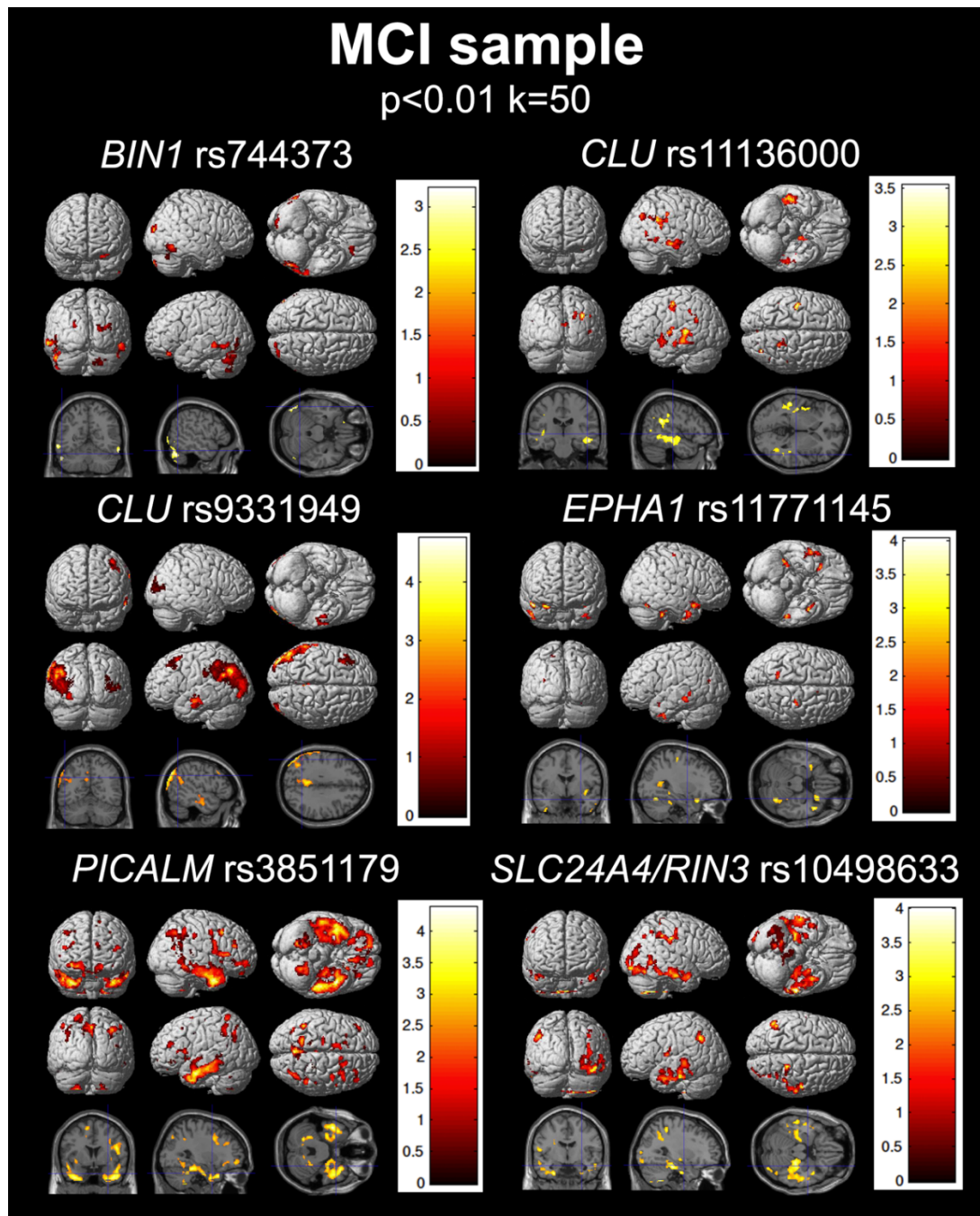
The selected genes under the AIC threshold of 0.157. In addition to reporting model parameters, I show [¹⁸F]Flortaucipir meta-ROI SUVR by copy number of risk alleles

| MCI Sample, Model R² = 0.2651 | | | | | |
|---|---------------------------|-----------------------|--------------------------------------|---|---|
| Covariates Selected | Parameter Estimate | Standard Error | p-value/FDR-corrected p-value | [¹⁸F]Flortaucipir SUVR by risk allele | [¹⁸F]Flortaucipir p-value |
| <i>BIN1</i> rs744373 | 0.086 | 0.041 | 0.0366 /0.1135 | 1.55/1.66/1.61 | 0.225 |
| <i>CLU</i> rs11136000 | -0.071 | 0.038 | 0.0647/0.1135 | 1.66/1.61/1.48 | 0.116 |
| <i>CLU</i> rs9331949 | 0.202 | 0.134 | 0.1386/0.1386 | 1.60/1.81 | 0.149 |
| <i>EPHA1</i> rs11771145 | 0.069 | 0.041 | 0.0946/0.1135 | 1.56/1.65/1.64 | 0.339 |
| <i>PICALM</i> rs3851179 | -0.079 | 0.046 | 0.0853/0.1135 | 1.66/1.53/1.63 | 0.114 |
| <i>SLC24A4/RIN3</i> rs10498633 | -0.069 | 0.040 | 0.0872/0.1135 | 1.65/1.52/1.53 | 0.123 |

Figure 14. Stepwise regression selected genes in the MCI group

SPM visualization of association patterns for regression selected genes.

Due to the exploratory nature of this analysis, the p-value was set at an uncorrected $p < 0.01$ and minimum cluster size of 50



DEM Sample

In DEM subjects, the regression model achieved an R^2 of 0.2545 (**Table 21**). *ZCWPW1* rs1476679 (coefficient=0.518, SE=0.274, p-value=0.0665) was associated to tau deposition at a tend level. Exploratory visualization of the patterns of association, as well as cluster and peak effects, can be seen in **Figure 15** and **Table 18**, respectively.

Table 21. Regression Selected Variants in a DEM Sample

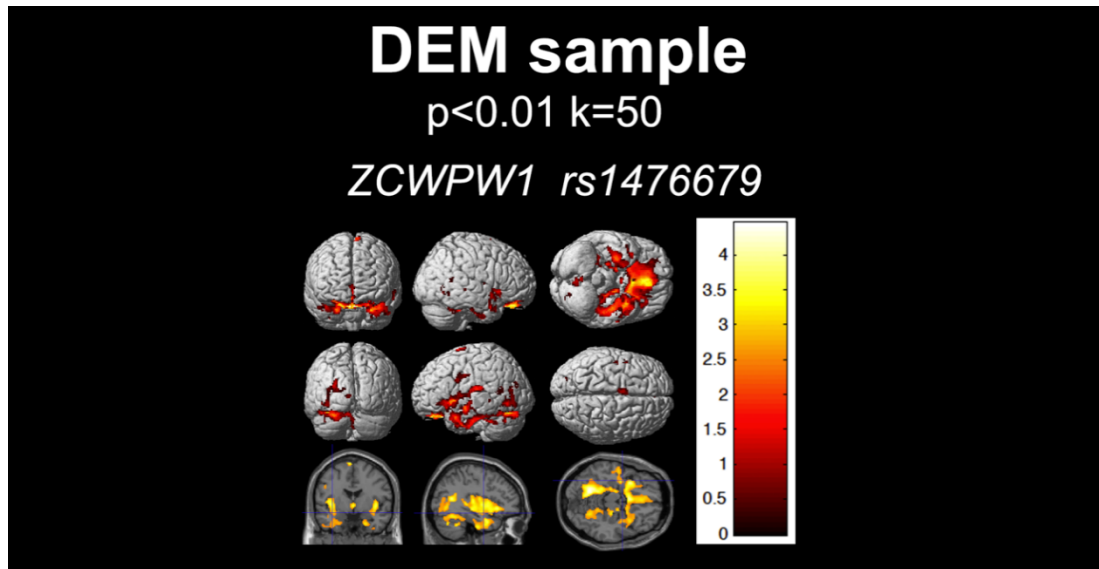
The selected genes under the AIC threshold of 0.157. In addition to reporting model parameters, I show [¹⁸F]Flortaucipir meta-ROI SUVR by copy number of risk alleles

| DEM Sample, Model R² = 0.2545 | | | | | |
|---|---------------------------|-----------------------|--------------------------------------|---|---|
| Covariates Selected | Parameter Estimate | Standard Error | p-value/FDR-corrected p-value | [¹⁸F]Flortaucipir SUVR by risk allele | [¹⁸F]Flortaucipir p-value |
| <i>ZCWPW1</i> rs1476679 | 0.518 | 0.274 | 0.0665/0.0665 | 2.28/2.06 /6.81 | <0.001 |

Figure 15. Stepwise regression selected genes in the DEM group

SPM visualization of association patterns for regression selected genes.

Due to the exploratory nature of this analysis, the p-value was set at a lenient uncorrected $p < 0.01$ and minimum cluster size of 50



4.4. Discussion:

To my knowledge, this is the first comprehensive analysis of the association of the top 20 AD risk variants with tau burden. This work highlights the importance of modeling genetic associations in AD, as well as other complex diseases, in a polygenic fashion. I replicated associations to tau previously reported for *ABCA7*, *BIN1*, *CLU*, *EPHA1*, *PICALM*, and *SLC24A4/RIN3*, meanwhile identifying novel associations for *ZCWPW1*^{140,181,184,207-217}. Like with my previous work^{113,199}, I also visualized the spatial associations using voxelwise regression maps and the table of FWE- or FDR- surviving clusters (**Figures 12, 13, 14, 15** and **Table 18**).

In total, I found 7 of the top 20 genes indicated in LOAD to have an association with tau burden. To better understand the potential role each gene may play in tau pathology, I have listed a brief literature review that includes probable functions as well as a previous association to tau (if applicable) and any associations to amyloidosis or neurodegeneration from the earlier publications using a similar technique and sample.

ABCA7

ATP-binding cassette subfamily A member 7 (*ABCA7*) encodes a 2,146 amino acid member of the ABC transporter family comprised of proteins involved in lipid transport and plays a role in macrophage-mediated phagocytosis^{156,218-221}. *ABCA7* expression is associated with tangle density¹⁸⁴. In my earlier work, *ABCA7* rs3752246 was associated with amyloidosis early in the disease course

(i.e., in CN and MCI) and with atrophy in the later disease stages (i.e. DEM)^{113,199}. Here, *ABCA7* association to the AD meta-ROI was found only in the pooled sample.

BIN1

Bridging integrator 1 (*BIN1*) encodes a 593 amino acid protein that may be involved with endocytosis of synaptic vesicles and trafficking as well as control of amyloid production²²². Additionally, the gene product of *BIN1* has been shown to directly interact with tau and further impact phosphorylation of tau²⁰⁷. *BIN1* was recently associated with increased binding of [¹⁸F]Flortaucipir²⁰⁸. I failed to find *BIN1* associations with amyloidosis or atrophy/hypometabolism in my prior work^{113,199}. Here I found significant *BIN1* associations with tau in the MCI sample.

CLU

Clusterin (*CLU*) encodes a 449 amino acid chaperone protein implicated in aggregation prevention of several proteins as well as in the regulation of cell proliferation²²³⁻²²⁵. In regards to tau, carrying the rs11136000 minor allele was associated with CSF tau levels in AD patients and intracellular CLU was found to interact with tau in cell culture²¹⁰. I previously found an association of the *CLU* rs9331949 variant with amyloidosis in DEM and hypometabolism in the CN and MCI^{113,199}. *CLU* rs11136000 was associated with amyloidosis and hypometabolism in the pooled sample. I found an association of the rs9331949

variant with tau SUVR in the pooled, CN and MCI sample, while the rs11136000 variant was associated at a trend level in the MCI sample.

EPHA1

EPH receptor A1 (*EPHA1*) is a 976 amino acid receptor tyrosine kinase protein that binds ephrin-A ligands participating in intercellular signaling upstream of angiogenesis and regulation of cell proliferation²²⁶⁻²²⁸, and as has recently been published, the *Drosophila* ortholog *Eph* was identified as a tau toxicity modulator²⁰⁹. I previously found an association of *EPHA1* rs11771145 to amyloidosis in a pooled, MCI, and DEM sample, to atrophy in a DEM sample and hypometabolism in a pooled sample^{113,199}. I also found an association of another *EPHA1* variant, rs11767557, to hypometabolism in a pooled sample^{113,199}. I found that rs11771145 was associated with meta-ROI tau deposition in an MCI sample.

PICALM

Phosphatidylinositol binding clathrin assembly protein (*PICALM*) encodes a 652 amino acid assembly protein which plays an essential role in clathrin-mediated endocytosis and specifically in the clearance of autophagy substrates like tau and amyloid precursor protein C-terminal fragment^{217,229,230}. *PICALM* overexpression significantly increased tau accumulation measured in cell culture as well as in an *in vivo* zebrafish model²¹⁷. *PICALM* was associated with

amyloidosis in a CN sample in my earlier work ^{113,199}. I found that *PICALM* was associated with tau burden in an MCI sample at a trend level ($p=0.0853$).

SLC24A4/RIN3

Solute carrier family 24 member 4 (*SLC24A4*) encodes a 622 amino acid protein involved in potassium-dependent sodium and calcium exchanger ²³¹, while the other gene located near the risk loci, Ras and rab interactor 3 (*RIN3*), encodes a 985 amino acid protein involved in guanine nucleotide exchange with small GTPases ^{187,232}. Additionally, peripheral hypomethylation of *RIN3* is associated with tangle pathology ²¹⁴. I previously found that *SLC24A4/RIN3* rs10498633 was associated with atrophy in a pooled, MCI and DEM sample, as well as with hypometabolism in a pooled and CN sample ^{113,199}. It seems that this variant is associated with tau and neurodegeneration to some degree through the entire cognitive spectrum, a fact that may indicate a gene of relative importance. I found that rs10498633 was associated with tau in the MCI sample.

ZCWPW1

Zinc finger CW-type and PPWP domain containing 1 (*ZCWPW1*) encodes a 648 amino acid protein with a potential role in epigenetic regulation ^{192,233}. I previously found that *ZCWPW1* rs1476679 was associated with amyloidosis in a pooled and DEM sample, as well as with atrophy in an MCI sample ^{113,199}. Here, I found a novel association of rs1476679 with AD meta-ROI tau SUVR in the DEM sample.

4.5. Strengths and limitations:

This study has several strengths and limitations of which merit discussion. One of the main strengths lies in the rigorous clinical, biomarker, and genetic characterization of all individuals enrolled in ADNI. ADNI uses standardized subject assessment, data collection and quality control practices as well as an imaging normalization to bring images from different scanner types and locations to their closest alignment. Another strength of ADNI is that it is a well-characterized cohort. A major limitation of the study is that I report only cross-sectional analyses, making it difficult to determine with absolute certainty that specific genetic variants exert stage-specific effects. However, leveraging the full dementia continuum, I suggest that there are differential early and late genetic influences on cortical tau burden. Another limitation of the work is the sample size, which was not large enough to visualize spatial associations in more than an exploratory fashion. I also believe the small sample size prevented finding more significant genes than *BIN1*. As more subjects in ADNI are scanned with [¹⁸F]Flortaucipir and more genotyping data is made available, the growing sample size should allow for more stringent thresholding and more power to detect significant associations of the variants with tau. Finally, ADNI is a research cohort that is not entirely representative of the general population, thus, the continuation of this study will aim to validate my findings in a large, independent, longitudinal cohort.

4.6. Conclusions:

Using a multivariable regression modeling technique across the cognitive continuum, I found associations of 7 of the top 20 AD risk genes to tau deposition in an AD-specific meta-ROI. Furthermore, using voxelwise regression, I found spatial association patterns, which should warrant more consideration as the sample size is increased in future iterations of this analysis.

Chapter 5. Summary and Future Directions

Studying Alzheimer's disease *in vivo* requires reliable and accessible disease biomarkers. Here, I report several studies that utilize neuroimaging features as biomarkers to better understand the driving factors of the heterogeneity seen in clinically diagnosed Alzheimer's age of disease onset, biomarker abnormalities and genetic risk. I first analyzed the impact of amyloid burden and age of cognitive symptom onset on neurodegeneration and tau burden relative to cognitively normal subjects. I then utilized an imaging genetics approach, looking at gene variant associations with both neurodegeneration and tau burden.

5.1. Neurodegenerative Changes in Early & Late-Onset Cognitive Impairment with and without Brain Amyloidosis:

Summary

Chapter 2 is a neuroimaging study that aimed to determine the extent of tau and neurodegenerative pathophysiology measured with tau PET ($[^{18}\text{F}]$ Flortaucipir), FDG PET and MRI in early-onset (EO) and late-onset (LO) ADNI cohorts stratified by amyloid positivity. To control for disease severity, I also stratified by clinical diagnosis, resulting in eight cognitively impaired groups and one amyloid negative CN group which was directly compared against all groups; EOAD_{MCI} , EOAD_{DEM} , $\text{EOnonAD}_{\text{MCI}}$, $\text{EOnonAD}_{\text{DEM}}$, LOAD_{MCI} , LOAD_{DEM} , $\text{LOnonAD}_{\text{MCI}}$ and $\text{LOnonAD}_{\text{DEM}}$. I included additional analyses comparing the LO and EO groups to either the older or younger half of the CN group, respectively. Voxelwise regression maps were made, comparing each group to CN subjects

and for all three modalities. Additionally, interpretation of voxelwise maps comparing groups of unequal sample sizes can be misleading. I, therefore, derived β -coefficient maps, which display effect sizes in each comparison.

Compared to EOAD_{MCI}, LOAD_{MCI} had significantly fewer years of education, while both EOAD groups had a significantly higher percentage of *APOE e4* homozygotes compared to LOAD subjects. Across the three modalities, all AD groups show large clusters of neurodegeneration and tau, though the MCI groups show less than DEM. The DEM groups largely show significance across the brain. This, in particular, underscores the importance of the coefficient maps, as both EO groups had much larger effect sizes than their diagnostic LO counterparts across the three modalities.

The EOnonAD_{MCI} group had a higher proportion of *APOE e4* carriers compared to the LOnonAD_{MCI} group. While I failed to find significant neurodegeneration in EOnonAD_{MCI}, I observed significant hypometabolism in EOnonAD_{DEM}. The lack of findings, particularly in the EOnonAD_{DEM} subjects may be because this group is largely heterogeneous.

LOnonAD, on the other hand, showed significant atrophy and hypometabolism across temporal and frontal lobes, a pattern of neurodegeneration seen in both primary age-related tauopathy (PART) and hippocampal sclerosis with TAR-DNA binding protein 43 (TDP-43) inclusions (HS-TDP-43)^{95,96}. However, due to the lack of findings on the tau scans, I believe the most likely etiology of the LOnonAD subjects to be limbic-predominant age-related TDP-43 encephalopathy (LATE)⁹⁷.

Future Directions

To further the work presented here, I would first begin with the inclusion of longitudinal imaging biomarkers. I believe this would greatly inform the study, filling gaps where I may now only speculate on what the biological process is. For example, the EOnonAD subjects who show no tau or neurodegeneration may still show an increased rate of tau accumulation and/or neurodegeneration compared to CN and LOnonAD subjects. Beyond that, the pattern of deposition or neurodegeneration seen in LOnonAD's may provide the information needed to understand more about the potential etiology of these subjects.

In addition to longitudinal imaging, a more complete cognitive assessment of the nonAD subjects would be helpful. Prospective studies focused on the nonAD subjects should include cross sectional and longitudinal batteries that may help to identify specific etiologies based on varying affected domains.

I believe adding a *post-mortem* validation for each of the LOnonAD (really all of the nonAD) subjects would be valuable. I would expect both nonAD groups to be heterogeneous, though I have specifically identified TDP-43 pathology as a potential driver of the signal seen in LOnonAD. TDP-43 is often found to have an age-related association; therefore, it would be hard to speculate whether or not this would be expected to be found in EOnonAD subjects as well.

The addition of other biomarkers to this analysis may also prove useful in ascertaining the nature of the nonAD etiology. The most obvious additions are plasma, and CSF markers of AD pathophysiology and neuronal damage, such as

A β , tau, neurofilament light chain, various metabolomic and lipidomic measures and measures of inflammation. Imaging markers of neuroinflammation or immune response are still in their relative infancy and currently are not even well understood. However, should one become available, it may be prudent to include. Beyond molecular imaging there are more complex MR sequences that would give information on white matter tract changes (diffusion imaging) and/or functional changes (functional MRI).

Finally, I believe future studies should include a genetic component, an intentionally vague suggestion because the genetic risk of sporadic EOAD is essentially unknown at this point. There are some who believe that there may not be much of a difference between the variant risk in EO vs LOAD, as the underlying pathology remains largely the same. I would argue that I am unsure even to what degree genetics plays in EOAD, be it more or less of a driving factor than in LOAD. I believe the differences in disease severity, in progression and most of all, in onset, are all factors that likely have a genetic component to them, which I believe crucial to not only understanding EOAD, but LOAD. To do this, I would start with GWAS to identify new hits that may explain some of the variability between EO and LOAD. I believe it would also be important to repeat a similar imaging genetics study presented in chapters 3 and 4 to measure relative variant contributions to amyloid, tau and neurodegeneration.

5.2. The effect of the top 20 Alzheimer's disease risk genes on gray matter density and FDG PET brain metabolism:

Summary

Chapter 3 explored the genetic risk alleles associated with imaging measures of neurodegeneration (FDG PET and MRI). I included risk variants identified in genome-wide association studies (GWAS) and meta-analysis of GWAS as significantly associated with AD, as well as variants near those found through GWAS that have previously been associated with brain amyloidosis ^{78-80,196-198}.

Following the reduction of variants after linkage disequilibrium analysis, all remaining 27 were included in multiple linear regression models with the variants included as predictors and either posterior cingulate cortex (PCC) SUVR (FDG) or gray-matter density (GMD) (MRI). Four models were run in each modality to tease apart the potential changing gene effects across the cognitive continuum (Pooled, NC, MCI and DEM models). The variants selected in the regression models were replicated using voxelwise regression to display patterns of association.

In the MRI analyses, I found *SLC24A4/RIN3* rs10498633 was significantly associated with GMD but found no associations in the NC group. However, both *SLC24A4/RIN3* rs10498633 and *ZCWPW1* rs1476679 were significantly associated with GMD, while *CELF1* rs10838725 was trending in the MCI group. *ABCA7* rs3752246, *EPHA1* rs11771145 and *INPP5D* rs35349669 were

significantly associated with GMD in the DEM sample, while *SLC24A4/RIN3* rs10498633 showed a trend-level association.

In the FDG PET analyses, *EPHA1* rs11767557 was significantly associated with hypometabolism in the pooled sample, while *MS4A6A* rs610932, *PTK2B* rs28834970 and *SLC24A4/RIN3* rs10498633 were associated at a trend-level. In the NC control group, *CD2AP* rs9349407, *NME8* rs2718058 and *SLC24A4/RIN3* rs10498533 were significantly associated with hypometabolism in PCC. Also in the NC group, *CELF1* rs10838725, *CR1* rs12034383 and *DSG2* rs8093731 had trending significance. In the MCI and DEM cohort, only *CLU* rs9331949 and *SORL1* rs11218343, respectively, showed trend-level associations.

Several variants show diagnosis-specific associations, which often followed the hypothetical biomarker progression proposed by Jack et al.¹¹⁴. In this model, neurodegeneration follows the buildup of amyloid and tau protein and begins in the late asymptomatic stages between NC and MCI¹¹⁴. A fitting example of this is seen in the *ABCA7* and *EPHA1* genes. Both genes were significantly associated with brain amyloidosis in my previous work, with their largest effect in the MCI cohort¹⁵³. Here, I found that both *ABCA7* and *EPHA1* associated with neurodegeneration in the DEM group, which follows the biomarker progression curve.

The reported associations of *ABCA7*, *INPP5D* and *ZCWPW1* to GMD, and of *CD2AP* to brain metabolism are novel.

5.3. Association of the top 20 Alzheimer's disease risk genes with [¹⁸F]Flortaucipir PET:

Summary

Chapter 4, like in the previous chapter, utilizes an imaging genetics approach to study associations of the top 20 AD risk genes, this time with [¹⁸F]Flortaucipir PET. As with before, genes were included in a multiple regression analysis as predictors while [¹⁸F]Flortaucipir PET meta-ROI SUVR was used as an outcome.

The meta-ROI used was an *a priori* AD-specific region determined by Clifford Jack and included the size-weighted Freesurfer regions corresponding to entorhinal, amygdala, parahippocampal, fusiform, inferior temporal, and middle temporal ROIs^{204,205}. Final regression outputs were reproduced in imaging space to visualize spatial patterns of gene variant associations.

I found there were significantly more male participants in the MCI group than in either CN or DEM and that DEM subjects had significantly less education than the other two groups. I also found that among all variants retained in the models, only *SLC24A4/RIN3* was significantly different in allele distribution among diagnostic groups, having more homozygous minor allele carriers in the MCI group. *APOE4* showed significant association with tau in the pooled, CN and MCI sample while only minimally so in the DEM group, even though there were significantly more homozygous carriers of the e4 allele in the DEM group.

Results from the regression analysis showed trend-level associations to tau for both *ABCA7* rs3752246 and *CLU* rs9331949 in the pooled sample, as well as *CLU* rs9331949 in the CN sample. In the MCI group, *BIN1* rs744373 was significantly associated, while *CLU* rs11136000, *EPHA1* rs11771145, *PICALM* rs3851179 and *SLC24A4/RIN3* rs10498633 were associated at a trend-level to tau. In the DEM sample, only a single variant was selected, *ZCWPW1* rs1476679, which was associated with tau at a trend-level. As with my previous work, I also visualized associations using voxelwise regression maps in SPM 113,199.

Despite no genes surviving FDR-correction (likely due to the smaller sample size), I was able to reproduce the associations to tau previously reported for *ABCA7*, *BIN1*, *CLU*, *EPHA1*, *PICALM*, and *SLC24A4/RIN3* ^{140,181,184,207-217}. The association of *ZCWPW1* to tau pathology has not been reported previously. In total, I found 7 of the top 20 genes indicated in LOAD to have an association with tau burden.

Future Directions for both 5.2. and 5.3.

Given the opportunity to further expand on this work I would first and foremost repeat the analysis using longitudinal imaging biomarkers. As mentioned previously, GMD does correlate with atrophy but the two are not synonymous. Measuring atrophy, instead, I believe would give more power to the study. The same can be true as well with both PET modalities i.e. measuring a decrease in brain metabolism and an increase in tau burden vs. at a single time point relative to a mean.

Specific to the imaging analysis of [¹⁸F]Flortaucipir PET, I would dramatically increase the sample size to more closely match that of the MRI and FDG PET analysis. This, of course, would largely get rid of any spurious associations and would hopefully result in more variants surviving multiple comparisons correction.

Additionally, I would include more variants in future analyses that have been identified since the inception of these studies. The current analysis is based on the GWAS and meta-analysis of GWAS from papers published in the early 2010s, which are nearly a decade old. Recently, there have been several massive GWAS/GWAX studies published which identify 13 new risk loci, not to mention slightly older GWAS which have occurred between 2013 and now ²³⁴⁻²³⁶. Inclusion of these as well as other genome-wide-significant loci would enrich the results and perhaps explain even more of the variance.

Finally, I believe it is necessary to continue this analysis across a variety of other races and ethnicities. We know that there are disparities in disease prevalence and severity across these groups for a variety of reasons, not the least of which is genetic ²³⁷⁻²⁴⁰. Future studies should first include multiple GWAS of each homogenous population. This, of course, has been difficult in the past. The results of these various GWAS would likely output several novel loci (possibly explaining some of the variability across race and ethnicity) as well as several overlapping loci (highlighting SNPs whose functions are central to the disease process). In line with this as well, is the sex-specific AD disparity, as we know women have a much greater risk. I believe GWAS hits would potentially be

able to explain this. Whether entirely new loci would appear or whether it would be the same loci with much greater effect sizes is unknown. The presented imaging genetics approach may be an effective route to parsing sex-specific differences for the currently known genome-wide significant loci and at the very least, in highlighting the variable effect size differences in genetic associations between male and female patients.

5.4. Conclusion:

The above work highlights the versatility of neuroimaging biomarkers to study the pathophysiology variations of clinically diagnosed AD and genetics of AD. Here, I studied tau and neurodegeneration in subjects divided by age of onset and amyloidosis. In amyloid positive subjects, earlier age of onset meant greater tau burden and neurodegeneration than their late-onset counterparts. For amyloid negative subjects, however, only the late-onset group displayed any significant neurodegeneration, which was in a non-Alzheimer's pattern and was suggestive of TDP-43 with hippocampal sclerosis. Using a neuroimaging genetics approach, I found variants of the top 20 Alzheimer's genes associated with FDG and [¹⁸F]Flortaucipir PET SUVR and MRI measures of medial temporal lobe thickness. Beyond replicating associations seen previously for many of the variants I found novel variant associations for all three modalities. Taken together, these results have 1) highlighted just how much age of onset impacts the progression of AD and indicated several groups which warrant future study and 2) identified several gene variants which may potentially garner further attention as drug targets or warrant further study on their own

References

- 1 Hebert, L. E., Weuve, J., Scherr, P. A. & Evans, D. A. Alzheimer disease in the United States (2010-2050) estimated using the 2010 census. *Neurology* **80**, 1778-1783, doi:10.1212/WNL.0b013e31828726f5 (2013).
- 2 Association, A. s. 2019 Alzheimer's Disease Facts and Figures. Report No. 1552-5260.
- 3 Huang, L. K., Chao, S. P. & Hu, C. J. Clinical trials of new drugs for Alzheimer disease. *J Biomed Sci* **27**, 18, doi:10.1186/s12929-019-0609-7 (2020).
- 4 Galasko, D. R. *et al.* Safety, tolerability, pharmacokinetics, and Abeta levels after short-term administration of R-flurbiprofen in healthy elderly individuals. *Alzheimer Dis Assoc Disord* **21**, 292-299, doi:10.1097/WAD.0b013e31815d1048 (2007).
- 5 Sampson, E. L., Jenagaratnam, L. & McShane, R. Metal protein attenuating compounds for the treatment of Alzheimer's dementia. *Cochrane Database Syst Rev*, CD005380, doi:10.1002/14651858.CD005380.pub5 (2014).
- 6 Rinne, J. O. *et al.* 11C-PiB PET assessment of change in fibrillar amyloid-beta load in patients with Alzheimer's disease treated with bapineuzumab: a phase 2, double-blind, placebo-controlled, ascending-dose study. *Lancet Neurol* **9**, 363-372, doi:10.1016/S1474-4422(10)70043-0 (2010).
- 7 Coric, V. *et al.* Safety and tolerability of the gamma-secretase inhibitor avagacestat in a phase 2 study of mild to moderate Alzheimer disease. *Arch Neurol* **69**, 1430-1440, doi:10.1001/archneurol.2012.2194 (2012).
- 8 Henley, D. *et al.* Preliminary Results of a Trial of Atabecestat in Preclinical Alzheimer's Disease. *N Engl J Med* **380**, 1483-1485, doi:10.1056/NEJMc1813435 (2019).
- 9 Aisen, P. S. *et al.* Tramiprosate in mild-to-moderate Alzheimer's disease - a randomized, double-blind, placebo-controlled, multi-centre study (the Alphase Study). *Arch Med Sci* **7**, 102-111, doi:10.5114/aoms.2011.20612 (2011).
- 10 Nicoll, J. A. *et al.* Neuropathology of human Alzheimer disease after immunization with amyloid-beta peptide: a case report. *Nat Med* **9**, 448-452, doi:10.1038/nm840 (2003).
- 11 Delnomdedieu, M. *et al.* First-In-Human safety and long-term exposure data for AAB-003 (PF-05236812) and biomarkers after intravenous infusions of escalating doses in patients with mild to moderate Alzheimer's disease. *Alzheimers Res Ther* **8**, 12, doi:10.1186/s13195-016-0177-y (2016).
- 12 Wessels, A. M. *et al.* Efficacy and Safety of Lanabecestat for Treatment of Early and Mild Alzheimer Disease: The AMARANTH and DAYBREAK-ALZ Randomized Clinical Trials. *JAMA Neurol*, doi:10.1001/jamaneurol.2019.3988 (2019).

- 13 Landen, J. W. *et al.* Ponezumab in mild-to-moderate Alzheimer's disease: Randomized phase II PET-PIB study. *Alzheimers Dement (N Y)* **3**, 393-401, doi:10.1016/j.trci.2017.05.003 (2017).
- 14 Landen, J. W. *et al.* Multiple-dose ponezumab for mild-to-moderate Alzheimer's disease: Safety and efficacy. *Alzheimers Dement (N Y)* **3**, 339-347, doi:10.1016/j.trci.2017.04.003 (2017).
- 15 Qiu, R. *et al.* Safety, Tolerability, Pharmacokinetics, and Pharmacodynamic Effects of PF-06751979, a Potent and Selective Oral BACE1 Inhibitor: Results from Phase I Studies in Healthy Adults and Healthy Older Subjects. *J Alzheimers Dis* **71**, 581-595, doi:10.3233/JAD-190228 (2019).
- 16 O'Neill, B. T. *et al.* Design and Synthesis of Clinical Candidate PF-06751979: A Potent, Brain Penetrant, beta-Site Amyloid Precursor Protein Cleaving Enzyme 1 (BACE1) Inhibitor Lacking Hypopigmentation. *J Med Chem* **61**, 4476-4504, doi:10.1021/acs.jmedchem.8b00246 (2018).
- 17 Doody, R. S. *et al.* A phase 3 trial of semagacestat for treatment of Alzheimer's disease. *N Engl J Med* **369**, 341-350, doi:10.1056/NEJMoa1210951 (2013).
- 18 Egan, M. F. *et al.* Randomized Trial of Verubecestat for Prodromal Alzheimer's Disease. *N Engl J Med* **380**, 1408-1420, doi:10.1056/NEJMoa1812840 (2019).
- 19 Alzheimer, A., Stelzmann, R. A., Schnitzlein, H. N. & Murtagh, F. R. An English translation of Alzheimer's 1907 paper, "Über eine eigenartige Erkrankung der Hirnrinde". *Clin Anat* **8**, 429-431, doi:10.1002/ca.980080612 (1995).
- 20 Braak, H. & Braak, E. Neuropathological staging of Alzheimer-related changes. *Acta Neuropathol* **82**, 239-259, doi:10.1007/bf00308809 (1991).
- 21 Serrano-Pozo, A., Frosch, M. P., Masliah, E. & Hyman, B. T. Neuropathological alterations in Alzheimer disease. *Cold Spring Harb Perspect Med* **1**, a006189, doi:10.1101/cshperspect.a006189 (2011).
- 22 Suh, Y. H. & Checler, F. Amyloid precursor protein, presenilins, and alpha-synuclein: molecular pathogenesis and pharmacological applications in Alzheimer's disease. *Pharmacol Rev* **54**, 469-525, doi:10.1124/pr.54.3.469 (2002).
- 23 Mohandas, E., Rajmohan, V. & Raghunath, B. Neurobiology of Alzheimer's disease. *Indian J Psychiatry* **51**, 55-61, doi:10.4103/0019-5545.44908 (2009).
- 24 Bateman, R. J. *et al.* Clinical and biomarker changes in dominantly inherited Alzheimer's disease. *N Engl J Med* **367**, 795-804, doi:10.1056/NEJMoa1202753 (2012).
- 25 Perl, D. P. Neuropathology of Alzheimer's disease. *Mt Sinai J Med* **77**, 32-42, doi:10.1002/msj.20157 (2010).
- 26 Jack, C. R., Jr. *et al.* Tracking pathophysiological processes in Alzheimer's disease: an updated hypothetical model of dynamic biomarkers. *Lancet Neurol* **12**, 207-216, doi:10.1016/S1474-4422(12)70291-0 (2013).

- 27 Lee, H. G. *et al.* Tau phosphorylation in Alzheimer's disease: pathogen or protector? *Trends Mol Med* **11**, 164-169, doi:10.1016/j.molmed.2005.02.008 (2005).
- 28 Wang, Y. & Mandelkow, E. Tau in physiology and pathology. *Nat Rev Neurosci* **17**, 5-21, doi:10.1038/nrn.2015.1 (2016).
- 29 Braak, H., Alafuzoff, I., Arzberger, T., Kretschmar, H. & Del Tredici, K. Staging of Alzheimer disease-associated neurofibrillary pathology using paraffin sections and immunocytochemistry. *Acta Neuropathol* **112**, 389-404, doi:10.1007/s00401-006-0127-z (2006).
- 30 Lee, S. H. *et al.* Antibody-Mediated Targeting of Tau In Vivo Does Not Require Effector Function and Microglial Engagement. *Cell Rep* **16**, 1690-1700, doi:10.1016/j.celrep.2016.06.099 (2016).
- 31 Paholikova, K. *et al.* N-terminal truncation of microtubule associated protein tau dysregulates its cellular localization. *J Alzheimers Dis* **43**, 915-926, doi:10.3233/JAD-140996 (2015).
- 32 Hyman, B. T. *et al.* National Institute on Aging-Alzheimer's Association guidelines for the neuropathologic assessment of Alzheimer's disease. *Alzheimers Dement* **8**, 1-13, doi:10.1016/j.jalz.2011.10.007 (2012).
- 33 McKhann, G. *et al.* Clinical diagnosis of Alzheimer's disease: report of the NINCDS-ADRDA Work Group under the auspices of Department of Health and Human Services Task Force on Alzheimer's Disease. *Neurology* **34**, 939-944 (1984).
- 34 Jack, C. R., Jr. *et al.* Introduction to the recommendations from the National Institute on Aging-Alzheimer's Association workgroups on diagnostic guidelines for Alzheimer's disease. *Alzheimers Dement* **7**, 257-262, doi:10.1016/j.jalz.2011.03.004 (2011).
- 35 Apostolova, L. G. Alzheimer Disease. *Continuum (Minneap Minn)* **22**, 419-434, doi:10.1212/CON.0000000000000307 (2016).
- 36 McKhann, G. M. *et al.* The diagnosis of dementia due to Alzheimer's disease: recommendations from the National Institute on Aging-Alzheimer's Association workgroups on diagnostic guidelines for Alzheimer's disease. *Alzheimers Dement* **7**, 263-269, doi:10.1016/j.jalz.2011.03.005 (2011).
- 37 Albert, M. S. *et al.* The diagnosis of mild cognitive impairment due to Alzheimer's disease: recommendations from the National Institute on Aging-Alzheimer's Association workgroups on diagnostic guidelines for Alzheimer's disease. *Alzheimers Dement* **7**, 270-279, doi:10.1016/j.jalz.2011.03.008 (2011).
- 38 Sperling, R. A. *et al.* Toward defining the preclinical stages of Alzheimer's disease: recommendations from the National Institute on Aging-Alzheimer's Association workgroups on diagnostic guidelines for Alzheimer's disease. *Alzheimers Dement* **7**, 280-292, doi:10.1016/j.jalz.2011.03.003 (2011).
- 39 Jagust, W. Imaging the evolution and pathophysiology of Alzheimer disease. *Nat Rev Neurosci* **19**, 687-700, doi:10.1038/s41583-018-0067-3 (2018).

- 40 Smith, R., Wibom, M., Pawlik, D., Englund, E. & Hansson, O. Correlation of In Vivo [[18F]]Flortaucipir With Postmortem Alzheimer Disease Tau Pathology. *JAMA Neurol* **76**, 310-317, doi:10.1001/jamaneurol.2018.3692 (2019).
- 41 Jack, C. R., Jr. *et al.* NIA-AA Research Framework: Toward a biological definition of Alzheimer's disease. *Alzheimers Dement* **14**, 535-562, doi:10.1016/j.jalz.2018.02.018 (2018).
- 42 Smits, L. L. *et al.* Early onset APOE E4-negative Alzheimer's disease patients show faster cognitive decline on non-memory domains. *Eur Neuropsychopharmacol* **25**, 1010-1017, doi:10.1016/j.euroneuro.2015.03.014 (2015).
- 43 Koedam, E. L. *et al.* Early-versus late-onset Alzheimer's disease: more than age alone. *J Alzheimers Dis* **19**, 1401-1408, doi:10.3233/JAD-2010-1337 (2010).
- 44 Smits, L. L. *et al.* Early onset Alzheimer's disease is associated with a distinct neuropsychological profile. *J Alzheimers Dis* **30**, 101-108, doi:10.3233/JAD-2012-111934 (2012).
- 45 Moller, C. *et al.* Different patterns of gray matter atrophy in early- and late-onset Alzheimer's disease. *Neurobiol Aging* **34**, 2014-2022, doi:10.1016/j.neurobiolaging.2013.02.013 (2013).
- 46 Heyman, A. *et al.* Early-onset Alzheimer's disease: clinical predictors of institutionalization and death. *Neurology* **37**, 980-984, doi:10.1212/wnl.37.6.980 (1987).
- 47 Filley, C. M., Kelly, J. & Heaton, R. K. Neuropsychologic features of early- and late-onset Alzheimer's disease. *Arch Neurol* **43**, 574-576, doi:10.1001/archneur.1986.00520060038014 (1986).
- 48 Katzman, R. Editorial: The prevalence and malignancy of Alzheimer disease. A major killer. *Arch Neurol* **33**, 217-218 (1976).
- 49 Bird, T. D., Stranahan, S., Sumi, S. M. & Raskind, M. Alzheimer's disease: choline acetyltransferase activity in brain tissue from clinical and pathological subgroups. *Ann Neurol* **14**, 284-293, doi:10.1002/ana.410140306 (1983).
- 50 Rossor, M. N., Iversen, L. L., Reynolds, G. P., Mountjoy, C. Q. & Roth, M. Neurochemical characteristics of early and late onset types of Alzheimer's disease. *Br Med J (Clin Res Ed)* **288**, 961-964 (1984).
- 51 Marshall, G. A., Fairbanks, L. A., Tekin, S., Vinters, H. V. & Cummings, J. L. Early-onset Alzheimer's disease is associated with greater pathologic burden. *J Geriatr Psychiatry Neurol* **20**, 29-33, doi:10.1177/0891988706297086 (2007).
- 52 Murray, M. E. *et al.* Neuropathologically defined subtypes of Alzheimer's disease with distinct clinical characteristics: a retrospective study. *Lancet Neurol* **10**, 785-796, doi:10.1016/S1474-4422(11)70156-9 (2011).
- 53 Sakamoto, S. *et al.* Differences in cerebral metabolic impairment between early and late onset types of Alzheimer's disease. *J Neurol Sci* **200**, 27-32 (2002).

- 54 Migliaccio, R. *et al.* Mapping the Progression of Atrophy in Early- and Late-Onset Alzheimer's Disease. *J Alzheimers Dis* **46**, 351-364, doi:10.3233/JAD-142292 (2015).
- 55 Lehmann, M. *et al.* Diverging patterns of amyloid deposition and hypometabolism in clinical variants of probable Alzheimer's disease. *Brain* **136**, 844-858, doi:10.1093/brain/aws327 (2013).
- 56 Scholl, M. *et al.* Distinct [18F]AV-1451 tau PET retention patterns in early- and late-onset Alzheimer's disease. *Brain* **140**, 2286-2294, doi:10.1093/brain/awx171 (2017).
- 57 Whitwell, J. L. *et al.* The role of age on tau PET uptake and gray matter atrophy in atypical Alzheimer's disease. *Alzheimers Dement*, doi:10.1016/j.jalz.2018.12.016 (2019).
- 58 Rabinovici, G. D. *et al.* Increased metabolic vulnerability in early-onset Alzheimer's disease is not related to amyloid burden. *Brain* **133**, 512-528, doi:10.1093/brain/awp326 (2010).
- 59 Chan, D. *et al.* Change in rates of cerebral atrophy over time in early-onset Alzheimer's disease: longitudinal MRI study. *Lancet* **362**, 1121-1122, doi:10.1016/S0140-6736(03)14469-8 (2003).
- 60 Kim, E. J. *et al.* Glucose metabolism in early onset versus late onset Alzheimer's disease: an SPM analysis of 120 patients. *Brain* **128**, 1790-1801, doi:10.1093/brain/awh539 (2005).
- 61 Karas, G. *et al.* Precuneus atrophy in early-onset Alzheimer's disease: a morphometric structural MRI study. *Neuroradiology* **49**, 967-976, doi:10.1007/s00234-007-0269-2 (2007).
- 62 Murrell, J., Farlow, M., Ghetti, B. & Benson, M. D. A mutation in the amyloid precursor protein associated with hereditary Alzheimer's disease. *Science* **254**, 97-99, doi:10.1126/science.1925564 (1991).
- 63 Chartier-Harlin, M. C. *et al.* Early-onset Alzheimer's disease caused by mutations at codon 717 of the beta-amyloid precursor protein gene. *Nature* **353**, 844-846, doi:10.1038/353844a0 (1991).
- 64 Goate, A. *et al.* Segregation of a missense mutation in the amyloid precursor protein gene with familial Alzheimer's disease. *Nature* **349**, 704-706, doi:10.1038/349704a0 (1991).
- 65 Citron, M. *et al.* Mutation of the beta-amyloid precursor protein in familial Alzheimer's disease increases beta-protein production. *Nature* **360**, 672-674, doi:10.1038/360672a0 (1992).
- 66 Pitsi, D. & Octave, J. N. Presenilin 1 stabilizes the C-terminal fragment of the amyloid precursor protein independently of gamma-secretase activity. *J Biol Chem* **279**, 25333-25338, doi:10.1074/jbc.M312710200 (2004).
- 67 Phiel, C. J., Wilson, C. A., Lee, V. M. & Klein, P. S. GSK-3alpha regulates production of Alzheimer's disease amyloid-beta peptides. *Nature* **423**, 435-439, doi:10.1038/nature01640 (2003).
- 68 Goldman, J. S. *et al.* Genetic counseling and testing for Alzheimer disease: joint practice guidelines of the American College of Medical Genetics and the National Society of Genetic Counselors. *Genet Med* **13**, 597-605, doi:10.1097/GIM.0b013e31821d69b8 (2011).

- 69 Gatz, M. *et al.* Role of genes and environments for explaining Alzheimer disease. *Arch Gen Psychiatry* **63**, 168-174, doi:10.1001/archpsyc.63.2.168 (2006).
- 70 Gatz, M. *et al.* Heritability for Alzheimer's disease: the study of dementia in Swedish twins. *J Gerontol A Biol Sci Med Sci* **52**, M117-125, doi:10.1093/gerona/52a.2.m117 (1997).
- 71 Mayeux, R. & Stern, Y. Epidemiology of Alzheimer disease. *Cold Spring Harb Perspect Med* **2**, doi:10.1101/cshperspect.a006239 (2012).
- 72 Duff, K. *et al.* Increased amyloid-beta42(43) in brains of mice expressing mutant presenilin 1. *Nature* **383**, 710-713, doi:10.1038/383710a0 (1996).
- 73 Corder, E. H. *et al.* Gene dose of apolipoprotein E type 4 allele and the risk of Alzheimer's disease in late onset families. *Science* **261**, 921-923, doi:10.1126/science.8346443 (1993).
- 74 Bettens, K., Sleegers, K. & Van Broeckhoven, C. Genetic insights in Alzheimer's disease. *Lancet Neurol* **12**, 92-104, doi:10.1016/S1474-4422(12)70259-4 (2013).
- 75 Harold, D. *et al.* Genome-wide association study identifies variants at CLU and PICALM associated with Alzheimer's disease. *Nature genetics* **41**, 1088-1093, doi:10.1038/ng.440 (2009).
- 76 Hollingworth, P. *et al.* Common variants at ABCA7, MS4A6A/MS4A4E, EPHA1, CD33 and CD2AP are associated with Alzheimer's disease. *Nat Genet* **43**, 429-435, doi:10.1038/ng.803 (2011).
- 77 Lambert, J. C. *et al.* Genome-wide association study identifies variants at CLU and CR1 associated with Alzheimer's disease. *Nat Genet* **41**, 1094-1099, doi:10.1038/ng.439 (2009).
- 78 Lambert, J. C. *et al.* Meta-analysis of 74,046 individuals identifies 11 new susceptibility loci for Alzheimer's disease. *Nat Genet* **45**, 1452-1458, doi:10.1038/ng.2802 (2013).
- 79 Naj, A. C. *et al.* Common variants at MS4A4/MS4A6E, CD2AP, CD33 and EPHA1 are associated with late-onset Alzheimer's disease. *Nat Genet* **43**, 436-441, doi:10.1038/ng.801 (2011).
- 80 Seshadri, S. *et al.* Genome-wide analysis of genetic loci associated with Alzheimer disease. *JAMA* **303**, 1832-1840, doi:10.1001/jama.2010.574 (2010).
- 81 Karch, C. M. & Goate, A. M. Alzheimer's disease risk genes and mechanisms of disease pathogenesis. *Biol Psychiatry* **77**, 43-51, doi:10.1016/j.biopsych.2014.05.006 (2015).
- 82 Beach, T. G., Monsell, S. E., Phillips, L. E. & Kukull, W. Accuracy of the clinical diagnosis of Alzheimer disease at National Institute on Aging Alzheimer Disease Centers, 2005-2010. *J Neuropathol Exp Neurol* **71**, 266-273, doi:10.1097/NEN.0b013e31824b211b (2012).
- 83 van der Flier, W. M., Pijnenburg, Y. A., Fox, N. C. & Scheltens, P. Early-onset versus late-onset Alzheimer's disease: the case of the missing APOE varepsilon4 allele. *Lancet Neurol* **10**, 280-288, doi:10.1016/S1474-4422(10)70306-9 (2011).

- 84 Konijnenberg, E. *et al.* Early-Onset Dementia: Frequency, Diagnostic Procedures, and Quality Indicators in Three European Tertiary Referral Centers. *Alzheimer Dis Assoc Disord* **31**, 146-151, doi:10.1097/WAD.000000000000152 (2017).
- 85 Petersen, R. C. *et al.* Alzheimer's Disease Neuroimaging Initiative (ADNI): clinical characterization. *Neurology* **74**, 201-209, doi:10.1212/WNL.0b013e3181cb3e25 (2010).
- 86 Folstein, M. F., Folstein, S. E. & McHugh, P. R. "Mini-mental state". A practical method for grading the cognitive state of patients for the clinician. *J Psychiatr Res* **12**, 189-198 (1975).
- 87 Morris, J. C. The Clinical Dementia Rating (CDR): current version and scoring rules. *Neurology* **43**, 2412-2414 (1993).
- 88 D., W. Wechsler Memory Scale – Revised. *Psychological Corporation; San, Antonio, TX: 1987.* (1987).
- 89 Fleisher, A. S. *et al.* Using positron emission tomography and florbetapir F18 to image cortical amyloid in patients with mild cognitive impairment or dementia due to Alzheimer disease. *Arch Neurol* **68**, 1404-1411, doi:10.1001/archneurol.2011.150 (2011).
- 90 Shaw, L. M. *et al.* Cerebrospinal fluid biomarker signature in Alzheimer's disease neuroimaging initiative subjects. *Ann Neurol* **65**, 403-413, doi:10.1002/ana.21610 (2009).
- 91 Risacher, S. L. *et al.* The role of apolipoprotein E (APOE) genotype in early mild cognitive impairment (E-MCI). *Front Aging Neurosci* **5**, 11, doi:10.3389/fnagi.2013.00011 (2013).
- 92 Jagust, W. J. *et al.* The Alzheimer's Disease Neuroimaging Initiative positron emission tomography core. *Alzheimers Dement* **6**, 221-229, doi:10.1016/j.jalz.2010.03.003 (2010).
- 93 Clark, C. M. *et al.* Cerebral PET with florbetapir compared with neuropathology at autopsy for detection of neuritic amyloid-beta plaques: a prospective cohort study. *Lancet Neurol* **11**, 669-678, doi:10.1016/S1474-4422(12)70142-4 (2012).
- 94 Shcherbinin, S. *et al.* Kinetics of the Tau PET Tracer [18F]AV-1451 (T807) in Subjects with Normal Cognitive Function, Mild Cognitive Impairment, and Alzheimer Disease. *J Nucl Med* **57**, 1535-1542, doi:10.2967/jnumed.115.170027 (2016).
- 95 Jellinger, K. A. *et al.* PART, a distinct tauopathy, different from classical sporadic Alzheimer disease. *Acta Neuropathol* **129**, 757-762, doi:10.1007/s00401-015-1407-2 (2015).
- 96 James, B. D. *et al.* TDP-43 stage, mixed pathologies, and clinical Alzheimer's-type dementia. *Brain* **139**, 2983-2993, doi:10.1093/brain/aww224 (2016).
- 97 Nelson, P. T. *et al.* Limbic-predominant age-related TDP-43 encephalopathy (LATE): consensus working group report. *Brain* **142**, 1503-1527, doi:10.1093/brain/awz099 (2019).

- 98 Lowe, V. J. *et al.* An autoradiographic evaluation of AV-1451 Tau PET in dementia. *Acta Neuropathol Commun* **4**, 58, doi:10.1186/s40478-016-0315-6 (2016).
- 99 Wren, M. C., Lashley, T., Arstad, E. & Sander, K. Large inter- and intra-case variability of first generation tau PET ligand binding in neurodegenerative dementias. *Acta Neuropathol Commun* **6**, 34, doi:10.1186/s40478-018-0535-z (2018).
- 100 McAleese, K. E. *et al.* TDP-43 pathology in Alzheimer's disease, dementia with Lewy bodies and ageing. *Brain Pathol* **27**, 472-479, doi:10.1111/bpa.12424 (2017).
- 101 Josephs, K. A. *et al.* Rates of hippocampal atrophy and presence of post-mortem TDP-43 in patients with Alzheimer's disease: a longitudinal retrospective study. *Lancet Neurol* **16**, 917-924, doi:10.1016/S1474-4422(17)30284-3 (2017).
- 102 Mackenzie, I. R., Rademakers, R. & Neumann, M. TDP-43 and FUS in amyotrophic lateral sclerosis and frontotemporal dementia. *Lancet Neurol* **9**, 995-1007, doi:10.1016/S1474-4422(10)70195-2 (2010).
- 103 Arai, T. *et al.* TDP-43 is a component of ubiquitin-positive tau-negative inclusions in frontotemporal lobar degeneration and amyotrophic lateral sclerosis. *Biochemical and biophysical research communications* **351**, 602-611, doi:10.1016/j.bbrc.2006.10.093 (2006).
- 104 Nag, S. *et al.* Hippocampal sclerosis and TDP-43 pathology in aging and Alzheimer disease. *Ann Neurol* **77**, 942-952, doi:10.1002/ana.24388 (2015).
- 105 Josephs, K. A. *et al.* Abnormal TDP-43 immunoreactivity in AD modifies clinicopathologic and radiologic phenotype. *Neurology* **70**, 1850-1857, doi:10.1212/01.wnl.0000304041.09418.b1 (2008).
- 106 Wilson, R. S. *et al.* TDP-43 pathology, cognitive decline, and dementia in old age. *JAMA neurology* **70**, 1418-1424, doi:10.1001/jamaneurol.2013.3961 (2013).
- 107 Nag, S. *et al.* TDP-43 pathology and memory impairment in elders without pathologic diagnoses of AD or FTLD. *Neurology* **88**, 653-660, doi:10.1212/WNL.00000000000003610 (2017).
- 108 Botha, H. *et al.* FDG-PET in tau-negative amnesic dementia resembles that of autopsy-proven hippocampal sclerosis. *Brain* **141**, 1201-1217, doi:10.1093/brain/awy049 (2018).
- 109 Grothe, M. *Towards a topographic imaging biomarker of TDP-43 pathology in amnesic dementia: patient stratification based on FDG-PET patterns in autopsy-confirmed cases* (2019).
- 110 Bejanin, A. *et al.* Antemortem volume loss mirrors TDP-43 staging in older adults with non-frontotemporal lobar degeneration. *Brain*, doi:10.1093/brain/awz277 (2019).
- 111 Rascovsky, K. *et al.* Sensitivity of revised diagnostic criteria for the behavioural variant of frontotemporal dementia. *Brain* **134**, 2456-2477, doi:10.1093/brain/awr179 (2011).

- 112 Baborie, A. *et al.* Pathological correlates of frontotemporal lobar degeneration in the elderly. *Acta Neuropathol* **121**, 365-371, doi:10.1007/s00401-010-0765-z (2011).
- 113 Apostolova, L. G. *et al.* Associations of the Top 20 Alzheimer Disease Risk Variants With Brain Amyloidosis. *JAMA neurology* **75**, 328-341, doi:10.1001/jamaneurol.2017.4198 (2018).
- 114 Jack, C. R., Jr. *et al.* Hypothetical model of dynamic biomarkers of the Alzheimer's pathological cascade. *Lancet Neurol* **9**, 119-128, doi:10.1016/S1474-4422(09)70299-6 (2010).
- 115 Tiraboschi, P., Hansen, L. A., Thal, L. J. & Corey-Bloom, J. The importance of neuritic plaques and tangles to the development and evolution of AD. *Neurology* **62**, 1984-1989 (2004).
- 116 Apostolova, L. G. *et al.* Three-dimensional gray matter atrophy mapping in mild cognitive impairment and mild Alzheimer disease. *Arch Neurol* **64**, 1489-1495, doi:10.1001/archneur.64.10.1489 (2007).
- 117 Apostolova, L. G. *et al.* Surface feature-guided mapping of cerebral metabolic changes in cognitively normal and mildly impaired elderly. *Mol Imaging Biol* **12**, 218-224, doi:10.1007/s11307-009-0247-7 (2010).
- 118 Wingo, T. S., Lah, J. J., Levey, A. I. & Cutler, D. J. Autosomal recessive causes likely in early-onset Alzheimer disease. *Arch Neurol* **69**, 59-64, doi:10.1001/archneurol.2011.221 (2012).
- 119 Sleegers, K. *et al.* The pursuit of susceptibility genes for Alzheimer's disease: progress and prospects. *Trends in genetics : TIG* **26**, 84-93, doi:10.1016/j.tig.2009.12.004 (2010).
- 120 Verghese, P. B., Castellano, J. M. & Holtzman, D. M. Apolipoprotein E in Alzheimer's disease and other neurological disorders. *Lancet Neurol* **10**, 241-252, doi:10.1016/S1474-4422(10)70325-2 (2011).
- 121 Farrer, L. A. *et al.* Effects of age, sex, and ethnicity on the association between apolipoprotein E genotype and Alzheimer disease. A meta-analysis. APOE and Alzheimer Disease Meta Analysis Consortium. *JAMA* **278**, 1349-1356 (1997).
- 122 Reiman, E. M. *et al.* Fibrillar amyloid-beta burden in cognitively normal people at 3 levels of genetic risk for Alzheimer's disease. *Proceedings of the National Academy of Sciences of the United States of America* **106**, 6820-6825, doi:10.1073/pnas.0900345106 (2009).
- 123 Lazaris, A. *et al.* Alzheimer risk genes modulate the relationship between plasma apoE and cortical PiB binding. *Neurol Genet* **1**, e22, doi:10.1212/NXG.000000000000022 (2015).
- 124 Andrawis, J. P. *et al.* Effects of ApoE4 and maternal history of dementia on hippocampal atrophy. *Neurobiol Aging* **33**, 856-866, doi:10.1016/j.neurobiolaging.2010.07.020 (2012).
- 125 Reiman, E. M. *et al.* Preclinical evidence of Alzheimer's disease in persons homozygous for the epsilon 4 allele for apolipoprotein E. *N Engl J Med* **334**, 752-758 (1996).

- 126 Mosconi, L. *et al.* Brain metabolic decreases related to the dose of the ApoE e4 allele in Alzheimer's disease. *J Neurol Neurosurg Psychiatry* **75**, 370-376 (2004).
- 127 Assareh, A. A. *et al.* Association of SORL1 gene variants with hippocampal and cerebral atrophy and Alzheimer's disease. *Curr Alzheimer Res* **11**, 558-563 (2014).
- 128 Cuenco, T. *et al.* Association of distinct variants in SORL1 with cerebrovascular and neurodegenerative changes related to Alzheimer disease. *Arch Neurol* **65**, 1640-1648, doi:10.1001/archneur.65.12.1640 (2008).
- 129 Ramirez, L. M. *et al.* Common variants in ABCA7 and MS4A6A are associated with cortical and hippocampal atrophy. *Neurobiol Aging* **39**, 82-89, doi:10.1016/j.neurobiolaging.2015.10.037 (2016).
- 130 Ma, J. *et al.* MS4A6A genotypes are associated with the atrophy rates of Alzheimer's disease related brain structures. *Oncotarget*, doi:10.18632/oncotarget.9563 (2016).
- 131 Kohannim, O. *et al.* Multilocus genetic profiling to empower drug trials and predict brain atrophy. *Neuroimage Clin* **2**, 827-835, doi:10.1016/j.nicl.2013.05.007 (2013).
- 132 Li, J. Q. *et al.* GWAS-Linked Loci and Neuroimaging Measures in Alzheimer's Disease. *Mol Neurobiol*, doi:10.1007/s12035-015-9669-1 (2016).
- 133 Biffi, A. *et al.* Genetic variation and neuroimaging measures in Alzheimer disease. *Arch Neurol* **67**, 677-685, doi:10.1001/archneurol.2010.108 (2010).
- 134 Chauhan, G. *et al.* Association of Alzheimer's disease GWAS loci with MRI markers of brain aging. *Neurobiol Aging* **36**, 1765 e1767-1716, doi:10.1016/j.neurobiolaging.2014.12.028 (2015).
- 135 Furney, S. J. *et al.* Genome-wide association with MRI atrophy measures as a quantitative trait locus for Alzheimer's disease. *Molecular psychiatry* **16**, 1130-1138, doi:10.1038/mp.2010.123 (2011).
- 136 Wang, H. F. *et al.* Bridging Integrator 1 (BIN1) Genotypes Mediate Alzheimer's Disease Risk by Altering Neuronal Degeneration. *J Alzheimers Dis* **52**, 179-190, doi:10.3233/JAD-150972 (2016).
- 137 Weiner, M. W. V., D.P.; Aisen, P.S.; Beckett, L.A.; Cairns, N.J.; Green, R.C.; Harvey, D.; Jack, C.R.; Jagust, W.; Liu, E.; Morris, J.C.; Petersen, R.C.; Saykin, A.J.; Schmidt, M.E.; Shaw, L.; Siuciak, J.A.; Soares, H.; Toga, A.W.; Trojanowski, J.Q.; Alzheimer's Disease Neuroimaging Initiative. The Alzheimer's Disease Neuroimaging Initiative: a review of papers published since its inception. *Alzheimer's Dementia* **8**, S1-68 (2012).
- 138 Wechsler, D. *Manual for the Wechsler Memory Scale - Revised.* (Psychological Corporation, 1987).
- 139 Thambisetty, M. *et al.* Effect of complement CR1 on brain amyloid burden during aging and its modification by APOE genotype. *Biol Psychiatry* **73**, 422-428, doi:10.1016/j.biopsych.2012.08.015 (2013).

- 140 Shulman, J. M. *et al.* Functional screening in *Drosophila* identifies Alzheimer's disease susceptibility genes and implicates Tau-mediated mechanisms. *Human molecular genetics* **23**, 870-877, doi:10.1093/hmg/ddt478 (2014).
- 141 Hughes, T. M. *et al.* Markers of cholesterol transport are associated with amyloid deposition in the brain. *Neurobiol Aging* **35**, 802-807, doi:10.1016/j.neurobiolaging.2013.09.040 (2014).
- 142 Nho, K. *et al.* The effect of reference panels and software tools on genotype imputation. *AMIA Annu Symp Proc* **2011**, 1013-1018 (2011).
- 143 Wyman, B. T. *et al.* Standardization of analysis sets for reporting results from ADNI MRI data. *Alzheimers Dement* **9**, 332-337, doi:10.1016/j.jalz.2012.06.004 (2013).
- 144 Jack, C. R., Jr. *et al.* Update on the magnetic resonance imaging core of the Alzheimer's disease neuroimaging initiative. *Alzheimers Dement* **6**, 212-220, doi:10.1016/j.jalz.2010.03.004 (2010).
- 145 Jack, C. R., Jr. *et al.* The Alzheimer's Disease Neuroimaging Initiative (ADNI): MRI methods. *J Magn Reson Imaging* **27**, 685-691, doi:10.1002/jmri.21049 (2008).
- 146 Jack, C. R., Jr. *et al.* Magnetic resonance imaging in Alzheimer's Disease Neuroimaging Initiative 2. *Alzheimers Dement* **11**, 740-756, doi:10.1016/j.jalz.2015.05.002 (2015).
- 147 Whitwell, J. L. Voxel-based morphometry: an automated technique for assessing structural changes in the brain. *J Neurosci* **29**, 9661-9664, doi:10.1523/JNEUROSCI.2160-09.2009 (2009).
- 148 Risacher, S. L. *et al.* Longitudinal MRI atrophy biomarkers: relationship to conversion in the ADNI cohort. *Neurobiol Aging* **31**, 1401-1418, doi:10.1016/j.neurobiolaging.2010.04.029 (2010).
- 149 Risacher, S. L. *et al.* Baseline MRI predictors of conversion from MCI to probable AD in the ADNI cohort. *Curr Alzheimer Res* **6**, 347-361 (2009).
- 150 Landau, S. M. *et al.* Associations between cognitive, functional, and FDG-PET measures of decline in AD and MCI. *Neurobiol Aging* **32**, 1207-1218, doi:10.1016/j.neurobiolaging.2009.07.002 (2011).
- 151 Jagust, W. J. *et al.* Relationships between biomarkers in aging and dementia. *Neurology* **73**, 1193-1199, doi:10.1212/WNL.0b013e3181bc010c (2009).
- 152 Akaike, H. in *Selected Papers of Hirotugu Akaike. Springer Series in Statistics (Perspectives in Statistics)* (Springer, 1998).
- 153 Apostolova, L. G., Risacher, S.L., Duran, T., Stage, E.C., Goukasian, N., West, J.D., Do, T., Grotts, J., Nho, K., Elashoff, D., Saykin, A.J. Examining the Effect of the Top 20 AD Risk Variants on Brain Amyloidosis, Structural Atrophy and Metabolism. (2016).
- 154 Wang, H. F. *et al.* Effect of EPHA1 genetic variation on cerebrospinal fluid and neuroimaging biomarkers in healthy, mild cognitive impairment and Alzheimer's disease cohorts. *J Alzheimers Dis* **44**, 115-123, doi:10.3233/JAD-141488 (2015).

- 155 Ge, T. *et al.* A kernel machine method for detecting effects of interaction between multidimensional variable sets: an imaging genetics application. *Neuroimage* **109**, 505-514, doi:10.1016/j.neuroimage.2015.01.029 (2015).
- 156 Kaminski, W. E. *et al.* Identification of a novel human sterol-sensitive ATP-binding cassette transporter (ABCA7). *Biochemical and biophysical research communications* **273**, 532-538, doi:10.1006/bbrc.2000.2954 (2000).
- 157 Li, H., Karl, T. & Garner, B. Understanding the function of ABCA7 in Alzheimer's disease. *Biochemical Society transactions* **43**, 920-923, doi:10.1042/BST20150105 (2015).
- 158 Satoh, K., Abe-Dohmae, S., Yokoyama, S., St George-Hyslop, P. & Fraser, P. E. ATP-binding cassette transporter A7 (ABCA7) loss of function alters Alzheimer amyloid processing. *The Journal of biological chemistry* **290**, 24152-24165, doi:10.1074/jbc.M115.655076 (2015).
- 159 Zhao, Q. F. *et al.* ABCA7 Genotypes Confer Alzheimer's Disease Risk by Modulating Amyloid-beta Pathology. *J Alzheimers Dis* **52**, 693-703, doi:10.3233/JAD-151005 (2016).
- 160 Sassi, C. *et al.* ABCA7 p.G215S as potential protective factor for Alzheimer's disease. *Neurobiol Aging*, doi:10.1016/j.neurobiolaging.2016.04.004 (2016).
- 161 Monzo, P. *et al.* Clues to CD2-associated protein involvement in cytokinesis. *Molecular biology of the cell* **16**, 2891-2902, doi:10.1091/mbc.E04-09-0773 (2005).
- 162 Liao, F. *et al.* Effects of CD2-associated protein deficiency on amyloid-beta in neuroblastoma cells and in an APP transgenic mouse model. *Molecular neurodegeneration* **10**, 12, doi:10.1186/s13024-015-0006-y (2015).
- 163 Dunstan, M., Gerrish, A., Thomas, R.S., Kidd, E., Morgan, T., Owens, H., and Williams J. The Effects of CD2AP Expression on APP Processing. *Alzheimers & Dementia* **11**, 858 (2015).
- 164 Cochran, J. N., Rush, T., Buckingham, S. C. & Roberson, E. D. The Alzheimer's disease risk factor CD2AP maintains blood-brain barrier integrity. *Human molecular genetics* **24**, 6667-6674, doi:10.1093/hmg/ddv371 (2015).
- 165 Maru, Y., Hirai, H., Yoshida, M. C. & Takaku, F. Evolution, expression, and chromosomal location of a novel receptor tyrosine kinase gene, eph. *Molecular and cellular biology* **8**, 3770-3776 (1988).
- 166 Torii, M., Hashimoto-Torii, K., Levitt, P. & Rakic, P. Integration of neuronal clones in the radial cortical columns by EphA and ephrin-A signalling. *Nature* **461**, 524-528, doi:10.1038/nature08362 (2009).
- 167 Hattori, M., Osterfield, M. & Flanagan, J. G. Regulated cleavage of a contact-mediated axon repellent. *Science* **289**, 1360-1365 (2000).
- 168 Yamazaki, T. *et al.* EphA1 interacts with integrin-linked kinase and regulates cell morphology and motility. *Journal of cell science* **122**, 243-255, doi:10.1242/jcs.036467 (2009).

- 169 Chen, G. *et al.* EphA1 receptor silencing by small interfering RNA has antiangiogenic and antitumor efficacy in hepatocellular carcinoma. *Oncology reports* **23**, 563-570 (2010).
- 170 Metzner, A. *et al.* Reduced proliferation of CD34(+) cells from patients with acute myeloid leukemia after gene transfer of INPP5D. *Gene Ther* **16**, 570-573, doi:10.1038/gt.2008.184 (2009).
- 171 Leung, W. H., Tarasenko, T. & Bolland, S. Differential roles for the inositol phosphatase SHIP in the regulation of macrophages and lymphocytes. *Immunol Res* **43**, 243-251, doi:10.1007/s12026-008-8078-1 (2009).
- 172 Hasegawa, J. *et al.* Autophagosome-lysosome fusion in neurons requires INPP5E, a protein associated with Joubert syndrome. *EMBO J*, doi:10.15252/embj.201593148 (2016).
- 173 Zhang, L., Sheng, R. & Qin, Z. The lysosome and neurodegenerative diseases. *Acta Biochim Biophys Sin (Shanghai)* **41**, 437-445 (2009).
- 174 Wolfe, D. M. *et al.* Autophagy failure in Alzheimer's disease and the role of defective lysosomal acidification. *Eur J Neurosci* **37**, 1949-1961, doi:10.1111/ejn.12169 (2013).
- 175 Orr, M. E. & Oddo, S. Autophagic/lysosomal dysfunction in Alzheimer's disease. *Alzheimers Res Ther* **5**, 53, doi:10.1186/alzrt217 (2013).
- 176 Zhang, Z. G., Li, Y., Ng, C. T. & Song, Y. Q. Inflammation in Alzheimer's Disease and Molecular Genetics: Recent Update. *Arch Immunol Ther Exp (Warsz)* **63**, 333-344, doi:10.1007/s00005-015-0351-0 (2015).
- 177 Farfel, J. M. *et al.* Relation of genomic variants for Alzheimer disease dementia to common neuropathologies. *Neurology* **87**, 489-496, doi:10.1212/WNL.0000000000002909 (2016).
- 178 Duriez, B. *et al.* A common variant in combination with a nonsense mutation in a member of the thioredoxin family causes primary ciliary dyskinesia. *Proceedings of the National Academy of Sciences of the United States of America* **104**, 3336-3341, doi:10.1073/pnas.0611405104 (2007).
- 179 Mahr, S. *et al.* Cis- and trans-acting gene regulation is associated with osteoarthritis. *American journal of human genetics* **78**, 793-803, doi:10.1086/503849 (2006).
- 180 Shi, D. *et al.* Association of single-nucleotide polymorphisms in RHOB and TXNDC3 with knee osteoarthritis susceptibility: two case-control studies in East Asian populations and a meta-analysis. *Arthritis research & therapy* **10**, R54, doi:10.1186/ar2423 (2008).
- 181 Liu, Y. *et al.* Association between NME8 locus polymorphism and cognitive decline, cerebrospinal fluid and neuroimaging biomarkers in Alzheimer's disease. *PloS one* **9**, e114777, doi:10.1371/journal.pone.0114777 (2014).
- 182 Kraev, A. *et al.* Molecular cloning of a third member of the potassium-dependent sodium-calcium exchanger gene family, NCKX3. *The Journal of biological chemistry* **276**, 23161-23172, doi:10.1074/jbc.M102314200 (2001).

- 183 Kraja, A. T. *et al.* Genetic analysis of 16 NMR-lipoprotein fractions in humans, the GOLDN study. *Lipids* **48**, 155-165, doi:10.1007/s11745-012-3740-8 (2013).
- 184 Yu, L. *et al.* Association of Brain DNA Methylation in SORL1, ABCA7, HLA-DRB5, SLC24A4, and BIN1 With Pathological Diagnosis of Alzheimer Disease. *JAMA neurology* **72**, 15-24, doi:10.1001/jamaneurol.2014.3049 (2015).
- 185 Li, X. F. & Lytton, J. An essential role for the K⁺-dependent Na⁺/Ca²⁺-exchanger, NCKX4, in melanocortin-4-receptor-dependent satiety. *The Journal of biological chemistry* **289**, 25445-25459, doi:10.1074/jbc.M114.564450 (2014).
- 186 Kajihio, H. *et al.* RIN3: a novel Rab5 GEF interacting with amphiphysin II involved in the early endocytic pathway. *Journal of cell science* **116**, 4159-4168, doi:10.1242/jcs.00718 (2003).
- 187 Kajihio, H. *et al.* Characterization of RIN3 as a guanine nucleotide exchange factor for the Rab5 subfamily GTPase Rab31. *The Journal of biological chemistry* **286**, 24364-24373, doi:10.1074/jbc.M110.172445 (2011).
- 188 Choi, J. H. *et al.* Early endosomal abnormalities and cholinergic neuron degeneration in amyloid-beta protein precursor transgenic mice. *J Alzheimers Dis* **34**, 691-700, doi:10.3233/JAD-122143 (2013).
- 189 Li, G. Rab GTPases, membrane trafficking and diseases. *Curr Drug Targets* **12**, 1188-1193 (2011).
- 190 Chapuis, J. *et al.* Increased expression of BIN1 mediates Alzheimer genetic risk by modulating tau pathology. *Molecular psychiatry* **18**, 1225-1234, doi:10.1038/mp.2013.1 (2013).
- 191 Beecham, G. W. *et al.* Genome-wide association meta-analysis of neuropathologic features of Alzheimer's disease and related dementias. *PLoS genetics* **10**, e1004606, doi:10.1371/journal.pgen.1004606 (2014).
- 192 He, F. *et al.* Structural insight into the zinc finger CW domain as a histone modification reader. *Structure* **18**, 1127-1139, doi:10.1016/j.str.2010.06.012 (2010).
- 193 Allen, M. *et al.* Late-onset Alzheimer disease risk variants mark brain regulatory loci. *Neurol Genet* **1**, e15, doi:10.1212/NXG.000000000000012 (2015).
- 194 Karch, C. M. *et al.* Expression of novel Alzheimer's disease risk genes in control and Alzheimer's disease brains. *PloS one* **7**, e50976, doi:10.1371/journal.pone.0050976 (2012).
- 195 Van Cauwenberghe, C., Van Broeckhoven, C. & Sleegers, K. The genetic landscape of Alzheimer disease: clinical implications and perspectives. *Genet Med* **18**, 421-430, doi:10.1038/gim.2015.117 (2016).
- 196 Harold, D. *et al.* Genome-wide association study identifies variants at CLU and PICALM associated with Alzheimer's disease. *Nat Genet* **41**, 1088-1093, doi:10.1038/ng.440 (2009).

- 197 Hollingworth, P. *et al.* Common variants at ABCA7, MS4A6A/MS4A4E, EPHA1, CD33 and CD2AP are associated with Alzheimer's disease. *Nat Genet* **43**, 429-435, doi:10.1038/ng.803 (2011).
- 198 Lambert, J. C. *et al.* Genome-wide association study identifies variants at CLU and CR1 associated with Alzheimer's disease. *Nat Genet* **41**, 1094-1099, doi:10.1038/ng.439 (2009).
- 199 Stage, E. *et al.* The effect of the top 20 Alzheimer disease risk genes on gray-matter density and FDG PET brain metabolism. *Alzheimers Dement (Amst)* **5**, 53-66, doi:10.1016/j.dadm.2016.12.003 (2016).
- 200 Petersen, R. C. & Negash, S. Mild cognitive impairment: an overview. *CNS Spectr* **13**, 45-53 (2008).
- 201 Petersen, R. C. *et al.* Mild cognitive impairment: clinical characterization and outcome. *Arch Neurol* **56**, 303-308, doi:10.1001/archneur.56.3.303 (1999).
- 202 Dubois, B. *et al.* Research criteria for the diagnosis of Alzheimer's disease: revising the NINCDS-ADRDA criteria. *Lancet Neurol* **6**, 734-746, doi:10.1016/S1474-4422(07)70178-3 (2007).
- 203 Wechsler, D. *Manual for the Wechsler Memory Scale-Revised*. (1987).
- 204 Jack, C. R., Jr. *et al.* Defining imaging biomarker cut points for brain aging and Alzheimer's disease. *Alzheimers Dement* **13**, 205-216, doi:10.1016/j.jalz.2016.08.005 (2017).
- 205 Maass, A. *et al.* Comparison of multiple tau-PET measures as biomarkers in aging and Alzheimer's disease. *Neuroimage* **157**, 448-463, doi:10.1016/j.neuroimage.2017.05.058 (2017).
- 206 Diedrichsen, J. A spatially unbiased atlas template of the human cerebellum. *Neuroimage* **33**, 127-138, doi:10.1016/j.neuroimage.2006.05.056 (2006).
- 207 Lasorsa, A. *et al.* Structural Basis of Tau Interaction With BIN1 and Regulation by Tau Phosphorylation. *Front Mol Neurosci* **11**, 421, doi:10.3389/fnmol.2018.00421 (2018).
- 208 Franzmeier, N., Rubinski, A., Neitzel, J., Ewers, M. & Alzheimer's Disease Neuroimaging, I. The BIN1 rs744373 SNP is associated with increased tau-PET levels and impaired memory. *Nat Commun* **10**, 1766, doi:10.1038/s41467-019-09564-5 (2019).
- 209 Dourlen, P. *et al.* Functional screening of Alzheimer risk loci identifies PTK2B as an in vivo modulator and early marker of Tau pathology. *Molecular psychiatry* **22**, 874-883, doi:10.1038/mp.2016.59 (2017).
- 210 Zhou, Y. *et al.* Intracellular clusterin interacts with brain isoforms of the bridging integrator 1 and with the microtubule-associated protein Tau in Alzheimer's disease. *PloS one* **9**, e103187, doi:10.1371/journal.pone.0103187 (2014).
- 211 Sullivan, S. E. *et al.* Candidate-based screening via gene modulation in human neurons and astrocytes implicates FERMT2 in Abeta and TAU proteostasis. *Human molecular genetics* **28**, 718-735, doi:10.1093/hmg/ddy376 (2019).

- 212 Martiskainen, H. *et al.* Transcriptomics and mechanistic elucidation of Alzheimer's disease risk genes in the brain and in vitro models. *Neurobiol Aging* **36**, 1221 e1215-1228, doi:10.1016/j.neurobiolaging.2014.09.003 (2015).
- 213 Li, C. & Gotz, J. Pyk2 is a Novel Tau Tyrosine Kinase that is Regulated by the Tyrosine Kinase Fyn. *J Alzheimers Dis* **64**, 205-221, doi:10.3233/JAD-180054 (2018).
- 214 Boden, K. A. *et al.* Methylation Profiling RIN3 and MEF2C Identifies Epigenetic Marks Associated with Sporadic Early Onset Alzheimer's Disease. *J Alzheimers Dis Rep* **1**, 97-108, doi:10.3233/ADR-170015 (2017).
- 215 Alexopoulos, P. *et al.* Interrelations between CSF soluble AbetaPPbeta, amyloid-beta 1-42, SORL1, and tau levels in Alzheimer's disease. *J Alzheimers Dis* **28**, 543-552, doi:10.3233/JAD-2011-110983 (2012).
- 216 Killick, R., Hughes, T. R., Morgan, B. P. & Lovestone, S. Deletion of Crry, the murine ortholog of the sporadic Alzheimer's disease risk gene CR1, impacts tau phosphorylation and brain CFH. *Neurosci Lett* **533**, 96-99, doi:10.1016/j.neulet.2012.11.008 (2013).
- 217 Moreau, K. *et al.* PICALM modulates autophagy activity and tau accumulation. *Nat Commun* **5**, 4998, doi:10.1038/ncomms5998 (2014).
- 218 Ikeda, Y. *et al.* Posttranscriptional regulation of human ABCA7 and its function for the apoA-I-dependent lipid release. *Biochemical and biophysical research communications* **311**, 313-318, doi:10.1016/j.bbrc.2003.10.002 (2003).
- 219 Wang, N. *et al.* ATP-binding cassette transporter A7 (ABCA7) binds apolipoprotein A-I and mediates cellular phospholipid but not cholesterol efflux. *The Journal of biological chemistry* **278**, 42906-42912, doi:10.1074/jbc.M307831200 (2003).
- 220 Kielar, D. *et al.* Adenosine triphosphate binding cassette (ABC) transporters are expressed and regulated during terminal keratinocyte differentiation: a potential role for ABCA7 in epidermal lipid reorganization. *J Invest Dermatol* **121**, 465-474, doi:10.1046/j.1523-1747.2003.12404.x (2003).
- 221 Abe-Dohmae, S. *et al.* Human ABCA7 supports apolipoprotein-mediated release of cellular cholesterol and phospholipid to generate high density lipoprotein. *The Journal of biological chemistry* **279**, 604-611, doi:10.1074/jbc.M309888200 (2004).
- 222 Miyagawa, T. *et al.* BIN1 regulates BACE1 intracellular trafficking and amyloid-beta production. *Human molecular genetics* **25**, 2948-2958, doi:10.1093/hmg/ddw146 (2016).
- 223 Wyatt, A. R. & Wilson, M. R. Identification of human plasma proteins as major clients for the extracellular chaperone clusterin. *The Journal of biological chemistry* **285**, 3532-3539, doi:10.1074/jbc.M109.079566 (2010).

- 224 Nizard, P. *et al.* Stress-induced retrotranslocation of clusterin/ApoJ into the cytosol. *Traffic* **8**, 554-565, doi:10.1111/j.1600-0854.2007.00549.x (2007).
- 225 Yerbury, J. J. *et al.* The extracellular chaperone clusterin influences amyloid formation and toxicity by interacting with prefibrillar structures. *FASEB J* **21**, 2312-2322, doi:10.1096/fj.06-7986com (2007).
- 226 Jin, P. *et al.* Novel splice variants derived from the receptor tyrosine kinase superfamily are potential therapeutics for rheumatoid arthritis. *Arthritis research & therapy* **10**, R73, doi:10.1186/ar2447 (2008).
- 227 Mosch, B., Reissenweber, B., Neuber, C. & Pietzsch, J. Eph receptors and ephrin ligands: important players in angiogenesis and tumor angiogenesis. *J Oncol* **2010**, 135285, doi:10.1155/2010/135285 (2010).
- 228 Pasquale, E. B. Eph receptors and ephrins in cancer: bidirectional signalling and beyond. *Nat Rev Cancer* **10**, 165-180, doi:10.1038/nrc2806 (2010).
- 229 Tebar, F., Bohlander, S. K. & Sorkin, A. Clathrin assembly lymphoid myeloid leukemia (CALM) protein: localization in endocytic-coated pits, interactions with clathrin, and the impact of overexpression on clathrin-mediated traffic. *Molecular biology of the cell* **10**, 2687-2702, doi:10.1091/mbc.10.8.2687 (1999).
- 230 Tian, Y., Chang, J. C., Fan, E. Y., Flajolet, M. & Greengard, P. Adaptor complex AP2/PICALM, through interaction with LC3, targets Alzheimer's APP-CTF for terminal degradation via autophagy. *Proceedings of the National Academy of Sciences of the United States of America* **110**, 17071-17076, doi:10.1073/pnas.1315110110 (2013).
- 231 Li, X. F., Kraev, A. S. & Lytton, J. Molecular cloning of a fourth member of the potassium-dependent sodium-calcium exchanger gene family, NCKX4. *The Journal of biological chemistry* **277**, 48410-48417, doi:10.1074/jbc.M210011200 (2002).
- 232 Saito, K. *et al.* A novel binding protein composed of homophilic tetramer exhibits unique properties for the small GTPase Rab5. *The Journal of biological chemistry* **277**, 3412-3418, doi:10.1074/jbc.M106276200 (2002).
- 233 Li, X. *et al.* Proteomic analyses reveal distinct chromatin-associated and soluble transcription factor complexes. *Mol Syst Biol* **11**, 775, doi:10.15252/msb.20145504 (2015).
- 234 Kunkle, B. W. *et al.* Genetic meta-analysis of diagnosed Alzheimer's disease identifies new risk loci and implicates Abeta, tau, immunity and lipid processing. *Nat Genet* **51**, 414-430, doi:10.1038/s41588-019-0358-2 (2019).
- 235 Jansen, I. E. *et al.* Genome-wide meta-analysis identifies new loci and functional pathways influencing Alzheimer's disease risk. *Nat Genet* **51**, 404-413, doi:10.1038/s41588-018-0311-9 (2019).
- 236 Marioni, R. E. *et al.* GWAS on family history of Alzheimer's disease. *Transl Psychiatry* **8**, 99, doi:10.1038/s41398-018-0150-6 (2018).

- 237 Mehta, K. M. & Yeo, G. W. Systematic review of dementia prevalence and incidence in United States race/ethnic populations. *Alzheimers Dement* **13**, 72-83, doi:10.1016/j.jalz.2016.06.2360 (2017).
- 238 Froehlich, T. E., Bogardus, S. T., Jr. & Inouye, S. K. Dementia and race: are there differences between African Americans and Caucasians? *J Am Geriatr Soc* **49**, 477-484, doi:10.1046/j.1532-5415.2001.49096.x (2001).
- 239 Chin, A. L., Negash, S. & Hamilton, R. Diversity and disparity in dementia: the impact of ethnoracial differences in Alzheimer disease. *Alzheimer Dis Assoc Disord* **25**, 187-195, doi:10.1097/WAD.0b013e318211c6c9 (2011).
- 240 Yaffe, K. *et al.* Effect of socioeconomic disparities on incidence of dementia among biracial older adults: prospective study. *BMJ* **347**, f7051, doi:10.1136/bmj.f7051 (2013).

Curriculum Vitae

Edwin Carl Stage Jr

EDUCATION

2015 - 2020 | Ph.D., Medical Neuroscience, Indiana University

2008 - 2012 | B.S., Biology, Ball State University

RESEARCH EXPERIENCE

June 2014 - December 2014 Research Assistant, Department of Hematology/Oncology

- In the laboratory of Rebecca Chan my experiences included the genotyping of mice, measuring relative protein levels via Western blotting, cell culture, mice husbandry, and dissection.

March 2015 - August 2015 Research Assistant, Department of Hematology/Oncology

- In the laboratory of Heiko Konig I was responsible for measuring protein levels, cell culture, and running pharmacologic efficacy tests on acute myeloid leukemia cells.

October 2015 - December 2015 Rotation student, Medical Neuroscience

- In the laboratory of Alexander Niculescu, I was a part of a novel genetic profiling of women with suicide ideation as well as creating a gene interaction database of genes which regulate circadian function.

March 2016 - May 2016 Rotation student, Medical Neuroscience

- In the laboratory of Jinhui Chen I was a part of a novel study of neuronal activity in mice after traumatic brain injury as well as looking at hippocampal neurogenesis post mild traumatic brain injury.

May 2016 - April 2020 Dissertation Research, Indiana Alzheimer Disease

Center/Department of Neurology

- In the laboratory of Liana Apostolova my research focus is centered around using neuroimaging techniques to quantitatively phenotype Alzheimer's disease. This includes projects centered on early vs. late-onset Alzheimer's disease and Suspected non-Alzheimer's disease, acetyl cholinesterase inhibitor use in mildly impaired subjects, and a study of GWAS-validated disease variants and their correlation with imaging biomarkers of amyloid, tau, FDG, and MRI.

AWARDS

2016 Alzheimer's Association of Greater Indiana Early Investigators Scholarship

Recipient

2016 AAIC Student Travel Fellowship

2016 AIC Registration Fellowship

2017 Alzheimer's Association of Greater Indiana Early Investigators Scholarship
Recipient

2017 Indiana Neuroimaging Symposium Travel Award

2018 Midwest Big Data Summer School Travel Award

2019 AAIC Student Travel Fellowship

2019 AIC Registration Fellowship

PROFESSIONAL AFFILIATIONS

International Society to Advance Alzheimer's Research (ISTAART)

American Academy of Neurology

PUBLICATIONS

- 1) Levey DF, Niculescu EM, Le-Niculescu H, Dainton HL, Phalen PL, Ladd TB, Weber H, Belanger E, Graham DL, Khan FN, Vanipenta NP, **Stage E**, Ballew A, Yard M, Gelbart T, Shekhar A, Schork NJ, Kurian SM, Sandusky GE, Salomon DR, Niculescu AB. Towards understanding and predicting suicidality in women: biomarkers and clinical risk assessment. Nat Molecular Psychiatry. 2016; 21:768–785.
- 2) **Stage E**, Duran T, Risacher SL, Goukasian N, Do TM, West JD, Wilhalme H, Nho K, Phillips M, Elashoff D, Saykin AJ, Apostolova LG. The effect of the top

- 20 Alzheimer disease risk genes on gray-matter density and FDG PET brain metabolism. *Alzheimer's and Dementia DADM*. 2016;5:53-66.
- 3) Apostolova LG, Risacher SL, Duran T, **Stage E**, Goukasian N, West JD, Do TM, Grotts J, Wilhalme H, Nho K, Phillips M, Elashoff D, Saykin AJ. Associations of the Top 20 Alzheimer Disease Risk Variants With Brain Amyloidosis. *JAMA Neurol*. 2018;75(3):328-341.
- 4) **Stage E**, Phillips M, Canela VH, Duran, T, Goukasian N, Risacher SL, Saykin AJ, Apostolova LG. Tau Burden and Neurodegenerative changes in Early & Late Onset Alzheimer and non-Alzheimer Pathology. Submitted revisions for *Alzheimer's Research and Therapy*.
- 5) Phillips M, **Stage E**, Lane KA, Gao S, Risacher SL, Goukasian N, Saykin AJ, Carrillo MC, Dickerson BC, Rabinovici GD, Apostolova LG. Neurodegenerative Patterns of Cognitive Clusters of Early Onset AD Subjects: Evidence for Disease Heterogeneity. *Dementia and Geriatric Cognitive Disorders*. 2020;48(3-4):131-142.

CONFERENCES AND PRESENTATIONS

- 1) Apostolova LG, Risacher SL, Duran T, **Stage E**, Goukasian N, West JD, Do TM, Grotts J, Wilhalme H, Nho K, Phillips M, Elashoff D, Saykin AJ. Examining the effect of the top 20 AD risk variants on brain amyloidosis, structural atrophy, and metabolism. AAIC 2016, Toronto, CAN, July 2016.*
- *Also presented at 2017 Bloomington Big Data Neuroscience workshop*

- 2) **Stage E**, Duran T, Goukasian N, West JD, Do TM, Grotts J, Wilhalme H, Nho K, Phillips M, Elashoff D, Risacher SL, Saykin AJ, Apostolova LG. Association of FDG-PET brain metabolism with Alzheimer's disease risk genes. AAIC 2016, Toronto, CAN, July 2016.*
**Also presented at the 2016 Alzheimer's Association Greater Indiana Chapter Scholarship Ceremony*
- 3) Duran T, **Stage E**, Goukasian N, West JD, Do TM, Grotts J, Wilhalme H, Nho K, Phillips M, Elashoff D, Risacher SL, Saykin AJ, Apostolova LG. Association of brain atrophy with Alzheimer's disease risk genes. AAIC 2016, Toronto, CAN, July 2016. **Oral**
- 4) Canela VH, **Stage E**, Phillips M, Duran T, Rabinovici G, Dickerson B, Carrillo M, De Santi S, Goukasian N, Risacher S, Apostolova L. Differences in brain metabolism in Early and Late Onset Alzheimer's disease and Suspect Non-Alzheimer's Pathophysiology, AAN 2017, Boston, MA, USA, April 2017.
- 5) **Stage E**, Phillips M, Duran T, Canela VH, Rabinovici G, Dickerson B, Carrillo M, De Santi S, Goukasian N, Risacher S, Apostolova L. Brain Atrophy in Early and Late Onset Alzheimer's Disease and Suspected Non-Alzheimer's Pathophysiology, AAN 2017, Boston, MA, USA, April 2017.
- 6) **Stage E**, Phillips M, Canela VH, Duran T, Goukasian N, Rabinovici GD, Dickerson BC, Carrillo MC, de Santi S, Risacher SL, Saykin AJ, Apostolova LG. Comparing Imaging Phenotypes of Amnesic Early Vs. Late-Onset Amyloid-Positive Mild Cognitive Impairment and Dementia ADNI Subjects.

2017 Alzheimer's Association International conference, London, UK, July 2017.*

**Also presented at 2017 Indiana Neuroimaging Symposium*

- 7) **Stage E**, Phillips M, Canela VH, Duran T, Goukasian N, Rabinovici GD, Dickerson BC, Carrillo MC, de Santi S, Risacher SL, Saykin AJ, Apostolova LG. Comparing Imaging Phenotypes of Amnesic Early Vs. Late-Onset Amyloid-Negative Mild Cognitive Impairment and Dementia ADNI Subjects. 2017 Alzheimer's Association International conference, London, UK, July 2017.*

**Also presented at the 2017 Alzheimer's Association Greater Indiana Chapter Scholarship Ceremony, 2017 Gill Symposium, 2017 IUSM Graduate Programs Poster Showcase, 2017 Indiana Neuroimaging Symposium*

- 8) Phillips M, **Stage E**, Canela VH, Duran T, Goukasian N, Rabinovici GD, Dickerson BC, Carrillo MC, de Santi S, Risacher SL, Saykin AJ, Apostolova LG. Neurodegenerative patterns of cognitive clusters of early onset AD subjects evidence for disease heterogeneity. 2017 Alzheimer's Association International conference, London, UK, July 2017. **Oral ***

**Also presented at 2017 Indiana Neuroimaging Symposium*

- 9) **Stage E**, Svaldi, D, Phillips M, Duran T, Risacher SL, Saykin AJ, Apostolova LG. ^{18}F -AV-1451 Binding Profile in early and late-onset Alzheimer's Disease and Suspected Non-Alzheimer Pathophysiology. 2018 Alzheimer's Association International Conference, Chicago, IL, USA, July 2018. **Oral ***

**Also presented at 2019 Human Amyloid Imaging Conference, 2019 International Conference on Alzheimer's and Parkinson's Diseases (BOTH ORAL), 2018 Gill Symposium*

- 10) Phillips M, Lane KA, Svaldi DO, Gao S, **Stage E**, Risacher SL, Saykin AJ, Apostolova LG. Longitudinal Patterns of Decline in Subtypes of Amnesic Early Onset AD. 2018 Alzheimer's Association International Conference, Chicago, IL, USA, July 2018.
- 11) Duran T, Woo E, Svaldi DO, Risacher SL, **Stage E**, Goukasian N, Hwang K, Nho K, West JD, Phillips M, Apostolova LG. Associations Between Cortical Thickness and Metamemory in Alzheimer's Disease. 2018 Alzheimer's Association International Conference, Chicago, IL, USA, July 2018.
- 12) **Stage E**, Svaldi, D, Sokolow, S, Risacher SL, Marosi, K, Rotter J, Saykin AJ, Apostolova LG. Prescribing Cholinesterase inhibitors in mild cognitive impairment – observations from the Alzheimer's Disease Neuroimaging Initiative. 2018 Clinical Trials on Alzheimer's Disease, Barcelona, Spain, October 2018.
- 13) **Stage E**, Svaldi, D, Phillips M, Duran T, Risacher SL, Saykin AJ, Apostolova LG. Early and Late-onset Alzheimer's disease and Suspected Non-Alzheimer Pathophysiology within the A/T/N Framework. 2019 Alzheimer's Association International Conference, Los Angeles, CA, USA, July 2019. **Oral***
**Also presented as a poster at AAIC and AIC 2019*
- 14) **Stage E**, Risacher SL, Goukasian N, Nho K, Saykin AJ, Apostolova LG. Global cortical [18F]Flortaucipir association with the top 20 Alzheimer's

disease risk genes. 2019 Alzheimer's Association International Conference, Los Angeles, CA, USA, July 2019. **Oral***

**Also presented as a poster at AAIC and AIC 2019*

15) Svaldi D, , Goñi J, Amico E, Risacher SL, **Stage E**, Charanya M, West JD, Dziedzic M, Saykin AJ, Apostolova LG. Covarying patterns of Functional Connectivity with Amyloid and Tau Deposition in Early Stage Alzheimer's Disease. 2019 Alzheimer's Association International Conference, Los Angeles, CA, USA, July 2019.